國 立 交 通 大 學

電子工程學系 電子研究所碩士班

碩 士 論 文

氧化鋯在雙穩態電阻切換式

記憶體的特性探討

The Properties of Bistable Resistivity Switching

Memory in Zirconium Oxide

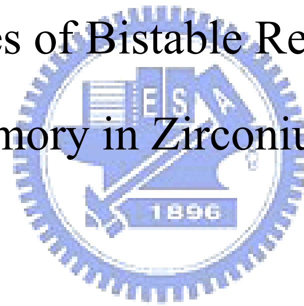

研 究 生：林昭正

指導教授：曾俊元 教授

中 華 民 國 九 十 四 年 六 月

氧化鋯在雙穩態電阻切換式
記憶體的特性探討

The Properties of Bistable Resistivity Switching
Memory in Zirconium Oxide

研 究 生：林昭正　　　　Student：Chao-Cheng Lin

指導教授：曾俊元　　　　Advisor：Tseung-Yuen Tseng

國 立 交 通 大 學

電子工程學系 電子研究所碩士班

碩 士 論 文

A Thesis

Submitted to Department of Electronics Engineering and Institute of Electronics

College of Electrical Engineering and Computer Science

National Chiao Tung University

in partial Fulfillment of the Requirements

for the Degree of

Master

in

Electronic Engineering

June 2005

Hsinchu, Taiwan, Republic of China

中華民國九十四年六月

氧化鋯在雙穩態電阻切換式
記憶體的特性探討

學生：林昭正　　　　　　　　　　指導教授：曾俊元 教授

國立交通大學電子工程學系電子研究所

摘要

隨著元件尺寸的持續縮小，傳統的非揮發式記憶體由於其基本機制因由而面臨許多問題的產生，因此，近年來許多新型態的非揮發式記憶體被廣泛的研究，以試圖能夠取代傳統的非揮發式記憶體。其中，電阻式切換記憶體因具有簡單的製程步驟，快速的反應時間，長時間的非揮發性記憶力以及較小尺寸面積，而成為一個很有可能的新世代非揮發式記憶體。

在這篇論文中，首先介紹了傳統是記憶體將面臨的一些問題，並且簡介了取代它的可能選擇以及各種曾經做過的電阻式切換記憶體。接著，介紹過去曾經被用來說明電阻式切換記憶體的幾種可能機制。而在實驗方面，我們利用溶膠-凝膠法製作氧化鋯的薄膜，並利用摻雜不同的元素以嘗試引發轉態特性。此外，我們量測氧化鋯的物性和電性以試圖找出其可能的電阻轉態機制。最後我們由整個實驗的結果歸納出雙穩態導電率在氧化鋯的一些特性等。

The Properties of Bistable Resistivity Switching Memory in Zirconium Oxide

Student : Chao-Cheng Lin Advisor : Tseung-Yuen Tseng

Department of Electronics Engineering and Institute of Electronics
National Chiao Tung University

Abstract

As the size of the device scales down, conventional nonvolatile memory has encountered some problems, such as the base mechanism. In recent years, many kinds of novel nonvolatile memories are investigated widely to substitute for the conventional nonvolatile memory. Among them, nonvolatile resistive memory may be a prior candidate for the new generation nonvolatile memory created by simpler process, faster reaction time, long time retention and smaller device area.

In this thesis, we first introduce some oncoming problems of the conventional nonvolatile memory and further describe the candidates for the replacement of it. Next, we present a few kinds of materials concerned with resistivity memory and some mechanisms have been used to explain the properties of the bistable resistivity phenomenon. In our experiment, we, however, employ Sol-Gel method to fabricate the zirconium oxide film and attempt to induce the bistable resistivity phenomenon by doping impurities into the film.

Besides, we measure variant physical and electrical properties to find out the mechanism of the bistable phenomenon. Finally, we make a summary on properties of the bistable resistivity in zirconium oxide with our experiment results.

E S A
1896

誌　　謝

首先，感謝指導教授曾俊元老師這兩年來給我的指導與教誨，每當實驗中遇到困惑不解之處或者遇到瓶頸時，老師總是能給予我很多好的建議使我能有更多的方法能夠去處理問題，突破難關，使得我能夠順利的完成碩士論文。在此對老師獻上至高的謝意，感謝兩年來的教導。

接著我要感謝實驗室的學長劉志益，學長總是給我在實驗上很多的建議，使得我在做實驗能夠犯較少的錯誤等，使得我從中學習到很多做實驗的方法以及精神，除此之外，我也要感謝我們實驗室的其他學長、同學以及學弟，總是給我很多的鼓勵以及幫助。

最後，我要感謝我最偉大的父母，多年來對我辛苦的教導以及栽培，使得我能夠長大成人，老爸老媽，感謝你們這些年來辛苦的工作來提供我生活上衣食無缺，以及感謝你們在精神上給我極大的支持，謝謝你們。

Contents

Chinese Abstract i

English Abstract ii

Acknowledgements iii

Chapter 1 Introduction

1.1 Conventional Nonvolatile Memory 1
- 1.1.1 Storing and Erasing 1
- 1.1.2 Retention 2
- 1.1.3 Long Write Time 2
- 1.1.4 High Operator Voltage 2
- 1.1.5 Endurance 3

1.2 Candidates 3
- 1.2.1 FeRAM 3
- 1.2.2 OUM 4
- 1.2.3 OBD 5
- 1.2.4 RRAM 6

1.3 Transition Metal Oxide 7
- 1.3.1 Titanium Oxide 7
- 1.3.2 Niobium Oxide 7
- 1.3.3 Nickel Oxide 8
- 1.3.4 Zirconium Oxide 8

1.4 Mechanisms 9
- 1.4.1 Filament 9
- 1.4.2 Phase Transformation 10
- 1.4.3 Charge Storage 11
- 1.4.4 States Modulation 11

1.6 Motivation and Strategies 13
- 1.6.1 Motivation 13
- 1.6.2 Strategies 14

Chapter 2 Experiment Detail

2.1 Bottom Electrode 15
- 2.1.1 Sputtering System 15
- 2.1.2 Preparation of Target 17
- 2.1.3 Deposition of Bottom Electrode 17

2.2 Transition Metal Oxide Film Samples 17
2.2.1 The Preparation of Solution 17
2.2.2 TMO Film 18
2.2.3 Deposition of Top Electrode 19
2.3 Physical characteristics 19
2.3.1 Scanning Electron Microscopy (SEM) 19
2.3.2 X-Ray Diffraction Analysis 20
2.4 Measurement System 20
2.5 Electrical Measurement 20

Chapter 3 Results and Discussion
3.1 X-Ray Results 22
3.1.1 Different Solution 22
3.1.2 The Properties of Crystallization 24
3.2 Morphology and Thickness of the ZrO_2 Film 24
3.3 Electrical properties 25
3.3.1 Static Properties of ZrO_2 Film 25
3.3.2 Dynamic Properties of ZrO_2 Film 26
3.3.3 Effect of Doping 27
3.3.4 Effect of Thickness 28
3.3.5 Electrical Characteristic of the Crystallized Type 29
3.3.6 Retention of ZrO_2 Film 30
3.3.7 Temperature Effect on The High Current Density State 30
3.3.8 Current fitting 31

Chapter 4 Conclusion

Table Captions

Table Captions

Table 1-1 Conduction processes in insulators

Table 2-1 Radius of Element

Fig. Captions

Chapter 1

Fig. 1.2.1-1 Equivalent circuit of capacitor-type FeRAM (a) and FET-type FeRAM [2]

Fig. 1.2.1-2 C-V characteristic of a ferroelectric device [2]

Fig. 1.2.3-1 The structure of the OBD device and its equivalent circuit [4]

Fig. 1.3.1-1 Switching cycle and current voltage behavior of a titanium dioxide film [5]

Fig. 1.3.3-1 Switching phenomenon in nickel oxide [6]

Fig. 1.3.2-1 Switching phenomenon in nickel oxide [7]

Fig. 1.4.2-1 the structure of OUM device[14]

Chapter 3

Fig. 3.1.1-1 X-Ray diffraction patterns of the sample with the solution of 0.05 M/L at temperature 500 ^oC

Fig. 3.1.1-2 X-Ray diffraction patterns of the sample with the solution of 0.05 M/L at temperature 700 ^oC

Fig. 3.1.1-3 X-Ray diffraction patterns of the sample with the solution of 0.1 M/L at temperature 500 ^oC

Fig. 3.1.1-4 X-Ray diffraction patterns of the sample with the solution of 0.1 M/L at temperature 700 ^oC

Fig. 3.1.1-5 X-Ray diffraction patterns of the sample with the solution of 0.5 M/L at temperature 500 ^oC

Fig. 3.1.1-6 X-Ray diffraction patterns of the sample with the solution of 0.5 M/L at temperature 700 ^oC

Fig. 3.1.1-7 X-Ray diffraction pattern of ZrO_2 film with solution of different mole concentration

Fig. 3.1.1-8 The relation between thickness of the film and mole concentration of the solution

Fig. 3.1.1-9 X-Ray diffraction patterns of the sample with the solution of 0.5 M/L at temperature 500 ^{o}C

Fig. 3.1.1-10 X-Ray diffraction patterns of the sample with the solution of 0.5 M/L at temperature 600 ^{o}C

Fig. 3.1.1-11 X-Ray diffraction patterns of the sample with the solution of 0.5 M/L at temperature 700 ^{o}C

Fig. 3.1.1-12 X-Ray diffraction patterns of the sample with the solution of 0.5 M/L at temperature 800 ^{o}C

Fig. 3.2-1 Plan-view of SEM with sample fabricated by using the solution of 0.3 mole concentration

Fig. 3.2-2 Plan-view of SEM with sample fabricated by using the solution of 0.3 mole concentration and thermal treatment at temperature 500 ^{o}C

Fig. 3.2-3 Plan-view of SEM with sample fabricated by using the solution of 0.3 mole concentration and thermal treatment at temperature 600 ^{o}C

Fig. 3.2-4 Plan-view of SEM with sample fabricated by using the solution of 0.3 mole concentration and thermal treatment at temperature 700 ^{o}C

Fig. 3.2-5 X-Ray diffraction pattern related to temperature of 500 ^{o}C in the furnace

Fig. 3.2-6 X-Ray diffraction pattern related to temperature of 600 ^{o}C in the furnace

Fig. 3.2-7 Cross section view of SEM with sample fabricated by using the solution of 0.05 mole concentration to deposit five layers of ZrO_2 films

Fig. 3.2-8 Cross section view of SEM with sample fabricated by using the solution of 0.1 mole concentration to deposit five layers of ZrO_2 films

Fig. 3.2-9 Cross section view of SEM with sample fabricated by using the solution of 0.5 mole concentration to deposit fore layers of ZrO_2 films

Fig. 3.3.1-1 Bistable switching current density versus voltage, sweeping of 1st time

Fig. 3.3.1-2 Bistable switching current density versus voltage sweeping of 5rd time

Fig. 3.3.2-1 Current density of ZrO_2 film with thickness of 30 nm measured by magnitude of pulse voltage of 12 volts with pulse width of 1ms, pulse delay 1 sec and readout voltage of -1 volt

Fig. 3.3.2-2 Current density of ZrO_2 film with thickness of 45 nm measured by magnitude of pulse voltage of 15 volts with pulse width of 1ms, pulse delay 1 sec and readout voltage of -1 volt

Fig. 3.3.3-1 Forming curve of non-doped ZrO_2 film of one layer deposited by solution of 0.1 mole concentration

Fig. 3.3.3-2 Forming curve of V doped ZrO_2 film of one layer deposited by solution of 0.1 mole concentration

Fig. 3.3.3-3 Forming curve of Cr ZrO_2 film of one layer deposited by solution of 0.1 mole concentration

Fig. 3.3.3-4 Forming curve of Mo ZrO_2 film of one layer deposited by solution of 0.1 mole concentration

Fig. 3.3.3-1 I-V curve of 5th sweeping time of non-doped ZrO_2 film

Fig. 3.3.3-1 I-V curve of 5th sweeping time of Mo doped ZrO_2 film

Fig. 3.3.4-1 I-V curve of the sample with thickness of 20 nm, sweeping of first time

Fig. 3.3.4-2 I-V curve of the sample with thickness of 30 nm, sweeping of first time

Fig. 3.3.4-3 I-V curve of the sample with thickness of 45 nm, sweeping of first time

Fig. 3.3.4-4 I-V curve of the sample with thickness of 82 nm, sweeping of first time

Fig. 3.3.4-5 I-V curve of the sample with thickness of 20 nm, sweeping of 5th time

Fig. 3.3.4-6 I-V curve of the sample with thickness of 30 nm, sweeping of 5th time

Fig. 3.3.4-7 I-V curve of the sample with thickness of 45 nm, sweeping of 5th time

Fig. 3.3.4-8 I-V curve of the sample with thickness of 82 nm, sweeping of 5th time

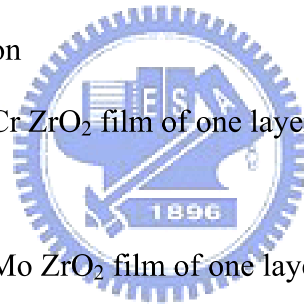

Fig. 3.3.4-9 The order of the current density versus thickness of the ZrO_2 film, sweeping of 1 time

Fig. 3.3.4-10 The order of the current density versus thickness of the ZrO_2 film, sweeping of 5 times

Fig. 3.3.5-1 I-V curve of ZrO_2 film deposited by solution of 0.5 mole concentration and thermal treatment in the furnace at temperature 600 ^{o}C for 30 min, 1st sweeping time

Fig. 3.3.5-2 I-V curve of ZrO_2 film deposited by solution of 0.5 mole concentration and thermal treatment in the furnace at temperature 600 ^{o}C for 30 min, 5th sweeping time

Fig. 3.3.5-3 X-Ray diffraction pattern of the ZrO_2 film deposited by solution of 0.5 mole concentration and thermal treatment in the furnace at temperature 600 ^{o}C for 30 min

Fig. 3.3.6-1 Retention for this sample, the magnitude of the pulse voltage is 30 volts and the pulse width is 1ms

Fig. 3.3.6-2 High-low leakage ration variation during retention test for this sample, the magnitude of the pulse voltage is 30 volts and the pulse width is 1ms

Fig. 3.3.7 High state current after thermal treatment divide by high state current before thermal treatment versus temperatur

Fig. 3.3.8-1 Static I-V curve of 0.1 M two layers ZrO_2 film

Fig. 3.3.8-2 Schottky emission process fitting of curve (a)

Fig. 3.3.8-3 Frenkel poole process current fitting of curve (a)

Fig. 3.3.8-4 Field emission process fitting of curve (a)

Fig. 3.3.8-5 Space-charge-limited process fitting of curve (a)

Fig. 3.3.8-6 Ohmic fitting of curve (a)

Fig. 3.3.8-7 Schottky emission process fitting of curve (b)

Fig. 3.3.8-8 Frenkel poole process current fitting of curve (b)

Fig. 3.3.8-9 Field emission process fitting of curve (b)

Fig. 3.3.8-10 Space-charge-limited process fitting of curve (b)

Fig. 3.3.8-11 Ohmic fitting of curve (b)

Fig. 3.3.8-12 Schottky emission process fitting of curve (c)

Fig. 3.3.8-13 Frenkel poole process current fitting of curve (c)

Fig. 3.3.8-14 Field emission process fitting of curve (c)

Fig. 3.3.8-15 Space-charge-limited process fitting of curve (c)

Fig. 3.3.8-16 Ohmic fitting of curve (c)

Fig. 3.3.8-17 Schottky emission process fitting of curve (d)

Fig. 3.3.8-18 Frenkel poole process current fitting of curve (d)

Fig. 3.3.8-19 Field emission process fitting of curve (d)

Fig. 3.3.8-20 Space-charge-limited process fitting of curve (d)

Fig. 3.3.8-21 Ohmic fitting of curve (d)

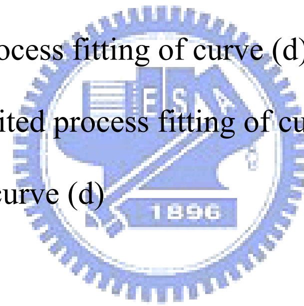

CHAPTER 1

INTRODUCTION

1.1 Conventional Nonvolatile Memory

Since the first nonvolatile memory device proposed by Kahng and Sze in 1967[1], the device has been studied widely for its application and then, various device structures have been made and nonvolatile memory devices have been extensively used in integrated circuit. In recent years, nonvolatile memory has been applied to human's life extensively, such as mobile phone, portable hard disk, mp3 walkman and so on. However, as the progress of the technology and science improve, the commercial nonvolatile memory, Flash memory, will face a number of challenges, such as retention, long writing time, high operator voltage and bad endurance, which are due to the base mechanism of the conventional nonvolatile memory.

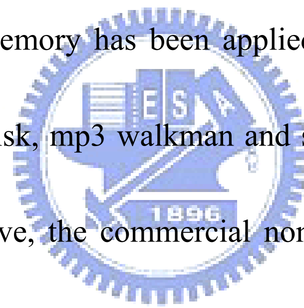

1.1.1 Storing and Erasing

The base structure of Flash is based on a modified n-type MOSFET which inserts a floating gate into the gate oxide. When a voltage of proper magnitude is applied on the gate electrode of the MOSFET, charges will be injected from the silicon substrate into the floating gate. The threshold voltage of the MOSFET, then, is altered to a higher threshold voltage state

and the channel conductance of the MOSFET shifts from the origin even if the external applied voltage is removed. In contrast, if now a voltage of proper magnitude and reverse polarity is applied on the device, the charge is removed from the floating gate and the threshold voltage returns to the non-charged state. Upon this operator mode, the states “1” and “0” can be stored in the device and then the data can be stored in this structure.

1.1.2 Retention

In order to reduce the area of the device, the gate oxide of a cell must be thinner to preserve adequate driving current but the thin gate oxide leads to leakage current between the floating gate and substrate so that the storage carriers will leak from the floating gate into the substrate. Therefore, Flash will lose its remembrance.

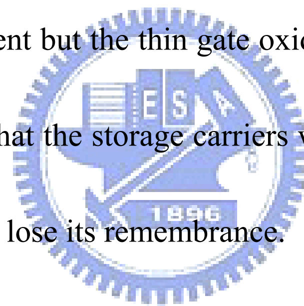

1.1.3 Long Write Time

As the mechanism mentioned above, Flash needs plenty of carriers tunneling into the floating gate, so that it needs a long write time to obtain enough carriers existing in the floating gate.

1.1.4 High Operator Voltage

Both the FN tunneling or the hot carrier need enough large electric field to take the

carrier into the floating gate, but with the device being scaled down, the voltage of a flash must reduce to an applicable range. Then, the high operator voltage becomes a problem for the Flash.

1.1.5 Endurance

The on and off operator on Flash will damage the gate oxide since the carriers, which possess high energy, tunnel across the gate oxide. Therefore, the gate oxide structure is destroyed.

Because there are a lot of challenges in the feature for the conventional nonvolatile memory, some new types of nonvolatile memory utilizing the mechanism that is different from Flash would become the coming generation nonvolatile memory device. Among these new types of nonvolatile memory, a few kinds of it, recently, have been studied widely. In order to know the advantages and the disadvantages with respect to conventional nonvolatile memory, the devices such as FeRAM, OUM, OBD, MRAM and RAM will be introduced in the following paragraphs.

1.2 Candidates

1.2.1 FeRAM

There are two types of FeRAMs which are the capacitor-type FERAM and FET-type

FERAM, as shown in Fig. 1.2.1-1(a) and Fig. 1.2.1-1(b)[2]. The FERAM uses the external voltage to polarize a ferroelectric film, and then it will contain different capacitance on the same voltage as shown in Fig. 1.2.1-2 [2]. Some drawbacks have been discovered, such as high processing temperatures. Ferroelectric thin films of the PZT family require a minimum of 723 K to convert fully into the perovskite phase from pyrochlore. What's more difficult is that a temperature of over 873 K, is required for SBT films to convert from fluorite to Aurivillius phase. Moreover, the toxicity of lead in semiconductor fabrication facility uses deadly arsin or phosphine. Surface and interface phenomena, the defect concentration in ferroelectric oxide is a thousand times more than that of a silicon chip, Fatigue, which may be due to a reduction of oxygen from the ferroelectric into the electrode, also reduces the performance. Scaling, on the other hand, has no detailed theory of finite size effects either for film thickness or edge effects [Ferroelctric memories].

1.2.2 OUM

The mechanism of phase change memory or ovonic unified memory (OUM) is phase change in a thin film chalcogenide material ($Ge_2Sb_2Te_5$-GST)[3]. When an external voltage is applied on film, enough current will move across the film and produce a joule heating. Its phase will be transformed from crystalline phase to amorphous state and vice versa. Therefore, different current order (about 10^4) as the on-state and off-state of the memory can be

controlled by the external applied voltage.

There are some advantages of the OUM. A conventional cell needs at least one transistor (e.g. Flash), but for the OUM cell, it only needs a MIM capacitance, so that the process of a OUM cell will be easier than that of a conventional memory, and can be fabricated more compactly. In addition, it possesses high write/read speed (50ns), long cycle life ($>10^{14}$), and is a nonvolatile memory. It was surprisingly found that OUM could be used as space-based application because of its radiation tolerance.

However, there are still several problems with the OUM. These include the high operation current (>1-3mA), the slow set writing speed (> 50ns), and the thermal fatigue of the phase change material.

1.2.3 OBD

OBD, organic bistable device, whose structure is a little different from a conventional organic RAM, consists of an organic/metal/organic trilayer structure, as shown in Fig. 1.2.3-1 [4]. The material of the middle metal layer is made up of multilayer nanoclusters with a very thin oxidized layer between the clusters so that the charge can easily tunnel through the thin oxidized layer. Therefore, when the applied voltage is high enough, the free carrier in the clusters will tunnel through the barrier, and then produce the charges inside the metallic cores of the nanoclusters. Consequently, this approach changes the conductance of the film

(becoming low resistance state), and is similar to the formation of a conducting channel in a transistor. When the applied voltage has been removed, the conductance of the films remains the same. If a reverse bias voltage has been applied on the film, the charges will be neutralized, and then the resistivity of the film will return to a high resistivity state.

1.2.4 RRAM

RRAM (resistance RAM), which can vary their resistance by appropriate voltage, was intensively investigated from the 1960s to 1980s for denser device and larger memory capacity. Nevertheless, some drawbacks, such as high operation voltage and current and poor endurance, made the studies of the resistance memory pause. Recently, with the promotion of the material science, the resistance memory has been studied again to solve the crisis of the conventional nonvolatile memory.

RRAM can be made from many materials, which comprise the pervoskite oxide, simple binary transition metal oxide and organic material etc. The pervoskite oxide, such as Cr-doped $SrTiO_3$, $SrZrO_3$, $Pr_{0.7}Ca_{0.3}MnO_3$, were reported to have bistable and reversible phenomena by applying proper voltage. The different RRAM system using the binary transition metal oxide which have been reported since 1960s are the most promising candidate for the application of the nonvolatile memory since they are compatible to CMOS process.

1.3 Transition Metal Oxide

Many kinds of transition metal oxides including nickel oxide, titanium oxide, niobium oxide, zirconium oxide had been found exhibiting switching phenomenon. We introduce these transition metal oxides based on their switching phenomenon in the following.

1.3.1 Titanium Oxide

In 1967, it was reported that reversible switching from initial high impedance to a low impedance state was made up of a titanium-titanium oxide-metal structure [5]. The film of titanium oxide was developed by anodization in an electrolyte of ammonium pentaborate in ethylene glycol. The electric characteristic was shown in the Fig. 1.3.1-1. The I-V characteristics in these figures showed some unstable properties of the film, which were uncontrolled switching as in 1.3.1-1(c), current controlled negative resistance as in 1.3.1-1(d) or ohmic region as in 1.3.1-1(e).

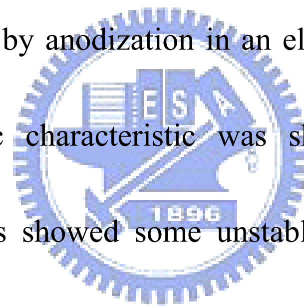

1.3.2 Niobium Oxide

The reversible switching of Nb oxide was studied from 1963 to 1973 [6]. In 1965, Nb-Nb_2O_5-metal diodes were formed by depositing 1 mm x 2 $\frac{1}{2}$ in. niobium strips anodizing the niobium in saturated boric acid electrolyte and then evaporating the metal counter electrode. The electric property of the film is as shown in Fig. 1.3.2-1 [7]. On the first

stage, curve a, shows a high conductance. If now we reverse the external applied voltage to over than 0.18 volt, the conductance will turn to a low one. However, when the applied voltage scans toward positive, the I-V curve will follow curve c, and as voltage increases over than 0.6 volt, the I-V curve will turn to curve a.

1.3.3 Nickel Oxide

Nickel oxide whose switching and negative resistance in thin films were discovered in 1970 [8] is widely investigated recently [9-11]. S. Seo et al. used dc reactive sputtering method to deposit the NiOx film, where the variable x is the ration of oxygen partial pressure to the ambient pressure, and they controlled a pressure of ambient Ar and O_2 gases to get various percentages of the oxygen in NiOx [11]. It was found that the bistable phenomena occurred when the x was smaller than 20%. The electrical characteristic of NiOx is as shown in Fig. 1.3.3-1 in which off-state current is increasing with the size of its top electrode but on-state is independent of the top electrode. Such phenomena had been attributed to the formation of a filament (this will be discussed in the next section).

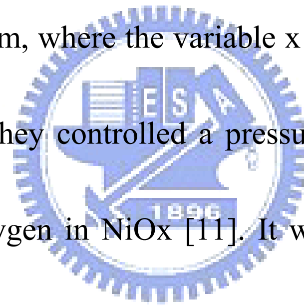

1.3.4 Zirconium Oxide

In 1970, K. C. Park and S. Basavaiah proposed a bistable switching fabricated with Zr-ZrO_2-Au structure. They first deposited zirconium on glass substrate using an electron

beam gun (E-beam), and then the zirconium oxide layers were formed either by vacuum depositing the metal oxide or by anodizing the electrode in a ethylene glycol solution of ammonium pentaborate[12]. The top electrode of gold was deposited on the zirconium oxide films by thermal evaporation, producing active junction areas of 10 mil x 25 mil.

The samples have some electrical properties:

(1) Fresh samples have giant resistances in excess of 10^8 Ω and their current is proportional to V^4.

(2) The thickness of the oxide layers ranges between 1000 to 1650 $\mathring{A}$.

(3) The forming fields ranges between 1 x 10^6 to 5 x 10^6 V/cm.

(4) The low state generally has a resistance of a few hundred Ω.

(5) The high state has a resistance of a hundreds KΩ.

(6) The mechanism is based on the filament discussed in the next section.

1.4 Mechanisms

There are many kinds of mechanism which have been proposed in the RRAM to explain why the switching phenomenon occurs.

1.4.1 Filament

In 1964, conducting filament was used to interpret the property of the switching

phenomenon [13]. The conducting filament will be formed when the external applied voltage is employed on a switching. Recently, the rediscovery that the switching phenomenon lies in polycrystalline NiO films has been reported again[9]. In the nickel oxide, it is observed that the bistable phenomenon is not only in the polycrystalline NiO films but also in the epitaxial ones, so the bistable phenomenon is not on the ground of the structural phase transition as remarked in the OUM device. On the other hand, It was found that the high state (low resistance state) held the same order current for a variant of top electrodes, yet the low state (high resistance state) increased its current as the area of the top electrode is increased. This characteristic was proposed to be caused by the formation and rupture of a conducting filament in the NiO films.

1.4.2 Phase Transformation

As mentioned in the section 1.2.2 OUM device, the phase transformation was found in the chalcogenide material[14]. In the phase change memory (Fig. 1.4.2-1), electric current of different magnitudes are conducted from a heater element to the chalcongenide material and joule heating is used to change the phase of the material. When OUM changes the phase from a crystalline state into an amorphous state, its resistance turns to a higher resistance state. However, if now, the conducting current is reduced to a middle region, the material converts its original states, high resistance state, into the low resistance and its phase, at the same time,

transmits back to the crystalline state.

1.4.3 Charge Storage

In 1967, J. G. Simmons and R. R Verderber proposed a mode to explain the memory state in a SiO film [15]. First, the film was fabricated by vacuum deposition of successive layers of aluminum, silicon monoxide and gold. They then used the electric measurement to analyze the characteristics of the films. It was shown that the film had a forming process and a memory states, high impendence state. In order to interpret these properties, it was hypothesized that there was a broad band of localized states produced by that gold ion injection into the insulator and by traps lying in amorphous insulator. Hence, when a different magnitude and rate of bias voltage is applied on the film, electrons injecting into the states and storing in the insulator cause the hysteresis curve.

ES 1896

1.4.4 States Modulation

Cr doped $SrTiO_3$ had been found to exhibit bistable switching states due to energy states modulation. Cr doped in $SrTiO_3$ as impurity in the $SrTiO_3$ film will induce more than two kinds of energy levels [16]. When a proper voltage is applied on the Cr doped $SrTiO_3$ film, causing the change of current density.

1.5 Carrier Transport in Insulating Films

In an insulator, six mechanisms proposed to explain transport of carriers leading to current flow are Schottky emission, Frenkel-Poole emission, Tunnel (field emission), Space-charge limited, Ohmic and Ionic conduction. Table 1-1 conduction processes in insulators summarizes the basic conduction processes in inulators [17].

When a metal contacts an insulator, their work function difference forms a barrier in band diagram with a barrier between the interface of metal and the insulator. The current, then, flows in the insulator by means of the fact that carriers with enough high thermal energy to surmount the barrier and to transport either from insulator to metal or from metal to insulator. A plot of lnJ versus $V^{1/2}$ produces a straight line with a slope determined by the permittivity of insulator.

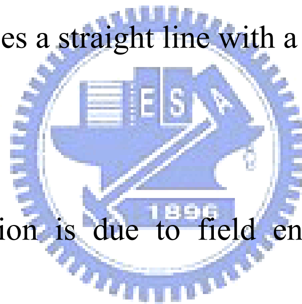

The Frenkel-Poole emission is due to field enhanced thermal excitation of trapped electrons into the conduction band. A plot of ln(J/V) versus $V^{1/2}$ yield a straight.

When an enough large field applies on a material, trapped electron can escape from a trapped state or electrons can tunnel from the metal Fermi energy into the insulator conduction band. The tunnel emission has the strongest dependence on the applied voltage but is not correlation to temperature.

Space-charge-limited result from a carrier injected into the insulator, where no compensating charge is present. The current for unipolar trap-free case is proportional to the square of the applied voltage.

At low voltage and high temperature, current is carrier by thermally excited electrons hopping from one isolated state to the next. This mechanism yields an ohmic characteristic exponentially dependent on temperature.

The ionic conduction is similar to a diffusion process. Generally the dc ionic conductivity decreases during the time the electric field is applied, because ions can't be readily injected into or extracted from the insulator. After the external applied voltage is removed, large internal fields remain causing a few ions to flow back toward their equilibrium position and hysteresis effects result.

1.6 Motivation and Strategies

1.6.1 Motivation

As the science and technology advances, there are more and more applications of Flash used in the life of mankind. Recent years, in order to solve the bottleneck for feature nonvolatile memory, a lot of different kinds of nonvolatile memory are proposed to replace the conventional ones. In these, it seems that RRAM is the more feasible to be a candidate for replacing Flash.

Although the resistance RAM had been studied for many years and plenty of mechanisms were proposed to explain the bistable phenomena, the real reason is not yet clarified. Nevertheless, all the three mechanisms mentioned above may be possible to be the

genuine occasion.

1.6.2 Strategies

In this study, a few impurity doped transition metal oxides produced by Sol-Gel method are investigated and some properties of samples are connected to the mechanisms. First, we use the Sol-Gel method to spin coat the impurity doped transition metal oxides on a substrate; the I-V characteristic are employed to find out bistable electrical properties. X-ray diffraction is, then, used to identify the film type and the crystallized states. The thickness and surface morphology of film are also observed and measured by SEM. In the end, some properties of the film are discussed and concluded.

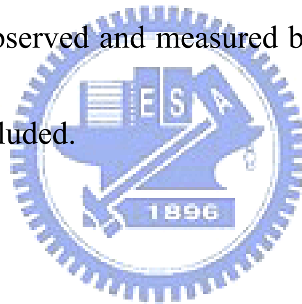

Chapter 2

Experimental Detail

In this chapter, we introduce the fabrication of bottom electrode using sputtering and present how to deposit a transition metal oxide film by Sol-Gel method. Both the physical and the electrical characteristic of the film were analyzed by X-Ray diffraction to identify the structure and the I-V measurement was used to observe its bistable properties.

The precursor solution is prepared by using both the acetic acid and the acetylacetone as solvent and some kinds of materials which include acetate, nitrate, propoxide, and ethoxide were also used as solutes.

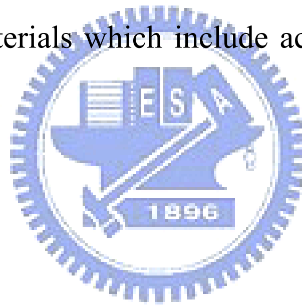

2.1 Bottom Electrode

2.1.1 Sputtering System

RF magnetron sputter is used in deposition of a variety of metallic films in VLSI fabrication, and it is also used in some applications to deposit dielectric film because sputtering method is not only matured but also simple and easy to apply. In our work, it is used for deposition of a bottom electrode on a substrate. We introduce it as the following.

The mechanism of the RF magnetron sputter is based on sputtering. First, the RF magnetron sputter system produces secondary electrons between two electrode plates where

the substrate and the target are seated respectively, and then the collision between the electrons and the inert gas which is pre-filled in the sputter chamber makes the inert gas be ionized. These ionized molecules move to the cathode and collide with it due to the Coulomb force. After the crash between the cathode and ions, the atoms on the target get the kinetic energy and thus escape from the cathode. Finally, these atoms would be deposited on the anode (substrate) and the film is therefore formed.

The RF magnetron sputter composed of 4 systems as discussed below.

(1) Vacuum system is mainly made up of a vacuum pump system. This system consisting of two major parts, a diffusion pump and a mechanical pump, and can control the pressure in the chamber.

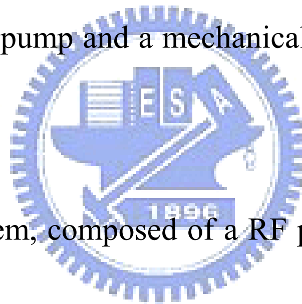

(2) Plasma generator system, composed of a RF power generator providing a maximum power of 600W is primarily employed to produce plasma. The system not only uses the secondary electrons to collide with the inert gas to produce plasma but utilizes RF coil to increase the residence time of the sputtered metallic particle.

(3) Gas flow system, which is mainly composed of the mass flow meter is used to control the ratio and flow rate of the gases during the deposition process.

(4) Cooling system, this part is used to cool the diffusion pump in the vacuum system, the magnet in the chamber and the metal chamber. When the diffusion pump operates, the pump increases the temperature to evaporate the oil and afterwards, the cooling system is used

to cool and control the pump temperature to prevent it from being too high. Furthermore, as the sputtering is in progress, the magnet temperature rises. It is well-known that if the temperature of a magnet material is too high, the magnetic force will be degraded. Therefore, the cooling system can protect the temperature of the magnet from being too high.

2.1.2 Preparation of Target

The sputtering target of LNO is prepared by conventional solid state ceramic powder-mixing way. La_2O_3 is blended with NiO in a stoichiometric ratio at La_2O_3 : NiO = 0.5 : 1. Then, the blended powder is ball milled for 12 hours to ascertain the particle size reduction and the homogeneity of the mixing. The blended powder is calcined at 1300 ^{0}C for 4 hours in air. Finally, the calcined powder is mixed into a disc of a 3-inch diameter.

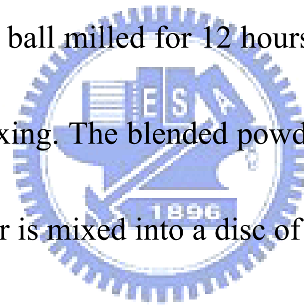

2.1.3 Deposition of Bottom Electrode

After the preparation of target, the La_2O_3 was deposited by sputtering on SiO_2 which is grown on a 4-inch bare silicon wafer, and then its thickness grows to about 2000 $\overset{o}{A}$.

2.2 Transition Metal Oxide Film Samples

2.2.1 The Preparation of Solution

Acetic acid [C2H4O2] and acetylacetone [C5H8O2] are used as solvent to dissolve

different kinds of dopants and starting chemicals including Zirkon (IV) propylate, propoxide, Nickel (II) acetate tetrahydrate, chromium (III) nitrate nonahydrate, niobium (V) ethoxide, molybdenum (II) acetate diamer, vanadium (V) oxide, magnesium acetate tetrahydrate and titanium (IV) ethoxide [Ti(OCH5)4] whose ionic radius is shown in table 2-1.

Acetic acid, first, is heated at the temperature of 80 ^{o}C for 10 minutes in order to remove partial water content. Materials, shown in table 2.2.1-2 are used as dopants to the solvent. Then, the solution is stirred and heated at temperature 80 ^{o}C for 30 minutes for synthesis. Finally, acetylacetone [C5H8O2] and Zirkon (IV) propylate, propoxide [Zr(OCH2CH2CH3)4] is mixed with the solution at temperature 80 ^{o}C for 1 hour.

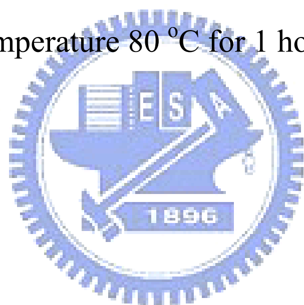

2.2.2 TMO Film

First, on a 4-inch silicon substrate, 2000 $\overset{o}{A}$ thick SiO_2 is grown and subsequently, LNO is sputtered as bottom electrode. The electrode is cut into 2.2 x 2.2 cm^2 square areas and then the squares are put in an oven in order to degas. After 2 hours, the film is spun on the substrate at two steps spin rates which are 1000 rpm and 3500 rpm respectively and whose duration are 5 seconds and 1 min separately. It is, then, heated on a hot plate at temperature 125 ^{o}C for 10 minutes so as to remove the wet and partial acetate content.

Second, the film undergoes two step heat treatments in a furnace. The first one is in order to remove residual water content and its temperature is 200 ^{o}C for 10 minutes. After the first

step, the pyrolysis, proceeds successively at temperature varying from 400 ^{o}C to 700 ^{o}C in order to remove organic compounds.

2.2.3 Deposition of Top Electrode

After the TMO film has formed, the top electrode, Al, is deposited on it with metal masks by a thermal coater. The metal masks are used to define different areas, and therefore the probe of the probe station could probe on these areas to measure electrical properties. The thermal coater is, first, pumped down to a pressure smaller than 10^{-6} and then the current passes through tungsten boat to heat the aluminum bullet and evaporate aluminum of about 3000 $\overset{o}{A}$ onto the TMO film at a deposition rate of about 8 $\overset{o}{A}$/s.

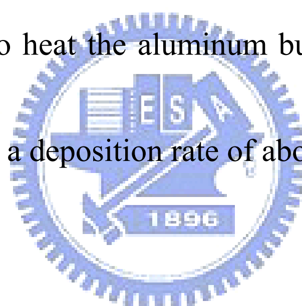

2.3 Physical characteristics

2.3.1 Scanning Electron Microscopy (SEM)

The film thickness is examined by scanning electron microscopy (SEM) using Hitachi model S4700I. The microstructures of thin films in the cross section are investigated by SEM. Besides, In order to know the relationship between the thickness of the films and solutions of different mole concentrations, we deposited different layers with mole concentrations varying from 0.05 mole/l to 0.5 mole/l.

2.3.2 X-Ray Diffraction Analysis

The film structure and the crystallization related to temperature is investigated by X-Ray diffraction. First, we use the solutions of 0.05 mole/l, 0.1 mole/l, 0.3 mole/l and 0.5 mole/l to deposit 1, 2 and 3 layers of the films. The samples are subsequently thermaly treated in a high temperature furnace and in a rapid thermal processing (RTA) furnace, respectively, with temperatures varying from 400 to 800 ^{o}C. Finally, these samples, were cut into about 0.5 x 0.5 cm^2, analyzed by a Rigaku Dmmax-B diffractometer with 0.02 degree beam divergence and operated at 30 KV x 20 mA with Cu $K\alpha$ radiation.

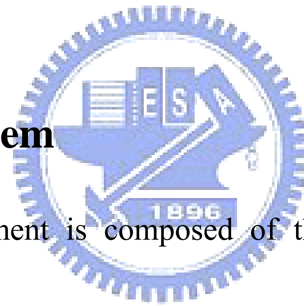

2.4 Measurement System

The system of measurement is composed of three parts, measurement machines, a personal computer, and Agilent VEE software. Measurement machines are made up of a probe station, one Agilent 4155C semiconductor parameter analyzer, one Agilent Agilent E5250A low leakage switch and one Agilent 81110A pulse generator. However, Agilent VEE software is used to control the measurement machines.

2.5 Electrical Measurement

In the RRAM, electrical properties can be divided into two parts, static and transient characteristics. The static one is measured by applying a static voltage with a rate of 0.5 V/s

sweeping from positive maximum to negative minimum and then scanning adversely. The waveform is shown in fig 2.5.0-1.

On the other hand, the transient property is measured by a sequence of steps interpreted in the following. First, a positive voltage whose magnitude is just a threshold voltage (will be explained in the next chapter) is applied on the sample with a short duration which can be adjusted by the Agilent VEE software and can vary from 1us to 0.99 s. The readout voltage is subsequently applied on the sample to extract the conductance state from the film.

Second, a negative voltage whose magnitude is also just a threshold voltage is applied on the sample for a short duration. After this step, the readout voltage is again applied on the sample to trace out another conductance state.

In conclusion, we, first, introduced how to sputter a LNO film involving sputtering system, preparation of target, and deposition of bottom electrode, and we also presented the fabrication of a transition metal oxide film sample, including how to make up solutions and the process of deposition of the sample. Furthermore, X-Ray and SEM are used to analyze the structure, crystallized properties, thickness and morphologies of the film. In the end, electrical analysis presented two kinds of states, that is, the static state and the transient state. The difference between these two states depends on what kind of wave form is applied.

Chapter 3

Results and Discussion

In this chapter, we show and discuss the results of X-Ray, SEM, electrical properties. First, the results of X-Ray related to different solutions are used to identify whether the structure of the films is correct or not. Furthermore, we investigate crystallization properties related to different temperatures. Second, the plane view of scanning electron microscopy (SEM) is employed to observe surface morphology and to measure the thickness of films with different solutions of mole concentration. Finally, we show the electrical characteristic of the film with different parameters of solution, thickness of film, RTA temperature, and furnace temperature and further discuss their relation.

3.1 X-Ray Results

3.1.1 Different Solution

As we mentioned in section 1.3, in the binary System, some transition metal oxides including TiO_2, ZrO_2, Nb_2O_5, NiO_2 and SiO etc. had been found to exhibit bistable phenomenon so that we use the different kinds of solutes, containing Zirkon (IV) propylate, propoxide, Nickel (II) acetate tetrahydrate and titanium (IV) ethoxide [Ti(OCH5)4], to make different types of solutions but the process of the solutions is the same as mentioned in section

2.2.2.

First of all, Fig. 3.1.1-1 ~ Fig. 3.1.1-6 show X-Ray diffraction patterns versus 2-theta of the samples made up with titanium (IV) ethoxide [Ti(OCH5)4] solvent. Here, all the samples are divided into two parts, Fig. 3.1.1-1, 3.1.1-3 and 3.1.1-5 and Fig. 3.1.1-2, 3.1.1-4 and 3.1.1-6, respectively by two rapid thermal annealing at temperatures of 500 and 700 ^{o}C. Fig. 3.1.1-1 and 3.1.1-2 present the X-Ray patterns of the samples which are fabricated with the solution of 0.05 mole concentration and Fig. 3.1.1-3 ~ Fig. 3.1.1-4 present the X-Ray diffraction patterns of the samples that are fabricated with the solution of 0.1 mole concentration. Finally, The Fig. 3.1.1-5 and Fig. 3.1.1-6, show the X-Ray pattern of the samples which are fabricated with the solution of 0.5 mole concentration. In these figures, the peaks at 2-theta are at about 23, 33 and 48 degrees are the diffraction pattern of LNO (100), Si (100) and LNO (200) planes, respectively, but there are no peaks of Ti oxide.

Next, Fig. 3.1.1-7 shows the X-Ray diffraction pattern of the samples using a solution with different mole concentrations and with the solvent of Zirkon (IV) propylate, propoxide, after rapid thermal annealing at temperature 700 ^{o}C. In this figure, the sample with 0.5 mole concentration solution has a weak peak at 2-theta of about 31 degree but there are no peaks for the samples with 0.05 and 0.1 mole concentration solutions. This result reveals that the film of the samples is ZrO_2 (111) plane but the samples with 0.05 and 0.1 mole concentration solutions are too thin to have the peak. We further present the relation between thickness and

mole concentration of the solution. Fig. 3.1.1-8 shows the thickness (measured by SEM and will show and discuss in the next section) versus the different mole concentrations of the solutions. Moreover, the weak peaks in Fig. 3.1.1-7 exhibits that the film is not crystallized well.

3.1.2 The Properties of Crystallization

In order to find out the properties of crystallization of the zircon oxide film with different temperatures of thermal treatment, we utilize different temperatures of a RTA furnace and a high temperature furnace to crystallize the film. Fig. 3.1.1-9 ~ Fig. 3.1.1-12 show X-Ray diffraction patterns with different RTA temperatures, 500, 600, 700 and 800 ^{o}C, of the 0.5 mole concentration solution. The peak of the X-Ray diffraction is too weak to observe but in these diagrams it is apparent that the higher the temperature of the thermal treatment is, the more crystallized the film is.

3.2 Morphology and Thickness of the ZrO_2 Film

In this section, the plane view of SEM is employed not only to study the properties of crystallization, directly and to compare with the X-Ray diffraction pattern mentioned in the above section, but also to observe the morphology of the ZrO_2 films. Besides, the cross section picture of SEM is used to measure the thickness of the films deposited by different solutions of mole concentrations.

Fig. 3.2-1 ~ Fig. 3.2-4 show the plane view of SEM of samples with temperatures of thermal treatment varied from 400 ^{o}C to 700 ^{o}C, respectively. First, there is no apparent grain in Fig. 3.2-1 and Fig. 3.2-2, implying that the crystallization of the film at temperature 400 ^{o}C and 500 ^{o}C is not complete but in Fig. 3.2-3 and Fig. 3.2-4 where the samples after thermal treatment at temperature 600 ^{o}C and 700 ^{o}C, the grain formation is more evident. To compare with X-Ray diffraction pattern, Fig. 3.2-5 and Fig. 3.2-6, we can further ascertain the properties of crystallization of ZrO_2 film made up by sol-gel method.

In the cross section view of SEM, as shown in Fig. 3.2-7 ~ Fig. 3.2-9, We deposited five, five and four layers of samples with respective solutions of 0.05, 0.1 and 0.5 mole concentration to get the average value of the thickness of the ZrO_2 film. Using this result, the figure 3.1.1-7 shows the relation between the thickness of the film and the solution of the mole concentration.

3.3 Electrical properties

3.3.1 Static Properties of ZrO_2 Film

The electrical property of static state is measured by a voltage of double sweeps from the magnitude of the maximum to the minimum at a rate of 0.5 V/s. The sample, first, was fabricated by the thermal coater with the metal mask to define the active region.

Fig. 3.3.1-1 shows an I-V curve of a ZrO_2 film with thickness of 82 nm at the double

sweeping of the first time. When the sweeping voltage had decreased to the negative threshold voltage, about -25 Volts in this sample, the magnitude of current density switched to a higher one.

In the opposite, when the sweeping voltage has increased to the positive threshold, the magnitude of current density switch to original state, low current density state. This bistable switching current density phenomenon is similar to that of Cr doped $SrTiO_3$ film. Fig. 3.1.1-2 shows the I-V curve of ZrO_2 film after 5 times' sweeping. The same, sample can change the current density with ratio of 1~2 orders by applying voltage up to threshold voltage, but it sometimes occurs that the curve at the maximal voltage is not closed. Moreover, the curve in the region of the positive voltage is more unstable than that in the opposed region. As shown in figure 3.3.1-1 or 3.3.1-2, the curve is not smooth in the region of the positive voltage so that the measurement of electrical properties is often in the region of the negative voltage.

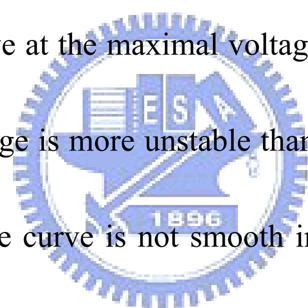

3.3.2 Dynamic Properties of ZrO_2 Film

The device is first formed by forming process that applies a pulse voltage with magnitude of threshold voltage causing the device in the low current density state. A sequence of voltage pulse, write-read-erase-read, with a proper pulse width and a designated cycle delay between the write and erase pulse voltage are employed to extract the dynamic properties from the ZrO_2 film.

Fig. 3.3.2-1 shows the dynamic properties of the ZrO_2 film with thickness of 30 nm measured by pulse voltage with pulse width of 0.5 s, pulse magnitude of 15 volts, readout voltage of -1 volt and cycle delay 1 sec. Different pulse widths have also been tested on the film with thickness of 30 nm, but the bistable switching phenomenon did not occur (the ratio of two states was less than 5 times). Besides, in the samples with thickness of about 30 nm, the fatigue property is often the pulse number of 10, and the maximum value of that is always less than pulse number of 20 with the 1 order ratio of two states.

Fig. 3.3.2-2 presents the dynamic properties of the ZrO_2 film with thickness of 45 nm. In the sample of 45 nm, the magnitude of pulse voltage is up to 15 volts that equaled to its threshold voltage of static property and the pulse width is also 0.5s. Fatigue for thickness of about 45 nm is often pulse number of 30.

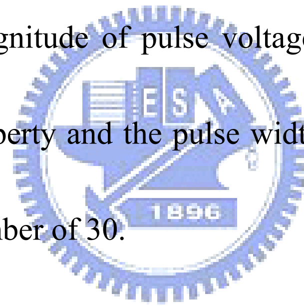

3.3.3 Effect of Doping

First, we doped the different kinds of transition metals to be an impurity into ZrO_2. As we had mentioned, in section 1.4.4 states modulation, the fact that if a voltage is applied on the Cr doped $SrTiO_3$, one mechanism assumes that Cr may act as an impurity and could release electrons leading to current conduction in the oxide. When an applied voltage up to threshold voltage, the valence of Cr could be transformed from initial type to another type causing free carriers in the film increasing or decreasing and thus resistivity is varied.

Transition metals, molybdenum, chromium, and vanadium were doped into ZrO_2 film. Fig. 3.3.3-1 ~ Fig. 3.3.3-4 show the I-V curve of the first time of a double sweeping (i.e. voltage sweep from positive maximal voltage to negative min voltage and sweep again with reverse process) on the non-dpoed, V, Cr and Mo doped ZrO_2 films of one layer deposited by solutions of 0.1 mole concentration. There are not only forming phenomena in the impurities doped films but also in the non-doped one. Fig. 3.3.3-5 ~ Fig. 3.3.3-8 show the I-V curves of the 5th time of the double sweeping on the films and the results are not stable; that is, the bistable switching phenomenon is observed in some samples but not in others.

Indeed, there is the bistable switching phenomenon in the ZrO_2 film and it does not need doping impurity into the film.

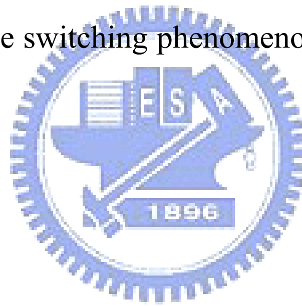

3.3.4 Effect of Thickness

The effect of thickness related to the I-V characteristic is studied on the samples fabricated by Sol-Gel method with solutions of 0.05, 0.1, 0.3 and 0.5 mole concentration.

Fig. 3.3.4-1~3.3.4-4 and Fig. 3.3.4-5~3.3.4-8 show the I-V curve of variant thickness, 20 nm, 30 nm, 45 nm and 82 nm, of ZrO_2 film correspond to first and the 5th sweeping time, respectively. It is apparent that the forming voltage increases as the thickness of ZrO_2 film increases. Besides, before and after the forming process, the current order of the high states of the samples respecting to different thickness is quite near. Fig. 3.3.4-9 and Fig. 3.3.4-10

exhibit the diagram of the order of current density at sweeping voltage of -1 volt versus variant thickness of the film at the 1st and the 5th sweeping time, respectively.

The magnitude of the high state current density is quite near and the thickness of the film do not affect the high state current suggesting that the bistable switching phenomenon in the ZrO_2 film may be due to the formation of the filament.

3.3.5 Electrical Characteristic of the Crystallized Type

There is bistable resistivity switching phenomenon in OUM device, having been mentioned before, that utilizes phase transition from two types, the crystallized and the amorphous type to produce resistivity switching.

In our experiments, the sample was first fabricated by Sol-Gel method with a solution of 0.5 mole concentration. Then, the sample was baked in the furnace at two temperatures. First, the sample was at the temperature of 200 ^{o}C. After 10 min, temperature was raised to 600 ^{o}C and the duration of thermal treatment at this temperature is 30 min.

The Fig. 3.3.5-1 and 3.3.5-2 show the I-V curve of the sample at the 1st and 5th sweeping time. The Fig. 3.3.5-3 is the X-Ray diffraction pattern of the film. bistable phenomenon occurs in the sample with temperature of thermal treatment up to 700 ^{o}C. At this temperature, the film had been crystallized, but bistable switching property still exists. This result suggests that the bistable states in the ZrO_2 film may not result from the phase transition

between two types.

3.3.6 Retention of ZrO_2 Film

Retention test was performed by applying a 0.5 s pulse voltage with magnitude of ± 30 volts to induce the high and low current state. Then the stress voltage of 1 volt was applied on the sample fabricated by Sol-Gel method with a solution of 0.5 mole concentration and the variation of leakage current versus time was measured. As shown in Fig. 3.3.6-1, the high current density shows a large drop after 60 seconds and then after about 1.8 hr, the high current density state drops down to another level about 0.05 A/cm^2. Fig. 3.3.6-2 shows the ratio between high and low current density state. The high current density state with about 8 times the low current density state did not show many changes after 8 hours' stress. In addition, voltage stress of -1 volt on the sample with low current density state shows a more stable status with respect to a high current density state. After 8 hr, the sample had not apparently changed, it was still in the original state.

3.3.7 Temperature Effect on The High Current Density State

In this experiment, aluminum (Al) was used as top electrode whose thickness was ~3000 $\overset{o}{A}$ deposited by thermal coater at a deposition rate of 8 $\overset{o}{A}$ and the metal was used to define device area of ~$9.615X10^{-4}$ cm^2.

After the top electrode had been deposited, the device was double swept with magnitude of ± 30 volts once, causing forming process to occur. Then, the sample was transformed into high current state by applying a voltage double sweep from 0 to -30 volts. The current was extracted by a readout voltage of -1 volt before thermal treatment in a furnace. The sample further was put into the furnace at temperature 100, 150 and 180 ^{o}C with duration 1 hr, respectively. After the sample was baked in the furnace, the current was again measured by the readout voltage of -1 volt.

Fig. 3.3.7 shows the normalized high state current versus temperature. The vertical coordinate of the figure is the high state current after thermal treatment divided by that before thermal treatment. The high state current was reduced to less than that before thermal treatment at the temperature of 180 degrees. The high state current still did not hold the original magnitude after thermal treatment of 150 ^{o}C but it remained unchanged for thermal treatment temperature of 100 ^{o}C.

3.3.8 Current fitting

Using the 0.1 M solution to deposit two layers ZrO_2 film on LNO substrate is employed to analysis process of current transport. The static I-V curve is show in fig. 3.3.8-1, where the curve is separated to fore portions. Fig. 3.3.8-2 ~ 3.3.8-5, Fig. 3.3.8-6 ~ 3.3.8-9, Fig. 3.3.8-10 ~ 3.3.8-13 and Fig. 3.3.8-14 ~ 3.3.8-17 show the current fitting of curve (a), (b), (c) and (d),

respectively. In fig. 3.3.8-1, I-V curve, the symmetry current density at positive bias region and negative region reveals the conduction process is dominated by the ZrO_2 film so conduction process of Schottky emission, space charge limited can be excluded. Indeed, the current conduction process at high and low state region may be due to Frenkel Pool emission.

Chapter 4

Conclusion

First, resistance switching of Sol-Gel derived ZrO_2 has been successfully demonstrated. The X-Ray diffraction confirms that the formation material is ZrO_2 film although the peak is very weak due to the fact that the crystallization is not good. Moreover, the thickness is related to different solutions of mole concentrations that have been measured with the cross section of SEM. The I-V curves in various kinds of impurities-doped ZrO_2 films do not have significant difference in resistivity switching phenomenon of the film providing a simpler process to fabricate ZrO_2 film with the states of modulation that may be excluded.

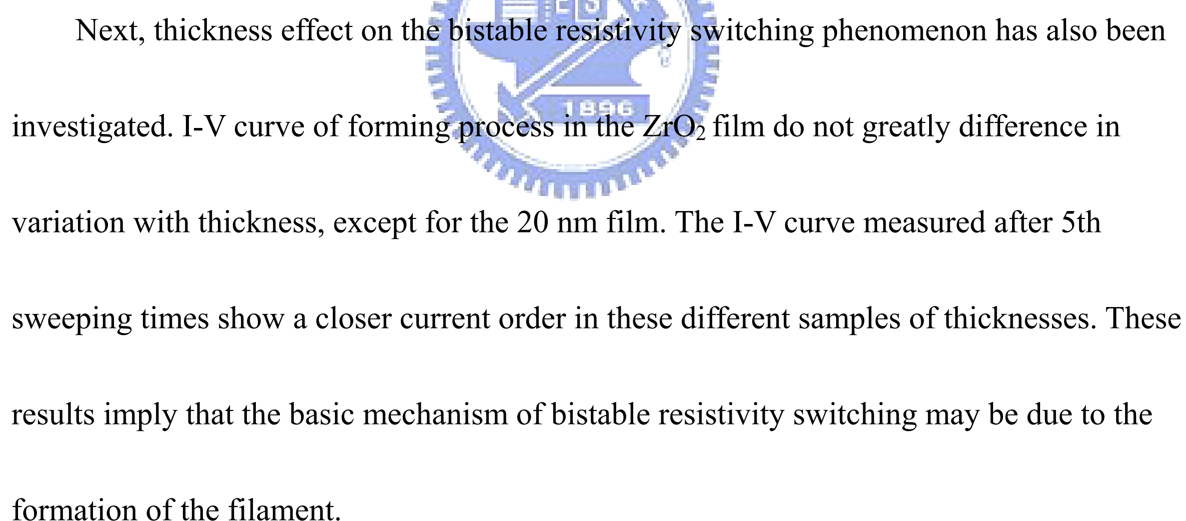

Next, thickness effect on the bistable resistivity switching phenomenon has also been investigated. I-V curve of forming process in the ZrO_2 film do not greatly difference in variation with thickness, except for the 20 nm film. The I-V curve measured after 5th sweeping times show a closer current order in these different samples of thicknesses. These results imply that the basic mechanism of bistable resistivity switching may be due to the formation of the filament.

Finally, reliability including temperature effect and retention is also examined. The result of temperature effect shows that the high current state in the ZrO_2 film is not degraded at a temperature up to 100 ^{o}C. Besides, the retention test present on ZrO_2 film reveals a near 8 times difference between high and low current density states after 8 hr stress.

Process	Voltage and Temperature Dependence
Schottky emission	$\sim T^2 \exp(+a\sqrt{V}/T - q\phi_B/kT)$
Frenkel-Poole emission	$\sim V \exp(+2a\sqrt{V}/T - q\phi_B/kT)$
Tunnel or field emission	$\sim V^2 \exp(-b/V)$
Space-charge limited	$\sim V^2$
Ohmic	$\sim V\exp(-c/T)$
Ionic conduction	$\sim \frac{V}{T}\exp(-d'/T)$

Table 1-1 Conduction Processes in Insulators

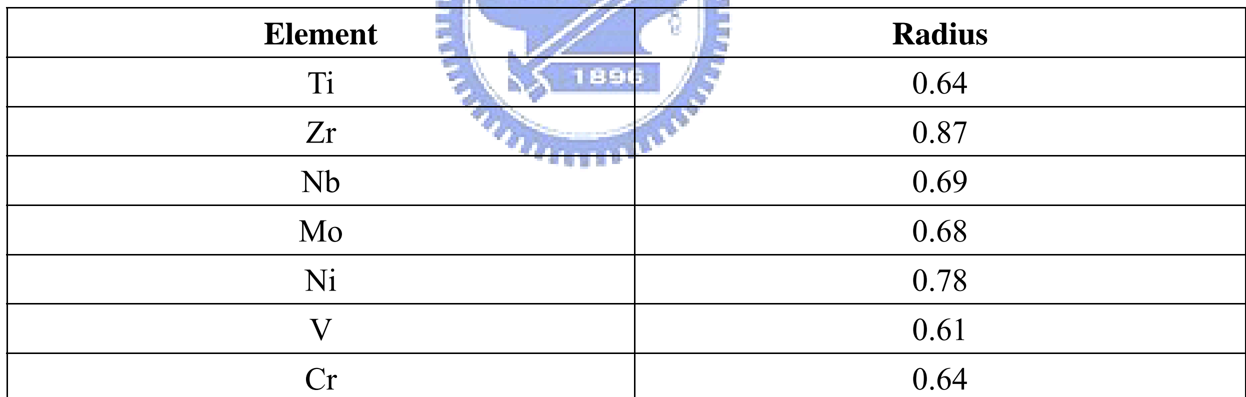

Element	**Radius**
Ti	0.64
Zr	0.87
Nb	0.69
Mo	0.68
Ni	0.78
V	0.61
Cr	0.64

Table 2-1 Radius of Element

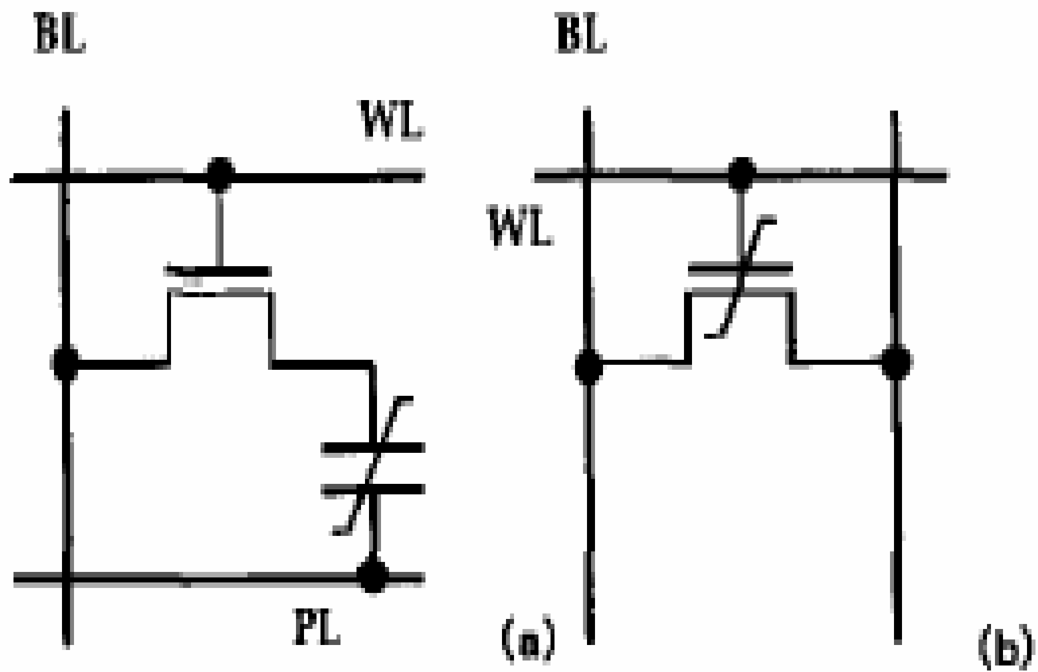

Fig. 1.2.1-1 Equivalent circuit of capacitor-type FeRAM (a) and FET-type FeRAM [2]

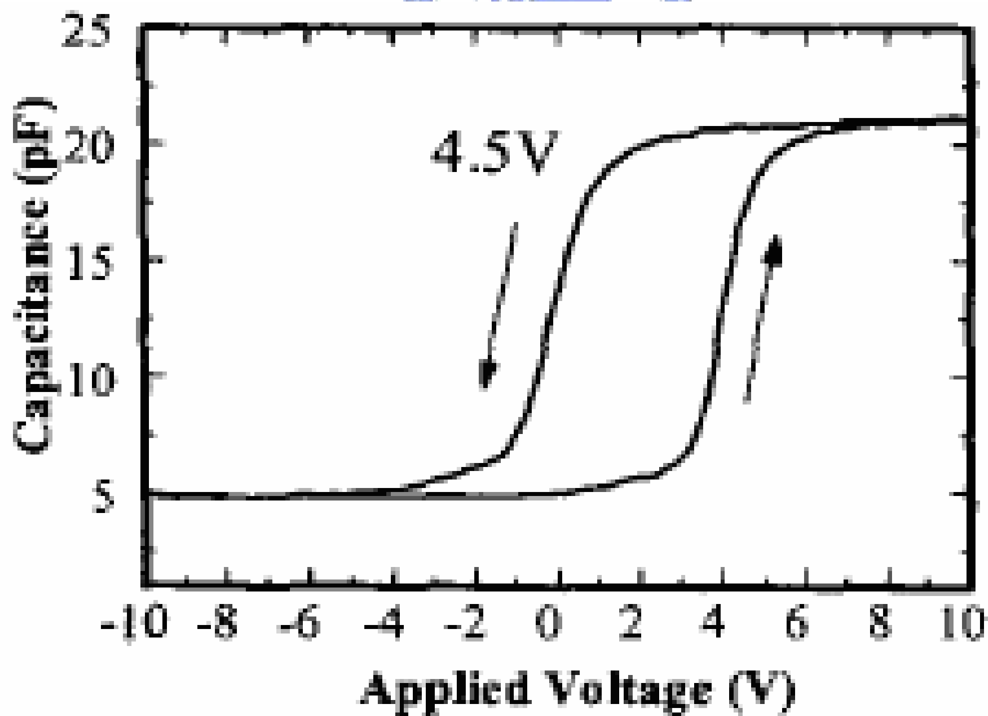

Fig. 1.2.1-2 C-V characteristic of a ferroelectric device [2]

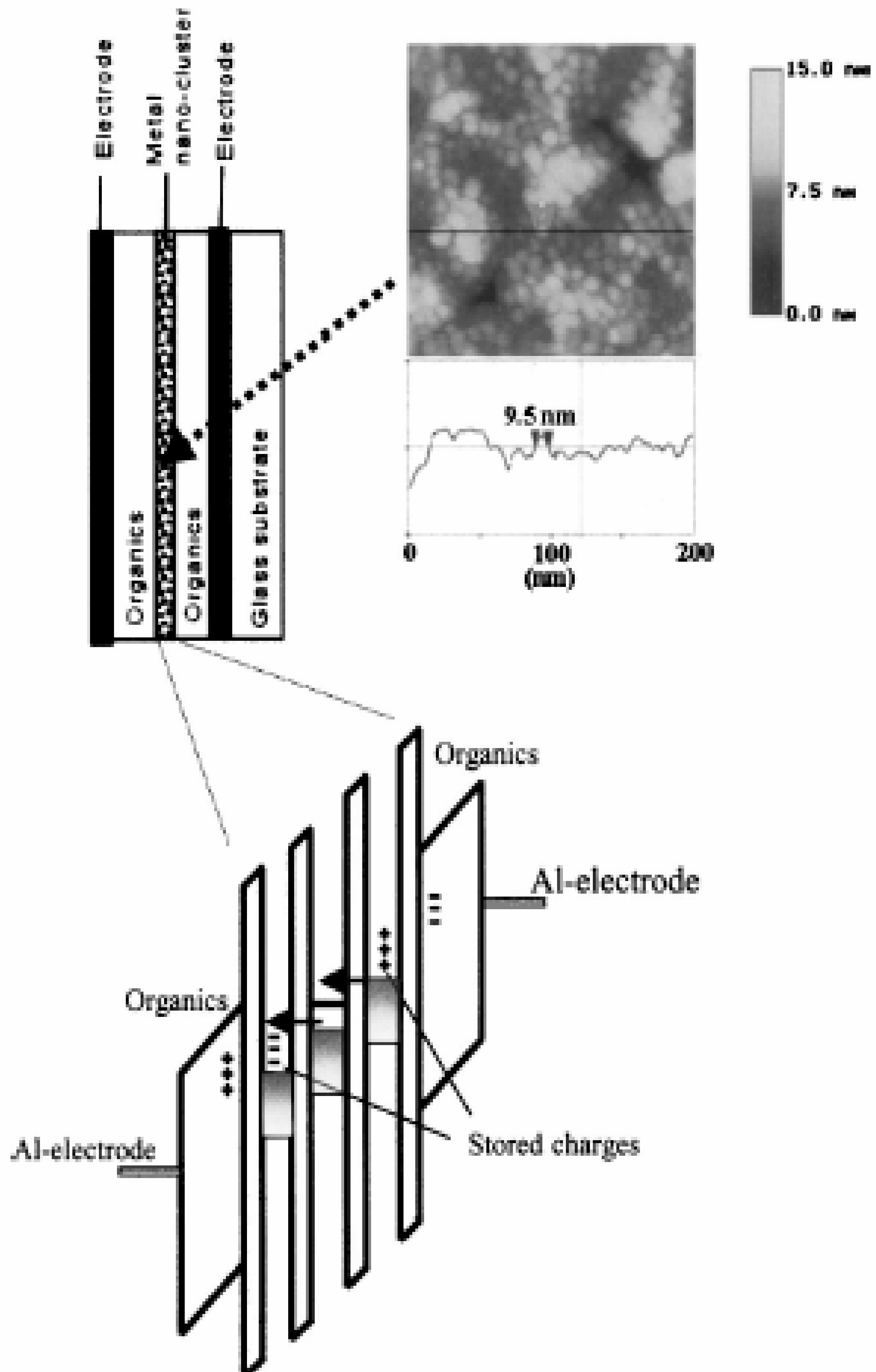

Fig. 1.2.3-1 The structure of the OBD device and its equivalent circuit [4]

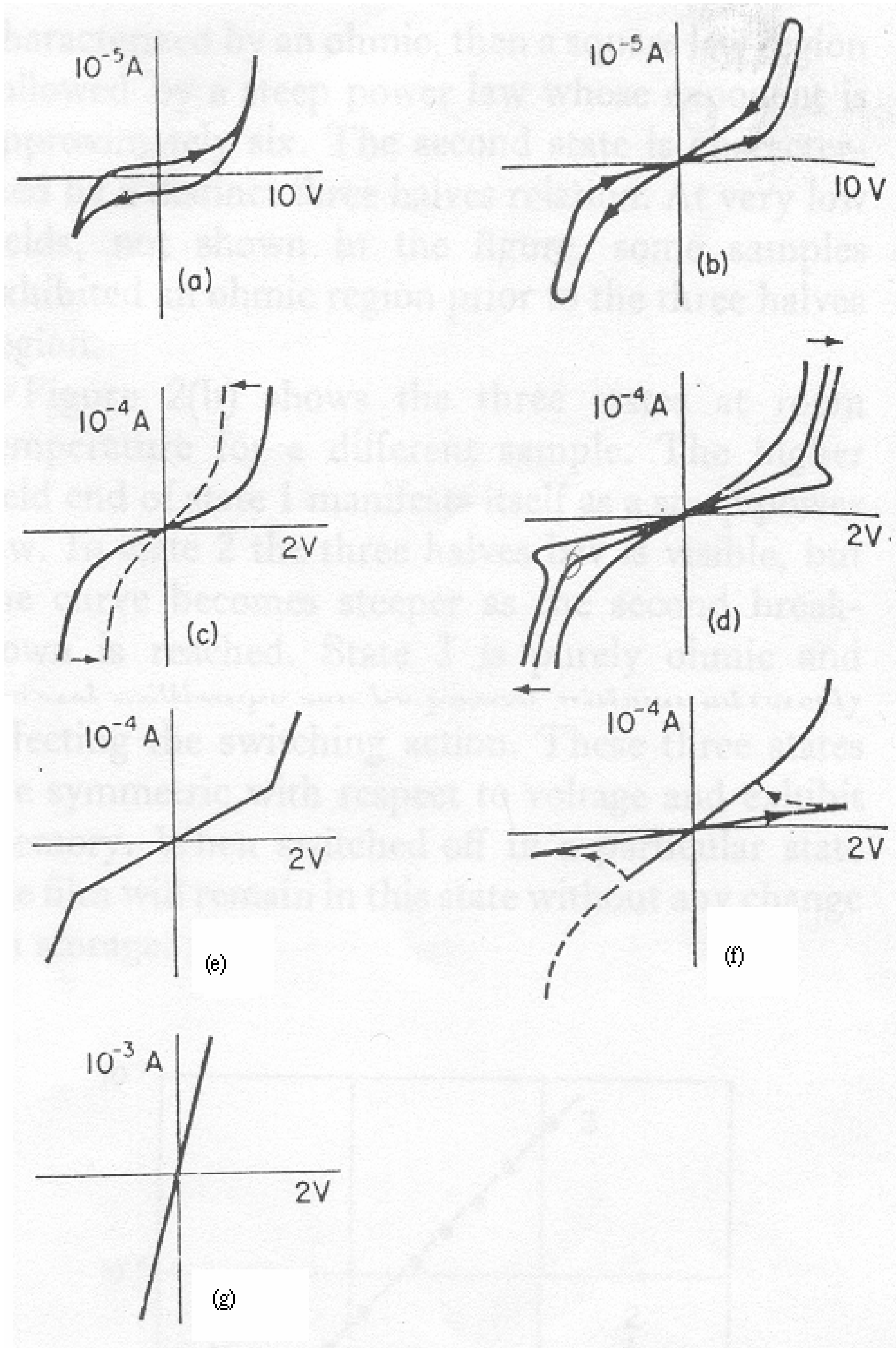

Fig. 1.3.1-1 Switching cycle and current voltage behavior of a titanium dioxide film[5]

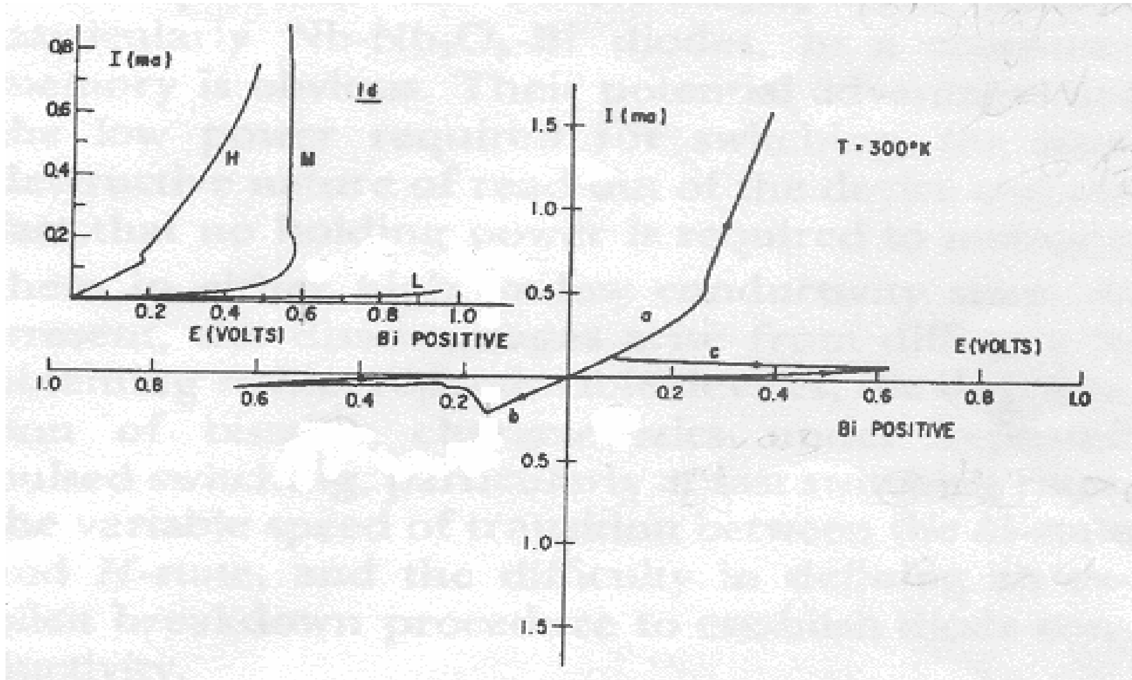

Fig. 1.3.3-1 Switching phenomenon in nickel oxide [6]

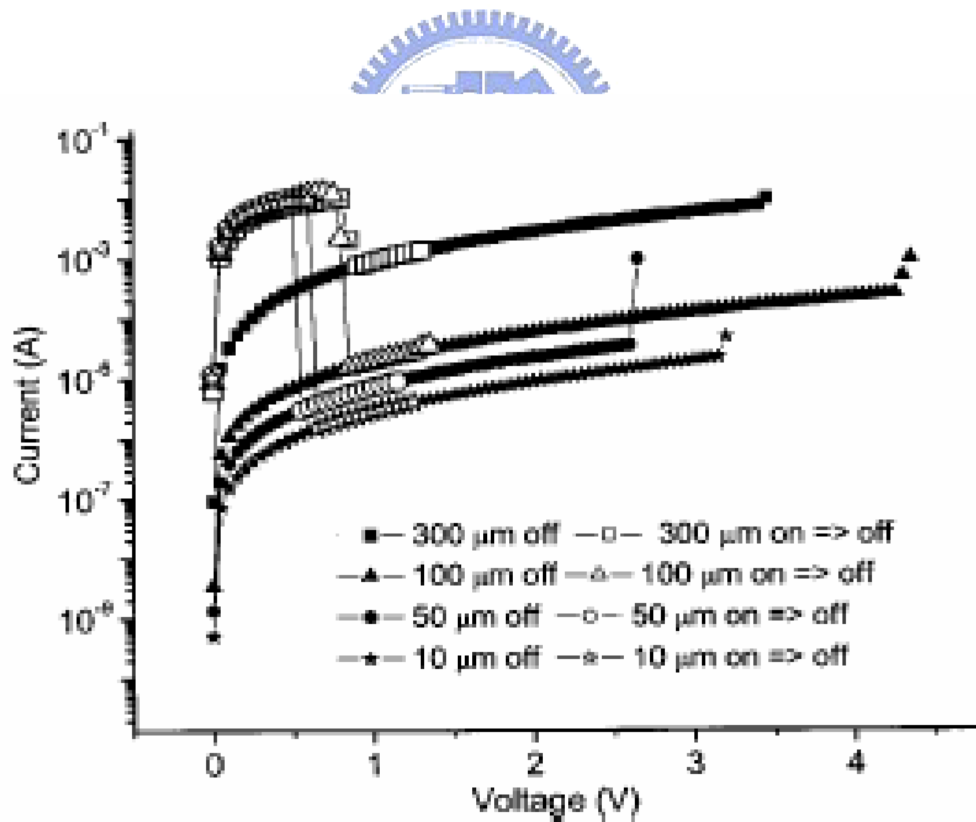

Fig. 1.3.2-1 Switching phenomenon in nickel oxide [7]

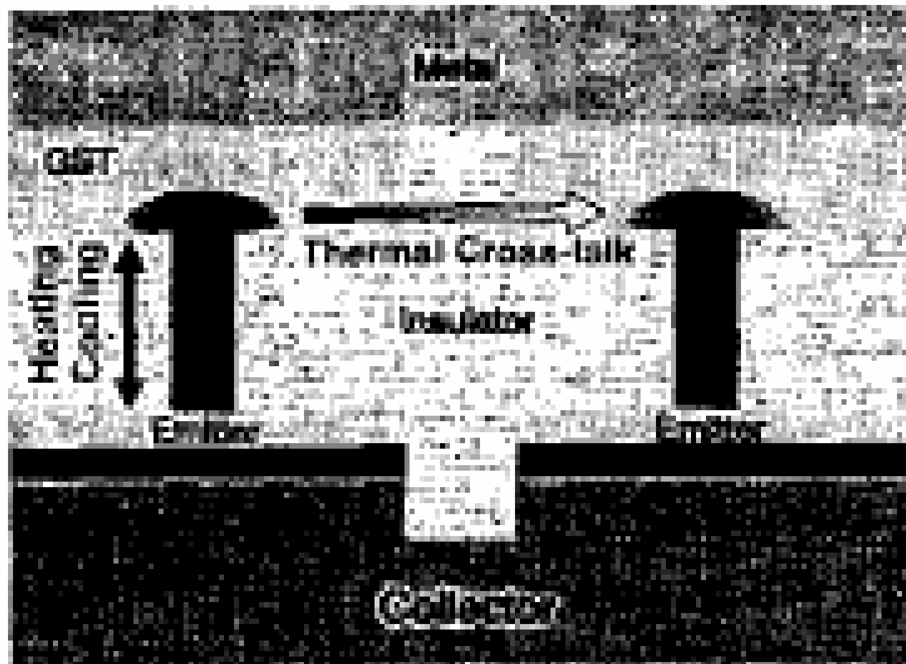

Fig. 1.4.2-1 the structure of OUM device[14]

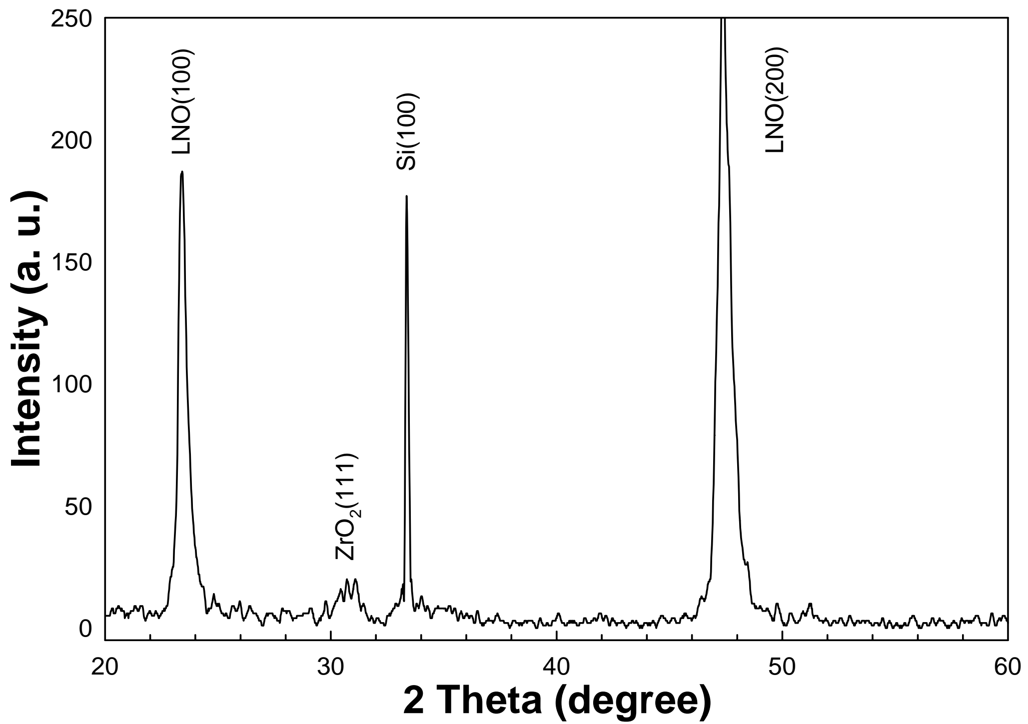

Fig. 3.1.1-1 X-Ray diffraction patterns of the sample with the solution of 0.05 M/L at temperature 500 ℃

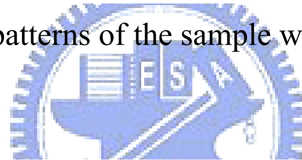

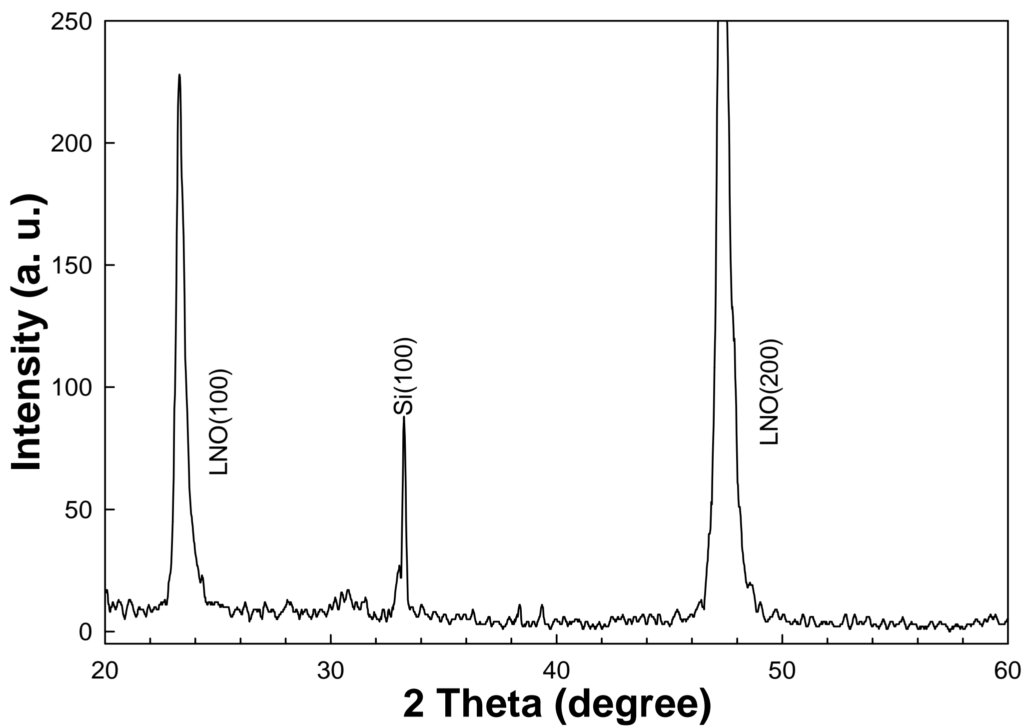

Fig. 3.1.1-2 X-Ray diffraction patterns of the sample with the solution of 0.05 M/L at temperature 700 ℃

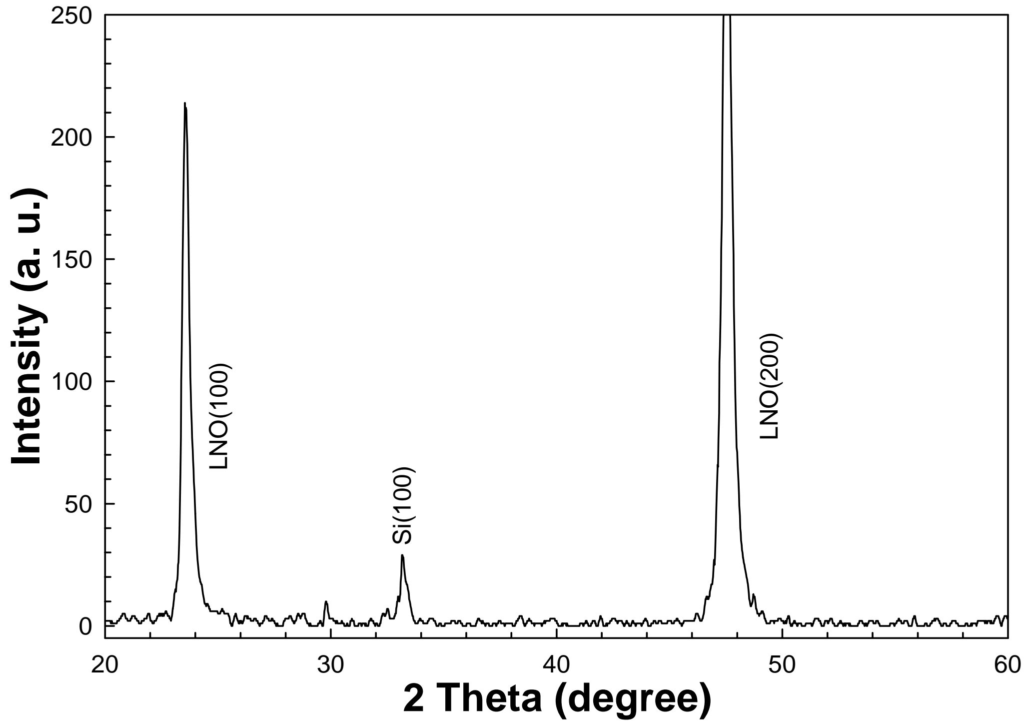

Fig. 3.1.1-3 X-Ray diffraction patterns of the sample with the solution of 0.1 M/L at temperature 500 ℃

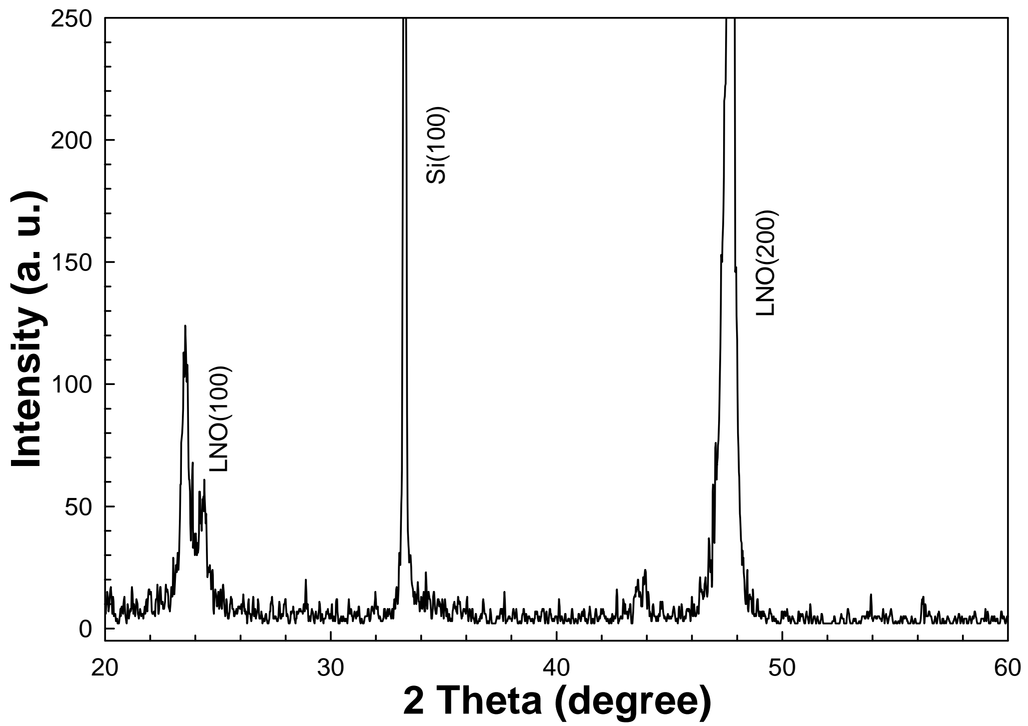

Fig. 3.1.1-4 X-Ray diffraction patterns of the sample with the solution of 0.1 M/L at temperature 700 ℃

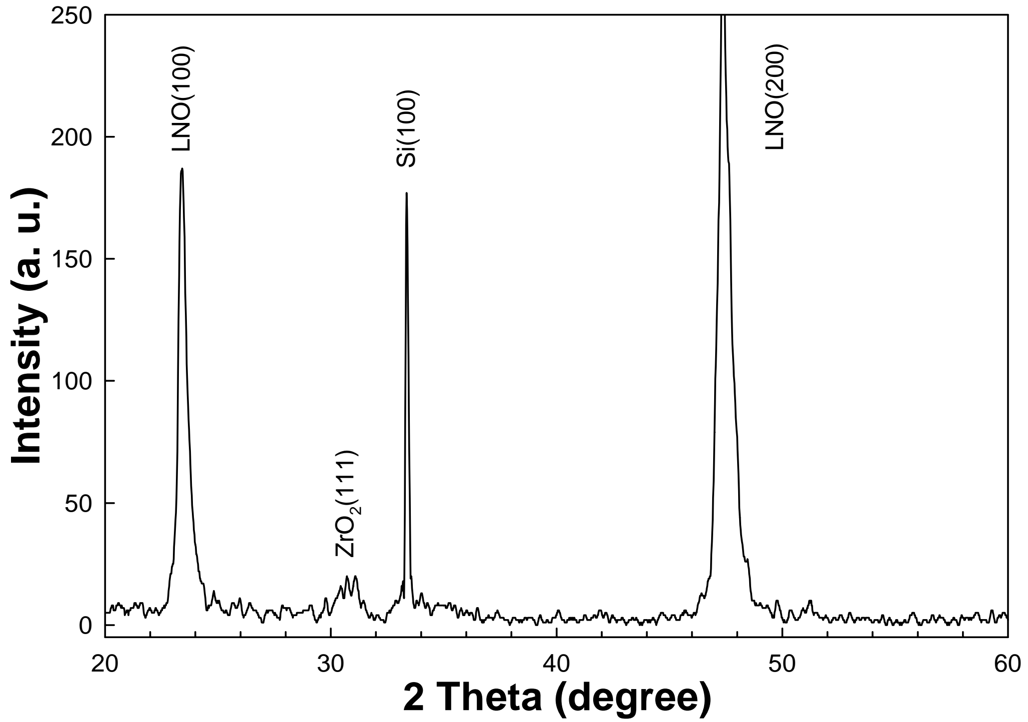

Fig. 3.1.1-5 X-Ray diffraction patterns of the sample with the solution of 0.5 M/L at temperature 500 ℃

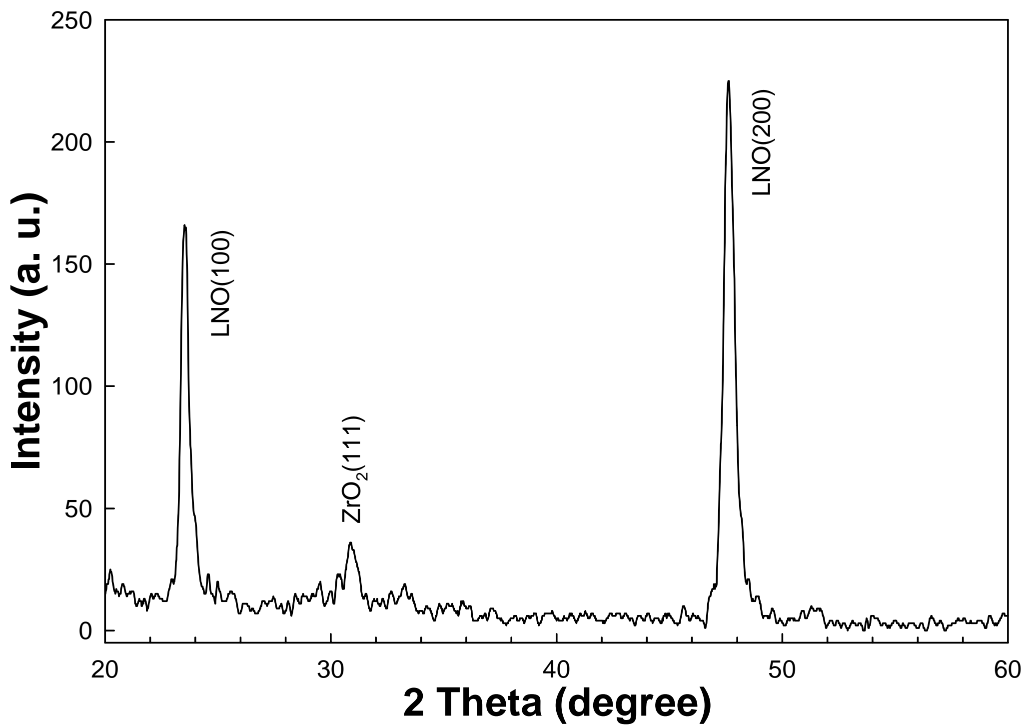

Fig. 3.1.1-6 X-Ray diffraction patterns of the sample with the solution of 0.5 M/L at temperature 700 ℃

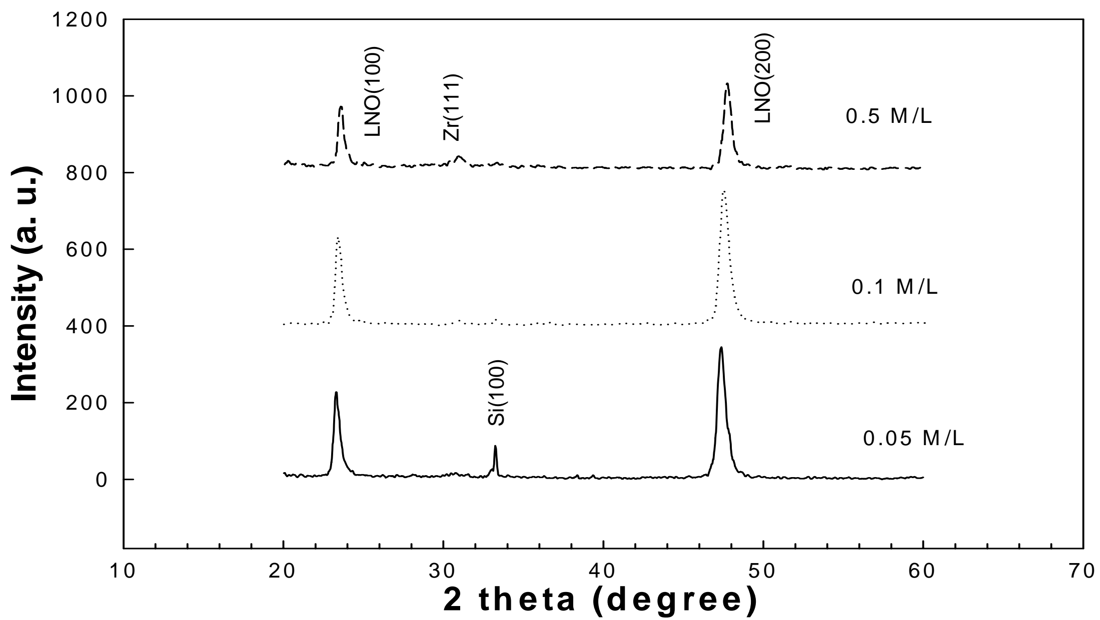

Fig. 3.1.1-7 X-Ray diffraction patterns of ZrO_2 film with solution of different mole concentration

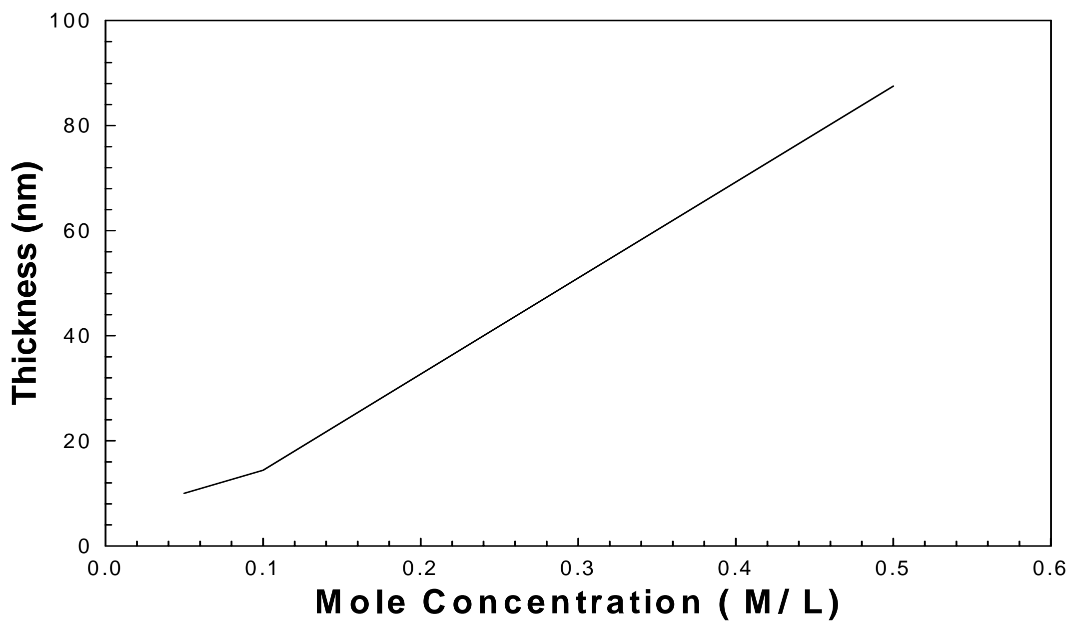

Fig. 3.1.1-7 The relation between thickness of the film and mole concentration of the solution

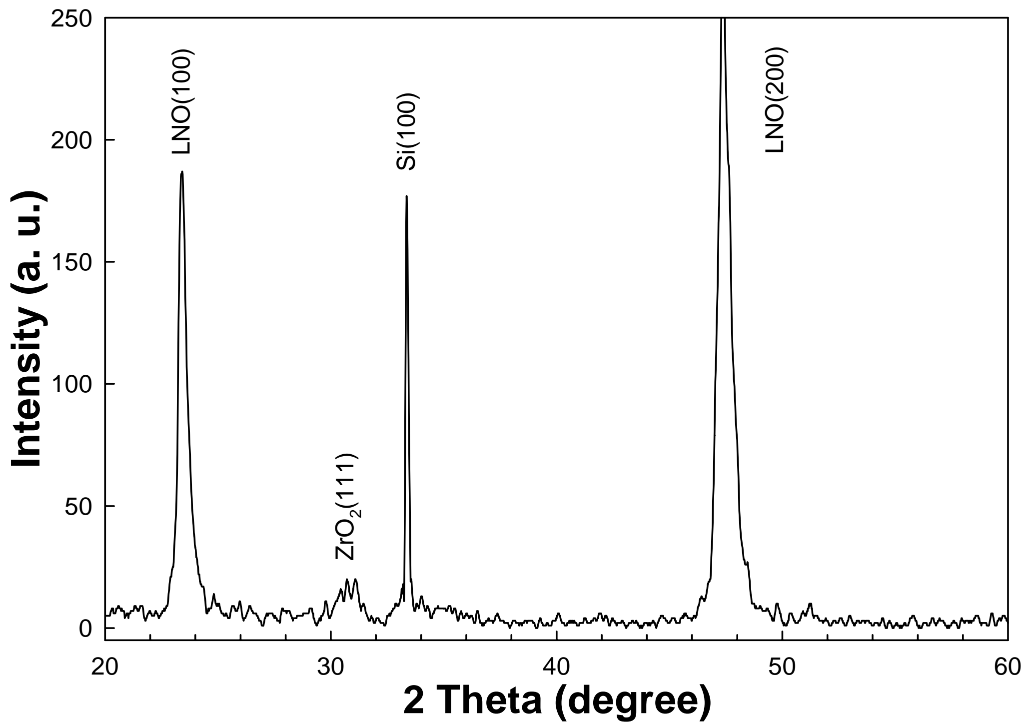

Fig. 3.1.1-9 X-Ray diffraction patterns of the sample with the solution of 0.5 M/L at temperature 500 ℃

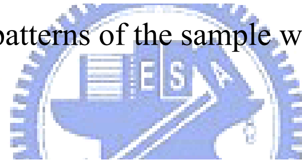
E S A

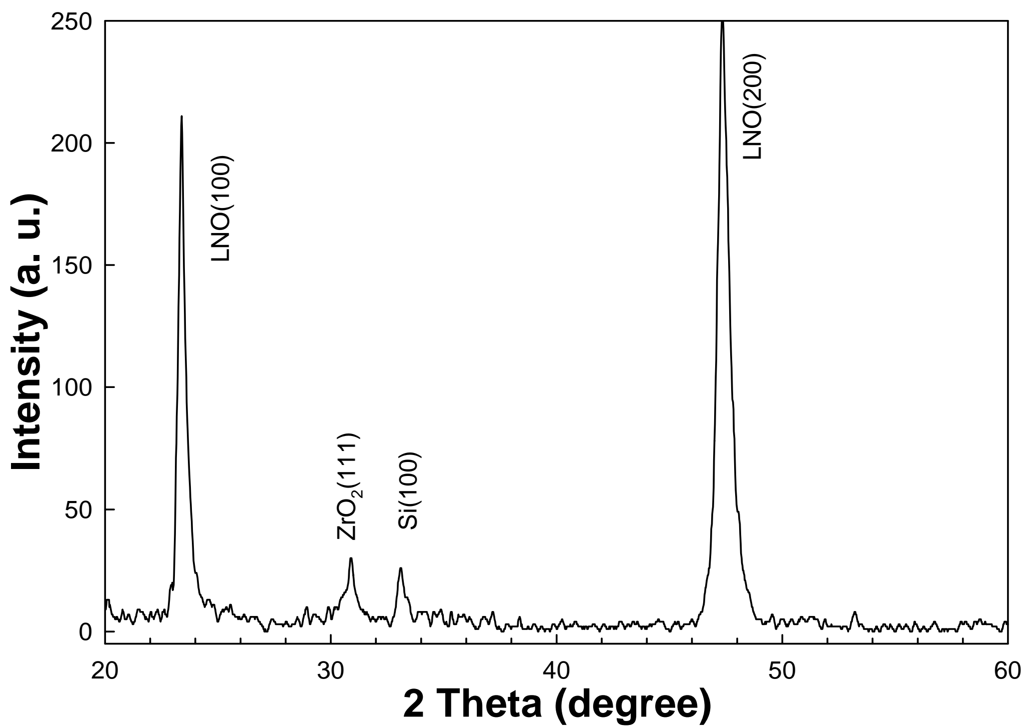

Fig. 3.1.1-10 X-Ray diffraction patterns of the sample with the solution of 0.5 M/L at temperature 600 ℃

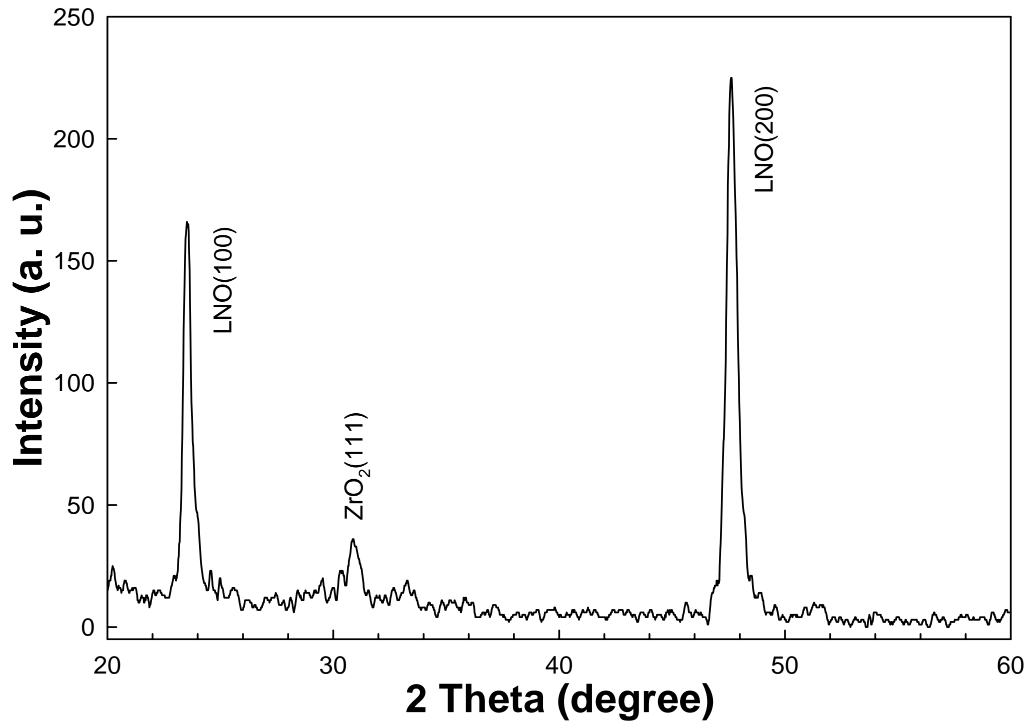

Fig. 3.1.1-11 X-Ray diffraction patterns of the sample with the solution of 0.5 M/L at temperature 700 ℃

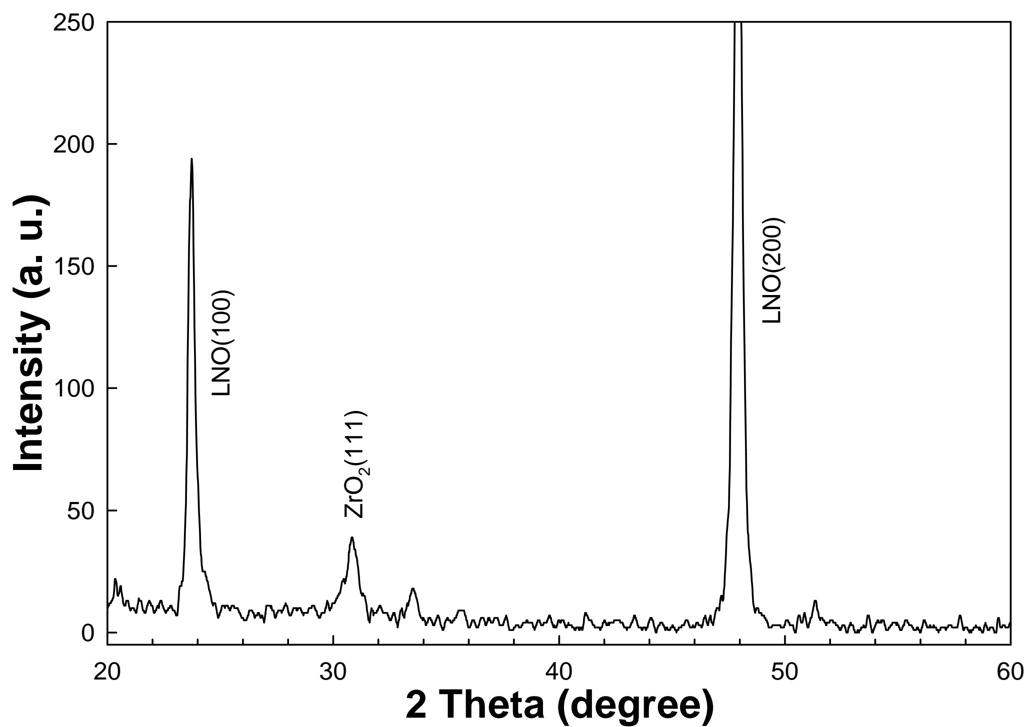

Fig. 3.1.1-12 X-Ray diffraction patterns of the sample with the solution of 0.5 M/L at temperature 800 ℃

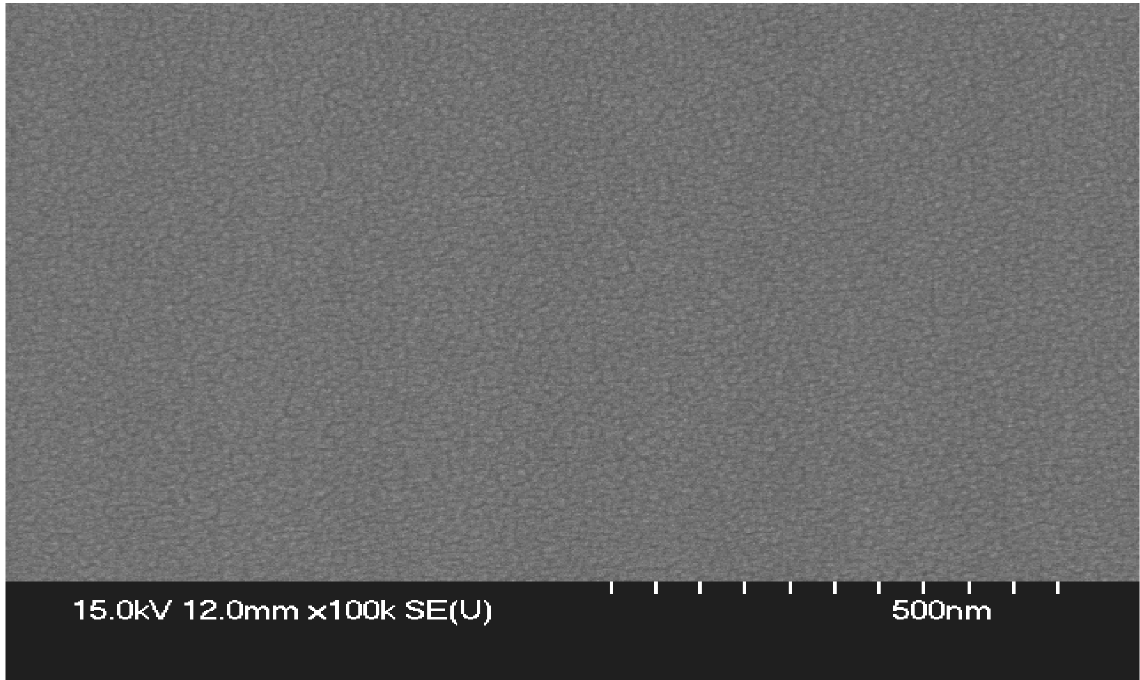

Fig. 3.2-1 Plane view of SEM with sample fabricated by using the solution of 0.3 mole concentration

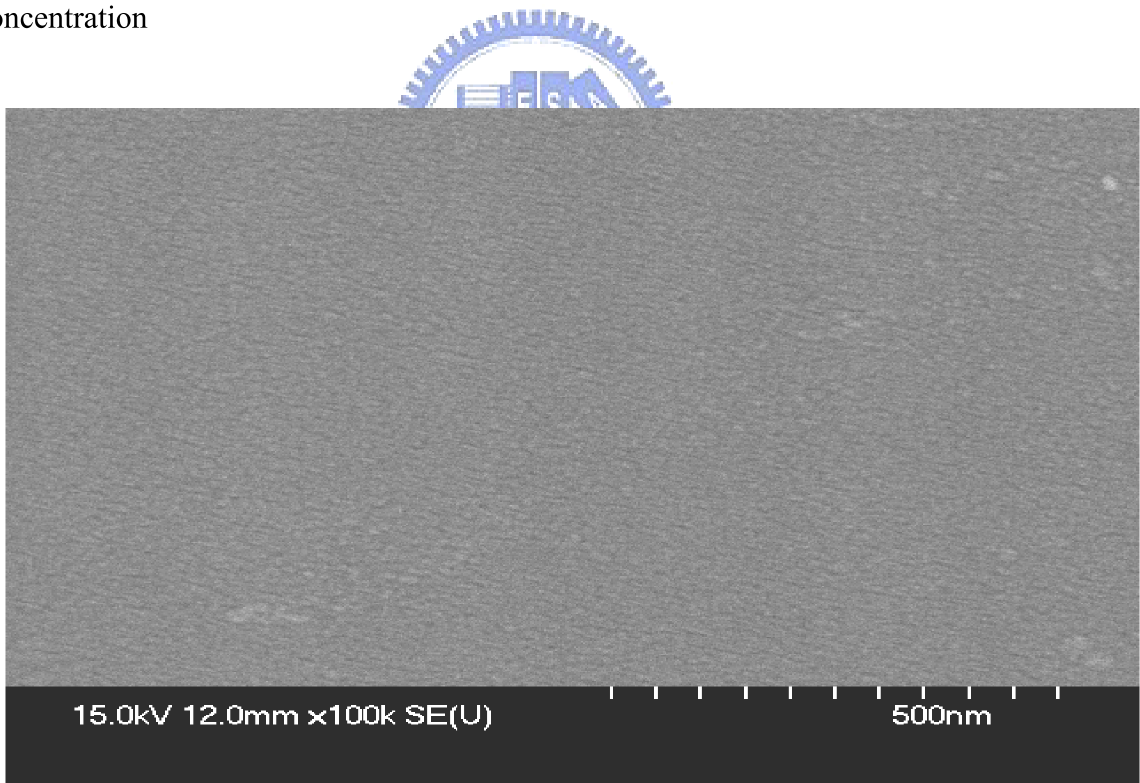

Fig. 3.2-2 Plane view of SEM with sample fabricated by using the solution of 0.3 mole concentration and thermal treatment at temperature 500 ℃

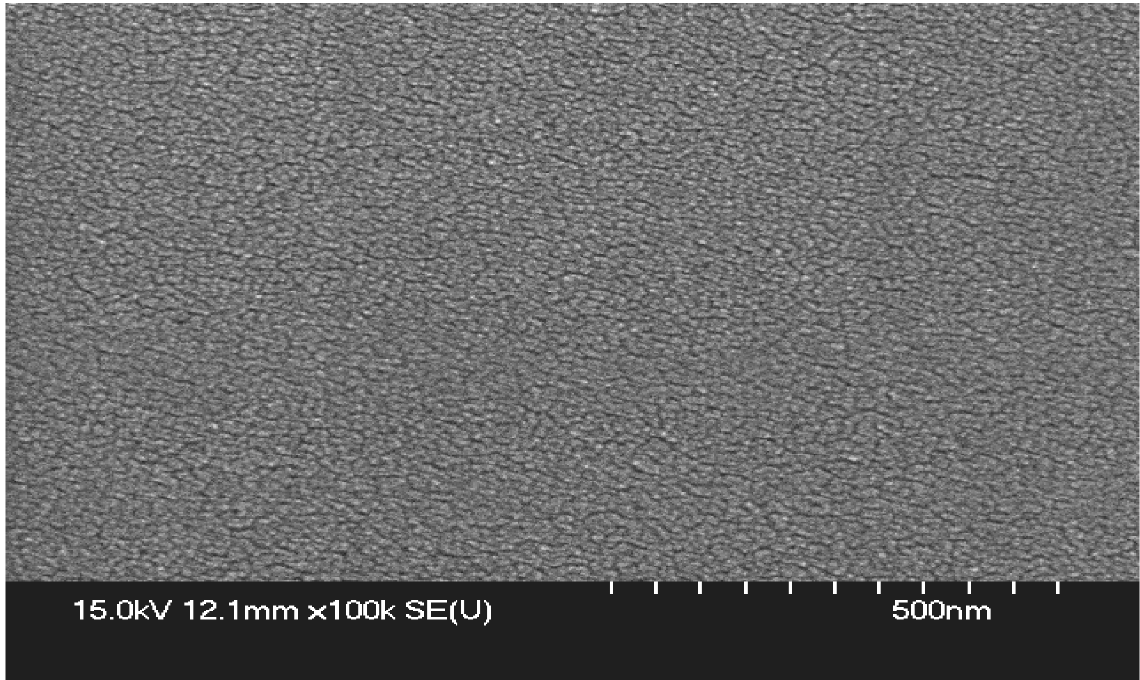

Fig. 3.2-3 Plane view of SEM with sample fabricated by using the solution of 0.3 mole concentration and thermal treatment at temperature 600 ℃

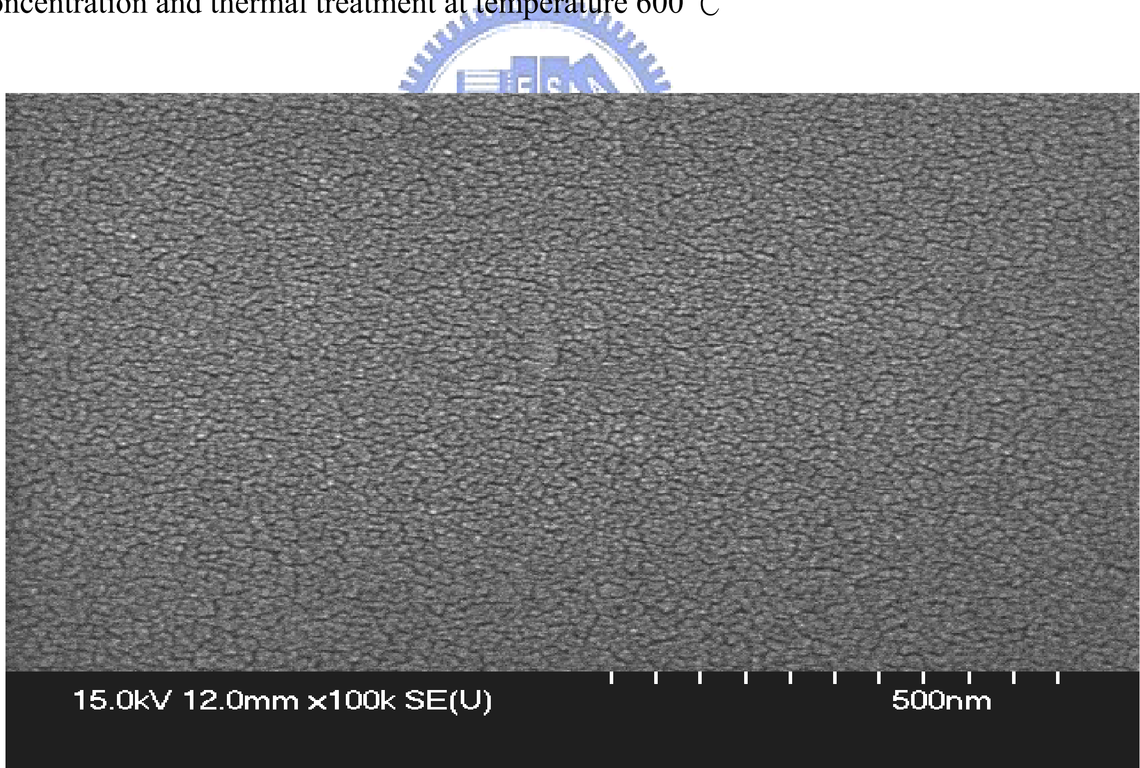

Fig. 3.2-4 Plane view of SEM with sample fabricated by using the solution of 0.3 mole concentration and thermal treatment at temperature 700 ℃

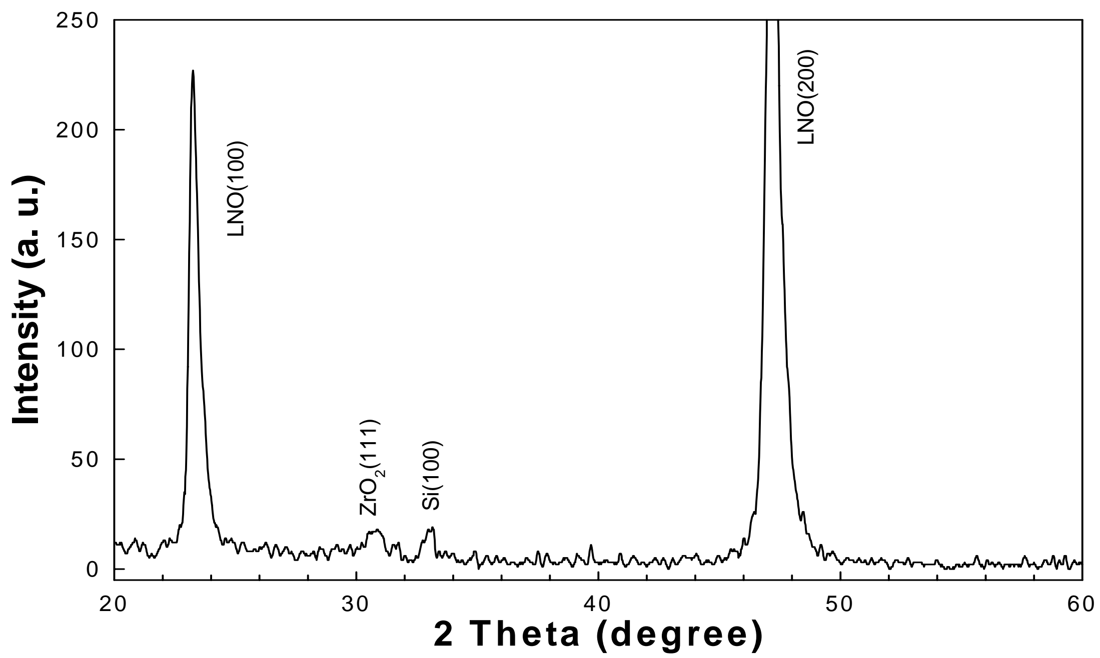

Fig. 3.2-5 X-Ray diffraction pattern related to temperature of 500 ^{o}C in the furnace

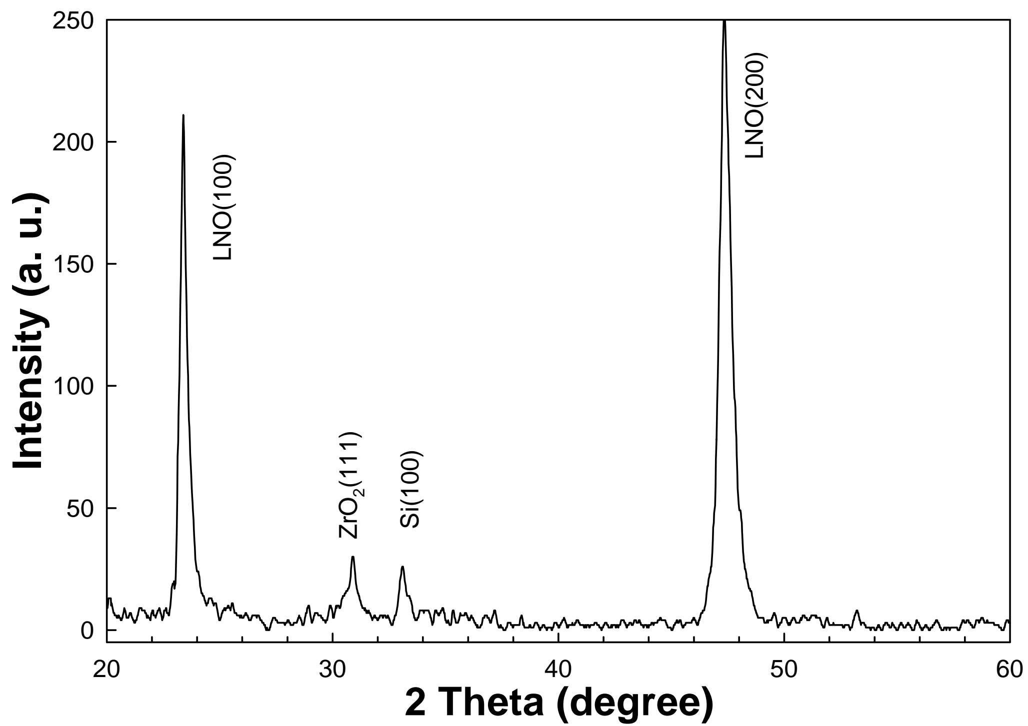

Fig. 3.2-6 X-Ray diffraction pattern related to temperature of 600 ^{o}C in the furnace

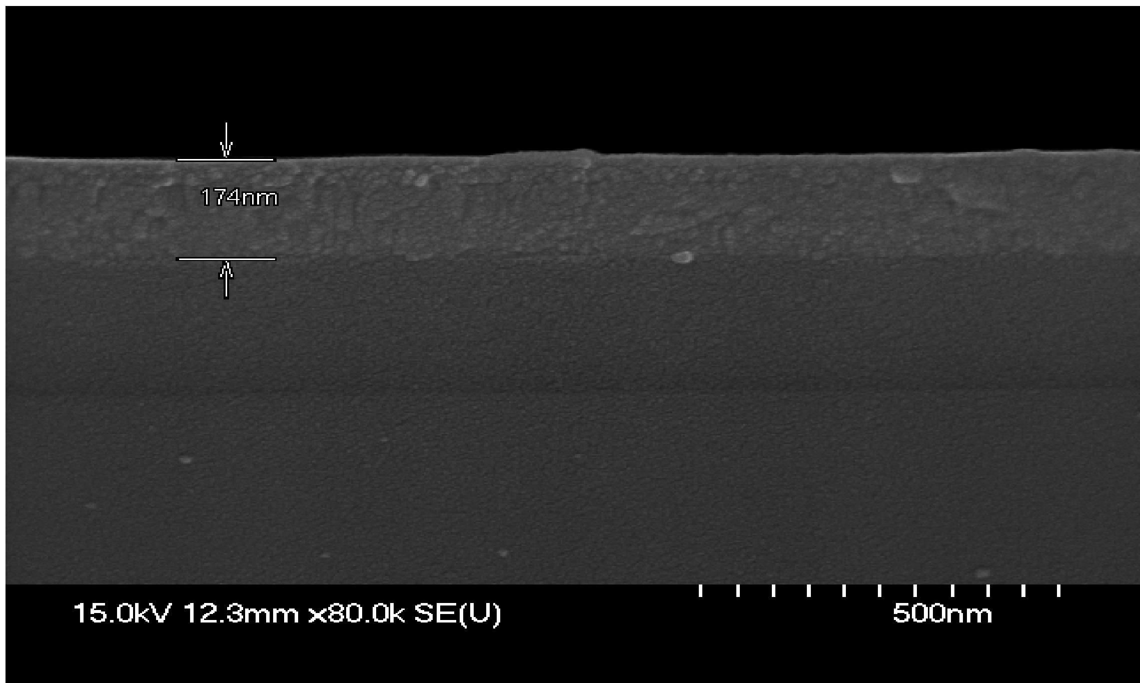

Fig. 3.2-7 cross section view of SEM with sample fabricated by using the solution of 0.05 mole concentration to deposit five layers of ZrO_2 films

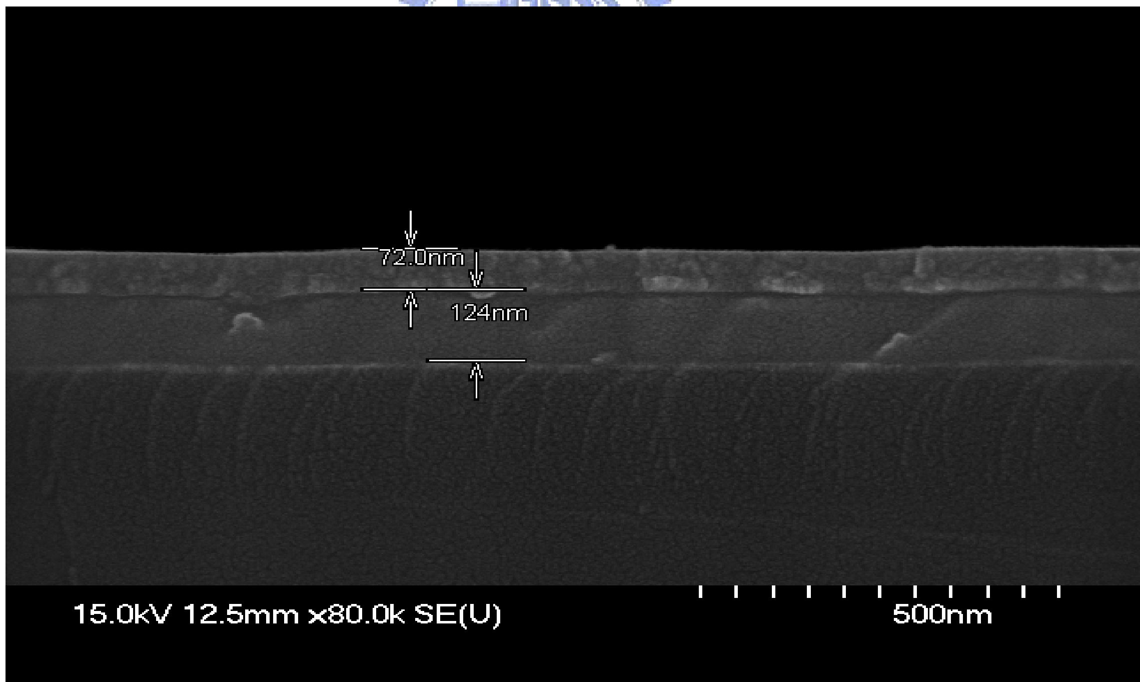

Fig. 3.2-8 cross section view of SEM with sample fabricated by using the solution of 0.1 mole concentration to deposit five layers of ZrO_2 films

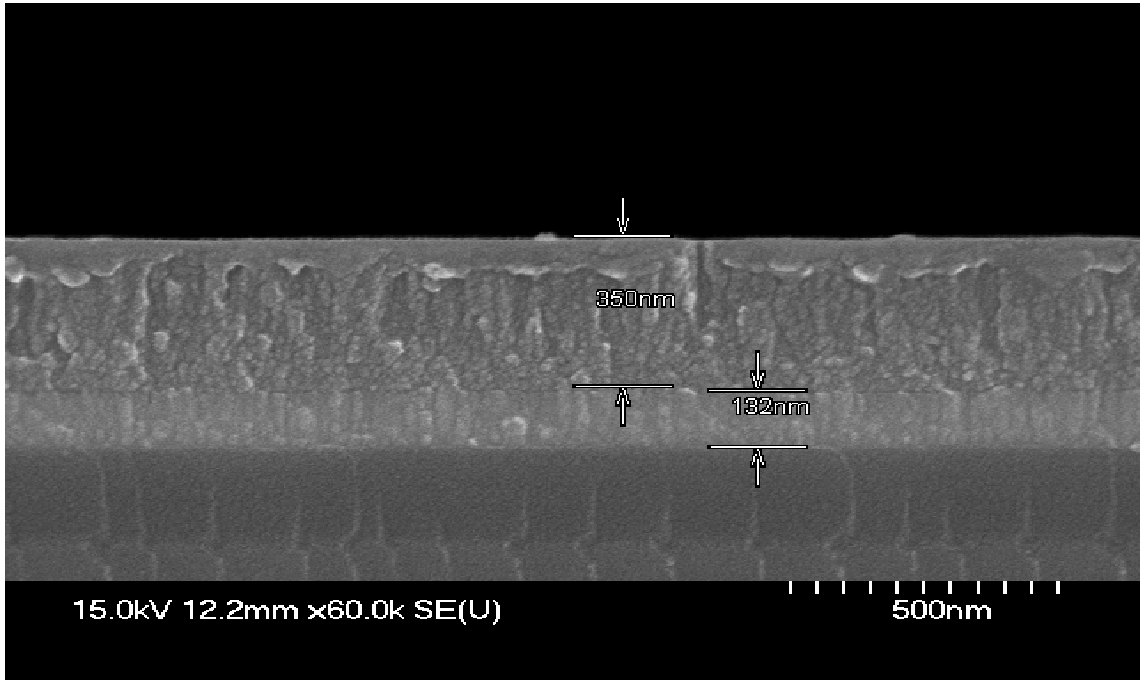

Fig. 3.2-9 cross section view of SEM with sample fabricated by using the solution of 0.5 mole concentration to deposit fore layers of ZrO_2 films

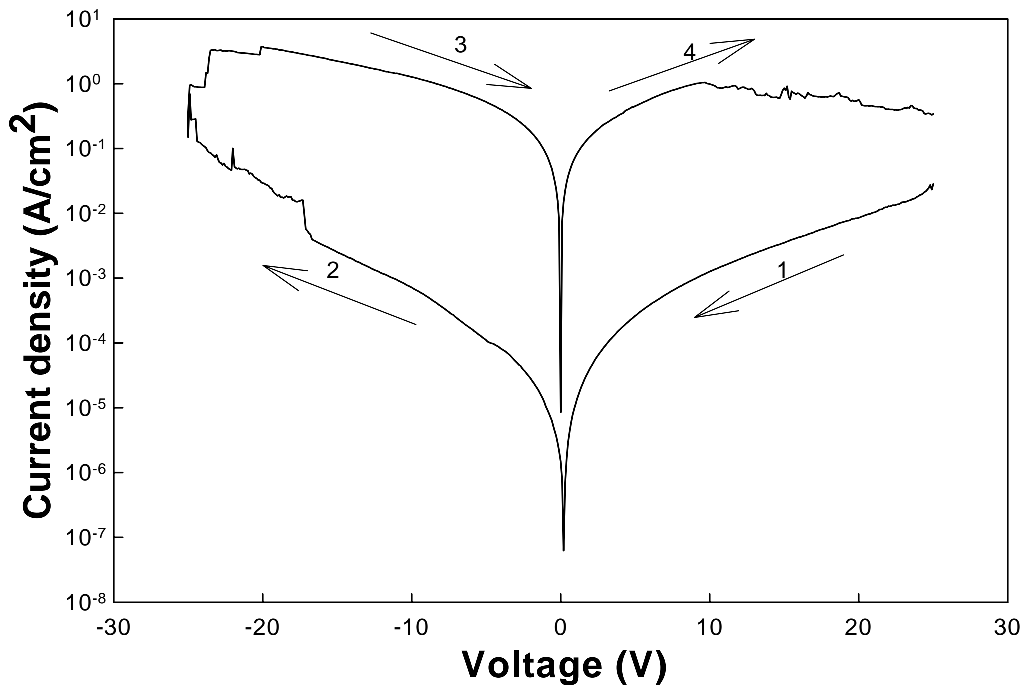

Fig. 3.3.1-1 Bistable switching current density versus voltage, sweeping of 1st time

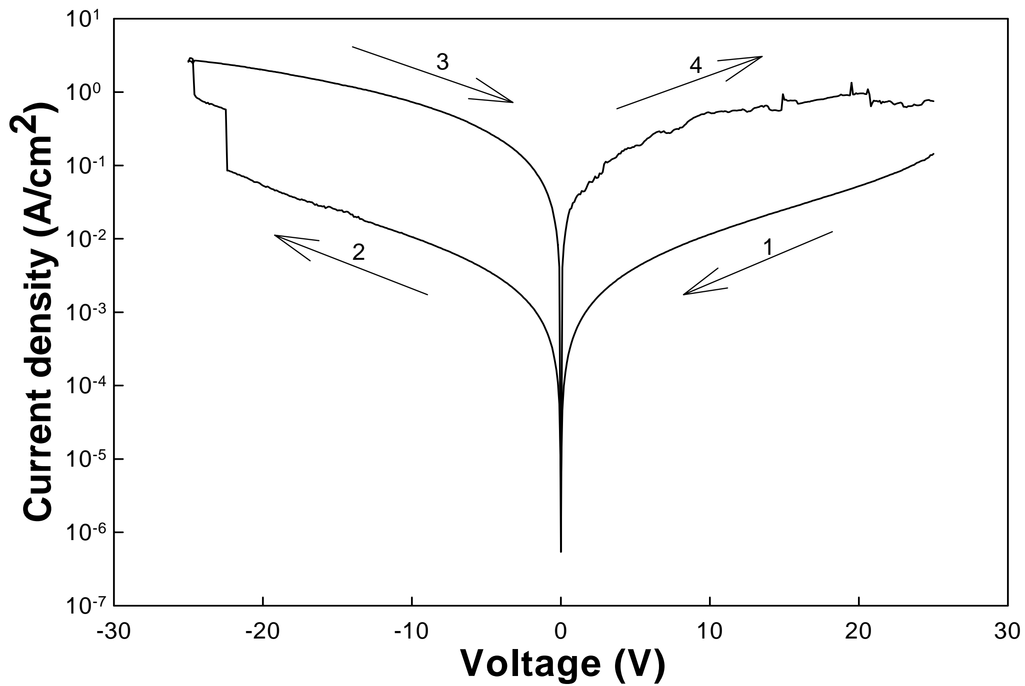

Fig. 3.3.1-2 Bistable switching current density versus voltage sweeping of 5rd time

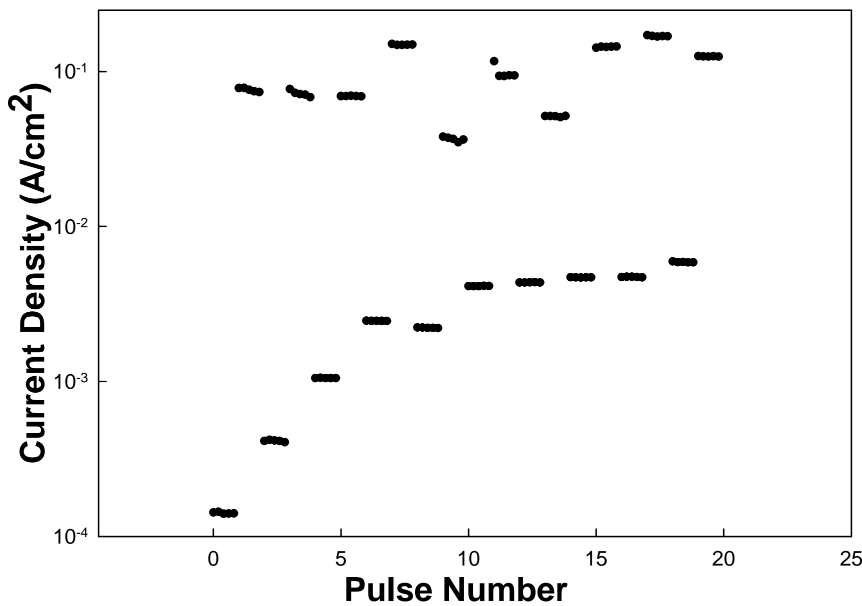

Fig. 3.3.2-1 Current density of ZrO_2 film with thickness of 30 nm measured by magnitude of pulse voltage of 12 volts with pulse width of 0.5s, pulse delay 1 sec and readout voltage of -1 volt

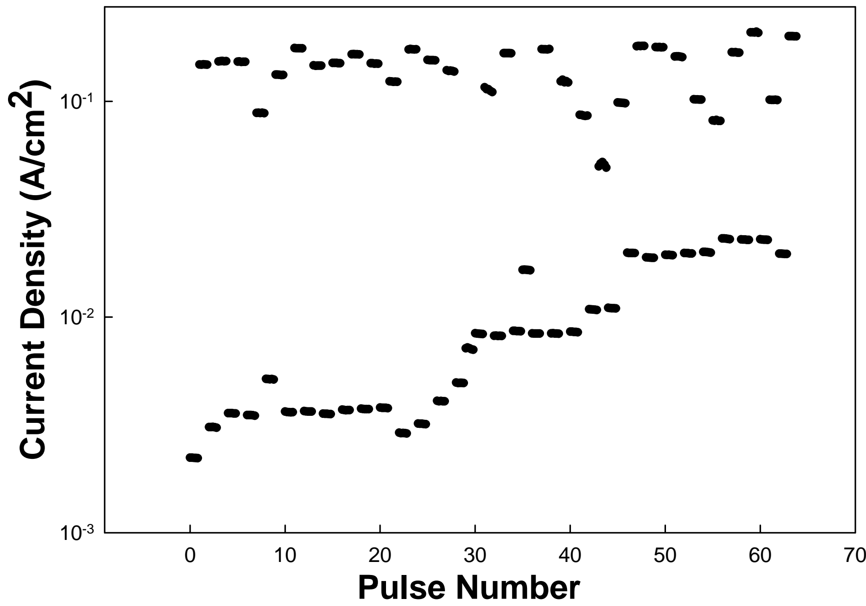

Fig. 3.3.2-2 Current density of ZrO_2 film with thickness of 45 nm measured by magnitude of pulse voltage of 15 volts with pulse width of 0.5 s, pulse delay 1 sec and readout voltage of -1 volt

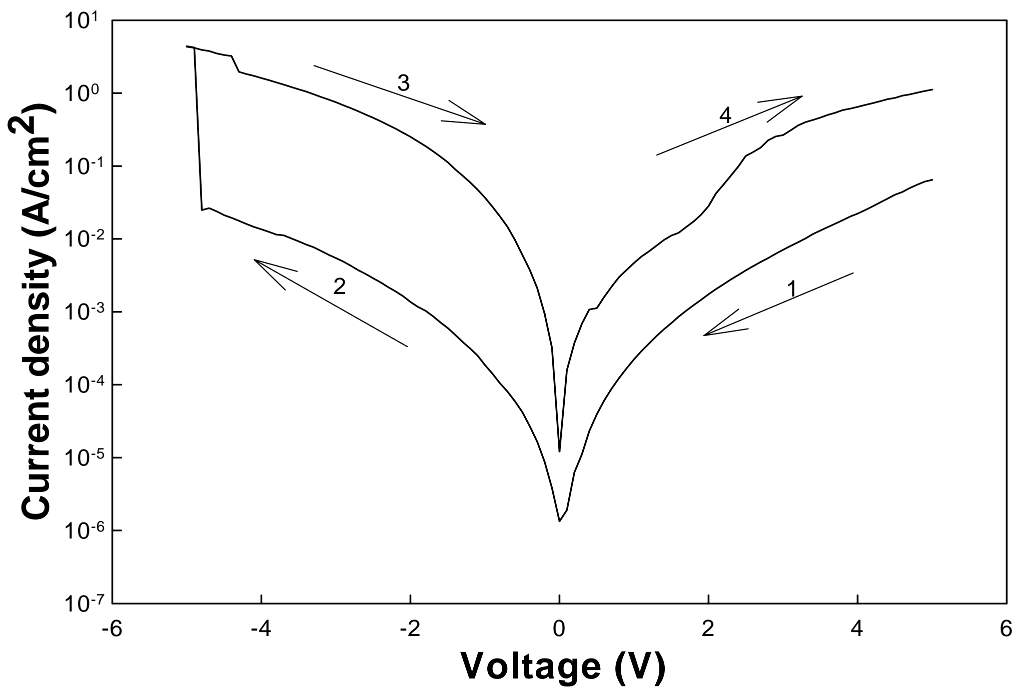

Fig. 3.3.3-1 forming curve of non-doped ZrO_2 film of one layer deposited by solution of 0.1 mole concentration

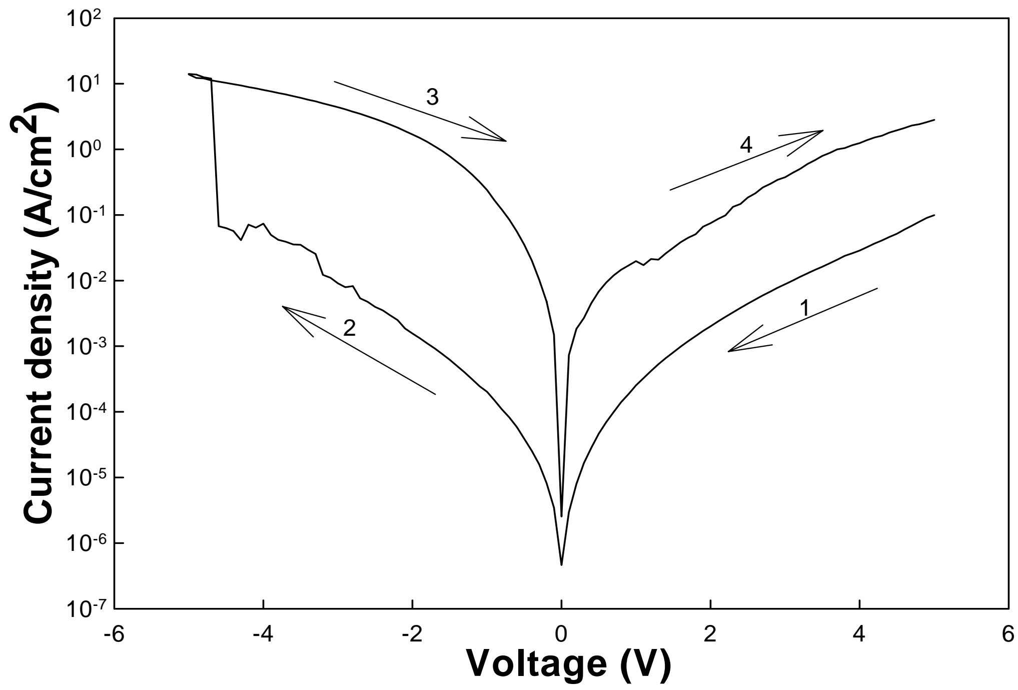

Fig. 3.3.3-2 forming curve of V doped ZrO_2 film of one layer deposited by solution of 0.1 mole concentration

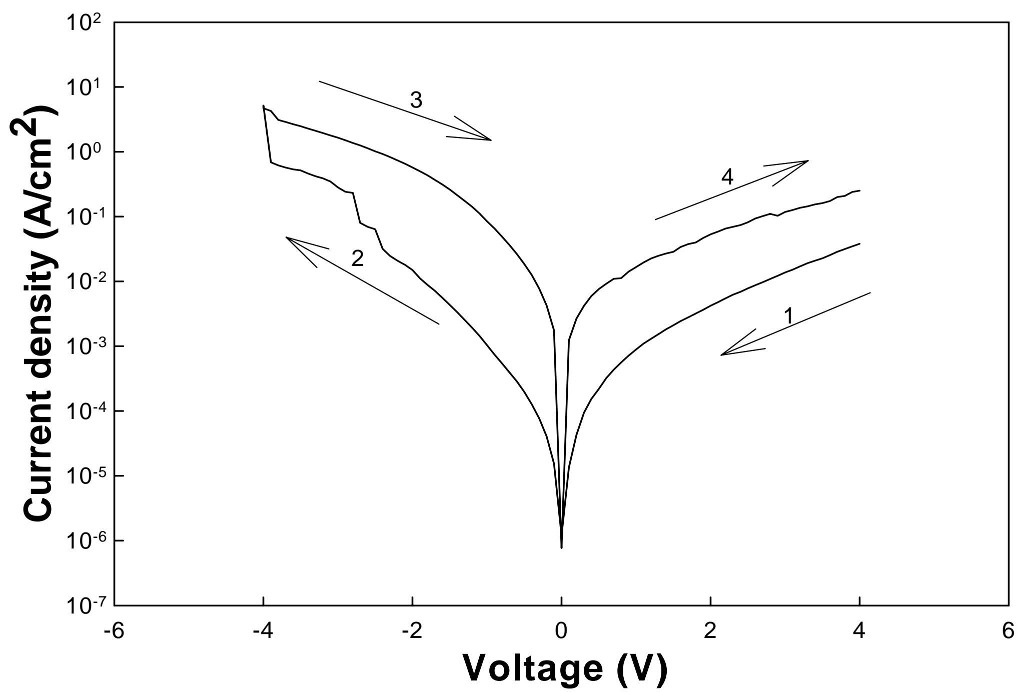

Fig. 3.3.3-3 forming curve of Cr ZrO_2 film of one layer deposited by solution of 0.1 mole concentration

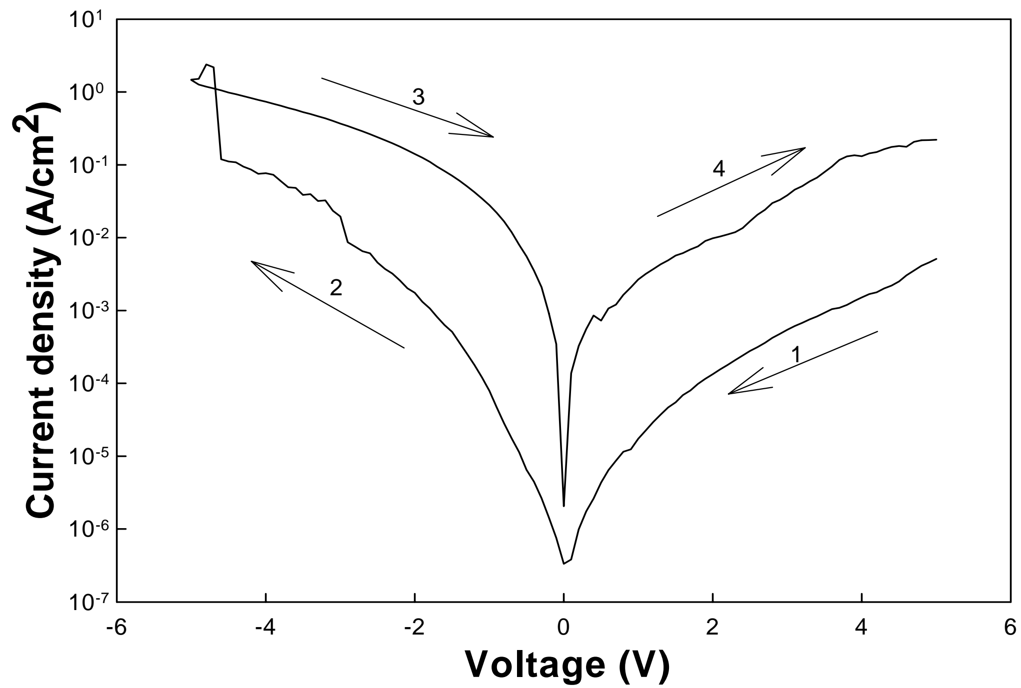

Fig. 3.3.3-4 forming curve of Mo ZrO_2 film of one layer deposited by solution of 0.1 mole concentration

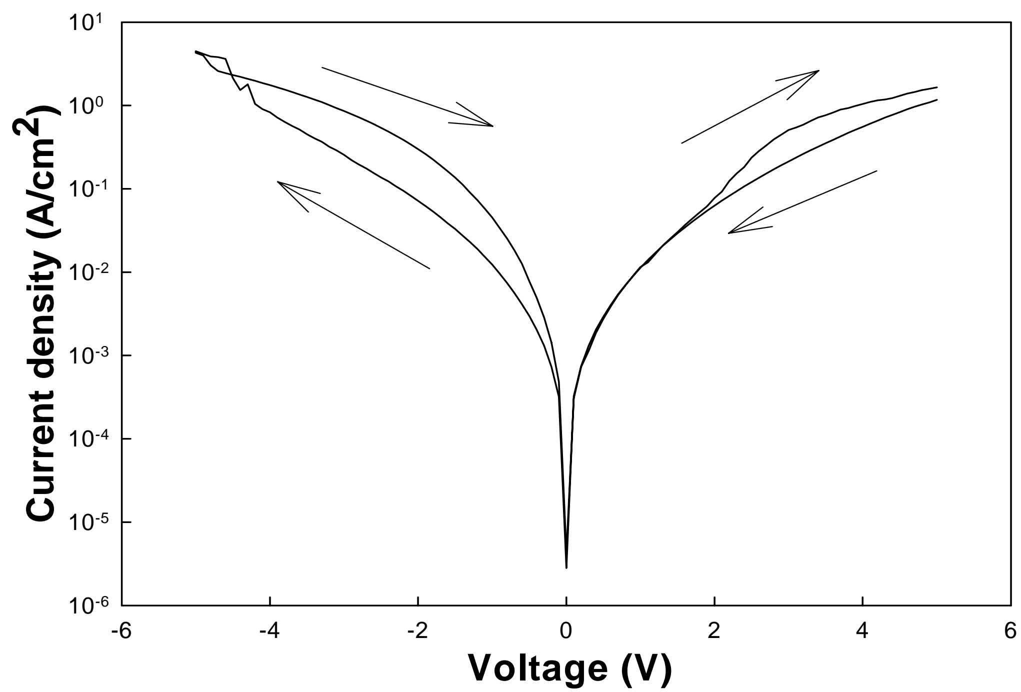

Fig. 3.3.3-1 I-V curve of 5th sweeping time of non-doped ZrO_2 film

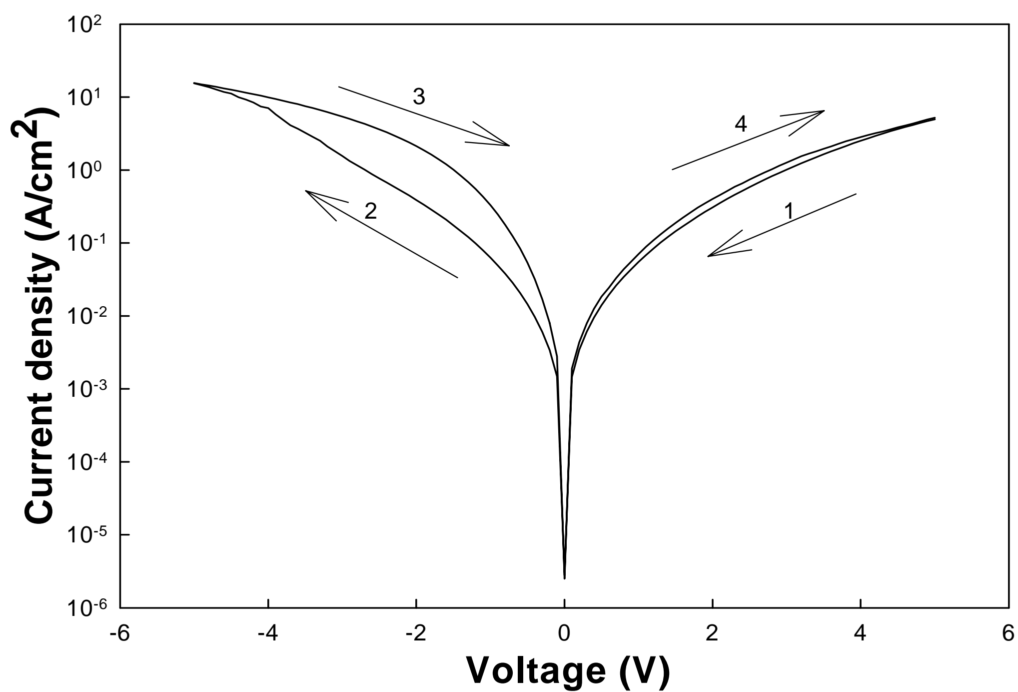

Fig. 3.3.3-1 I-V curve of 5th sweeping time of V doped ZrO_2 film

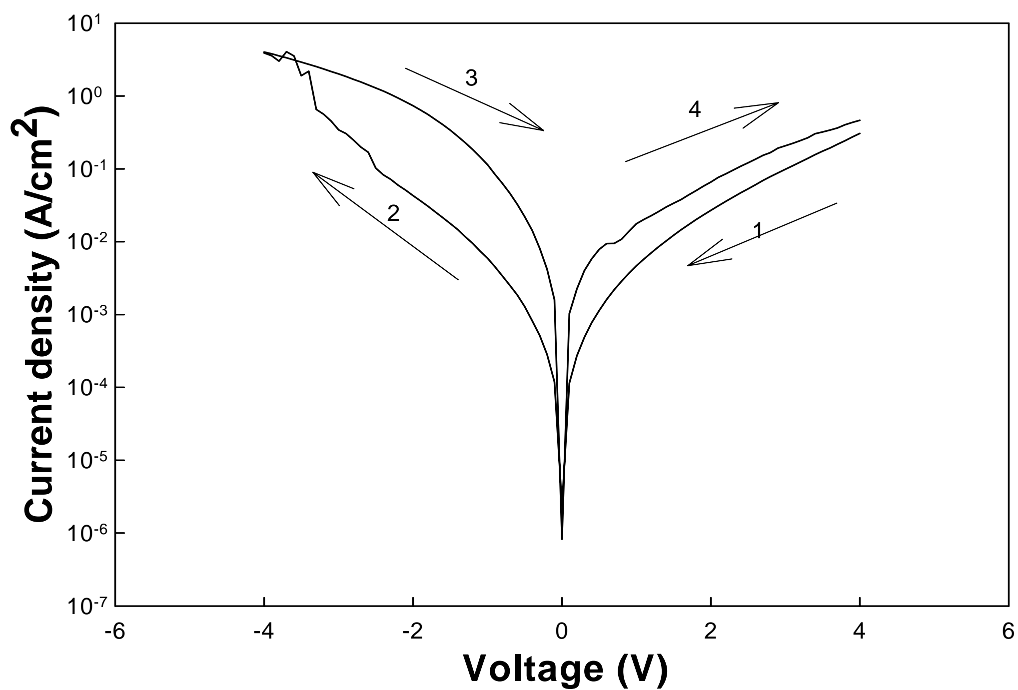

Fig. 3.3.3-1 I-V curve of 5th sweeping time of Cr doped ZrO_2 film

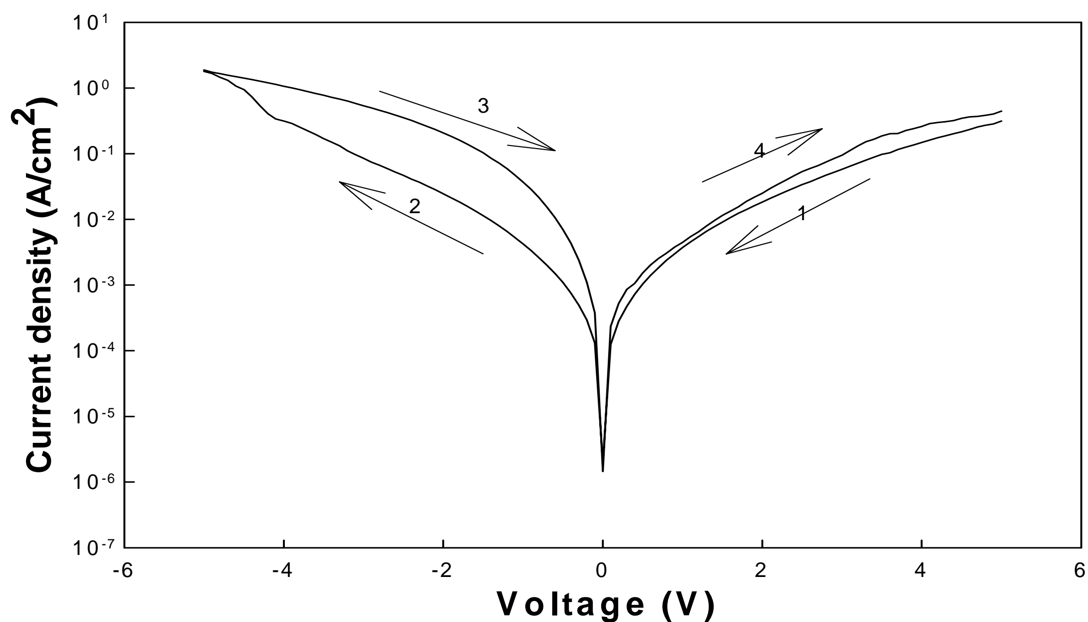

Fig. 3.3.3-1 I-V curve of 5th sweeping time of Mo doped ZrO_2 film

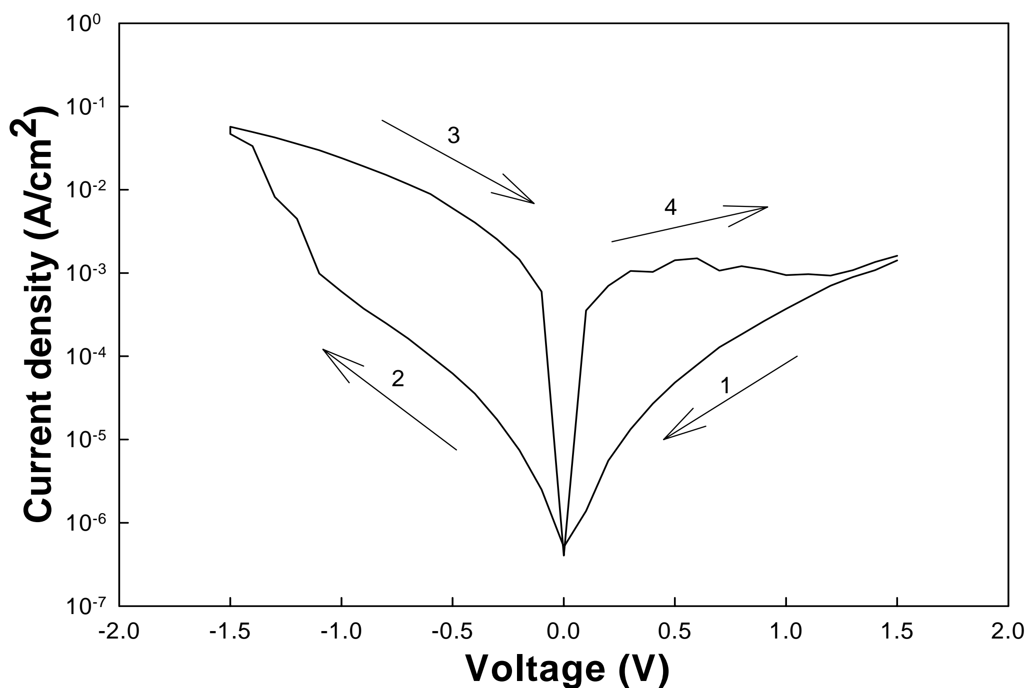

Fig. 3.3.4-1 I-V curve of the sample with thickness of 20 nm, sweeping of first time

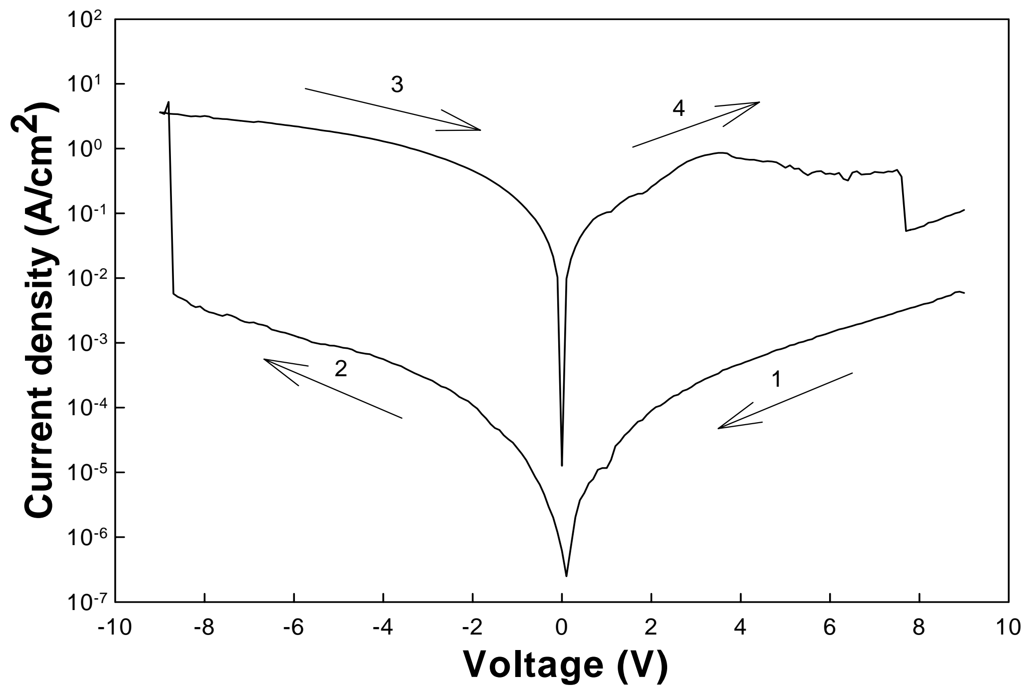

Fig. 3.3.4-2 I-V curve of the sample with thickness of 30 nm, sweeping of first time

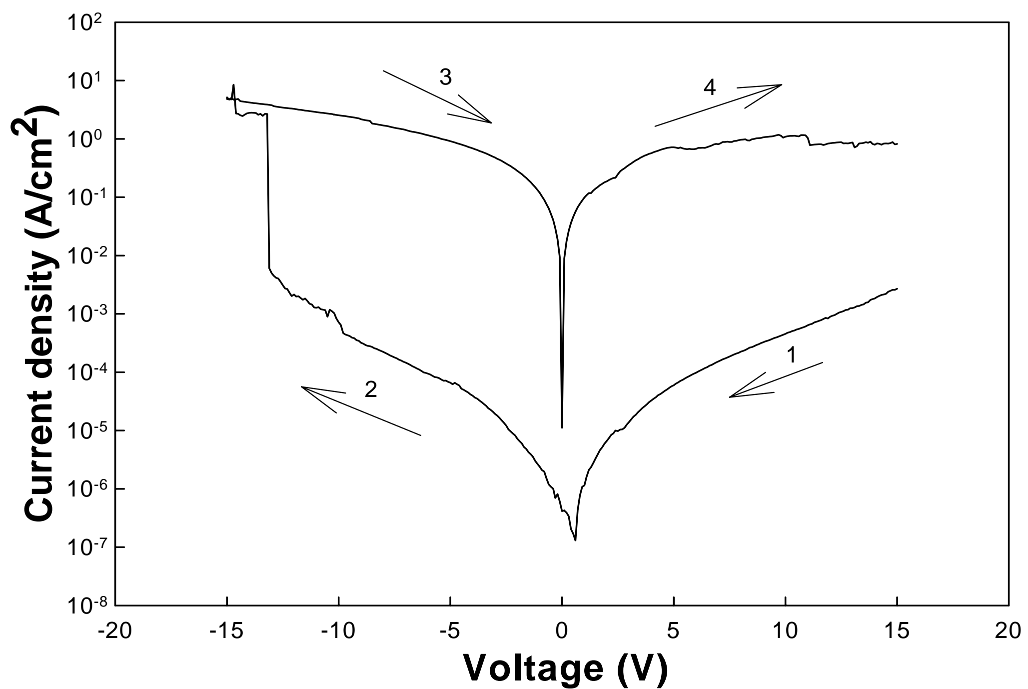

Fig. 3.3.4-3 I-V curve of the sample with thickness of 45 nm, sweeping of first time

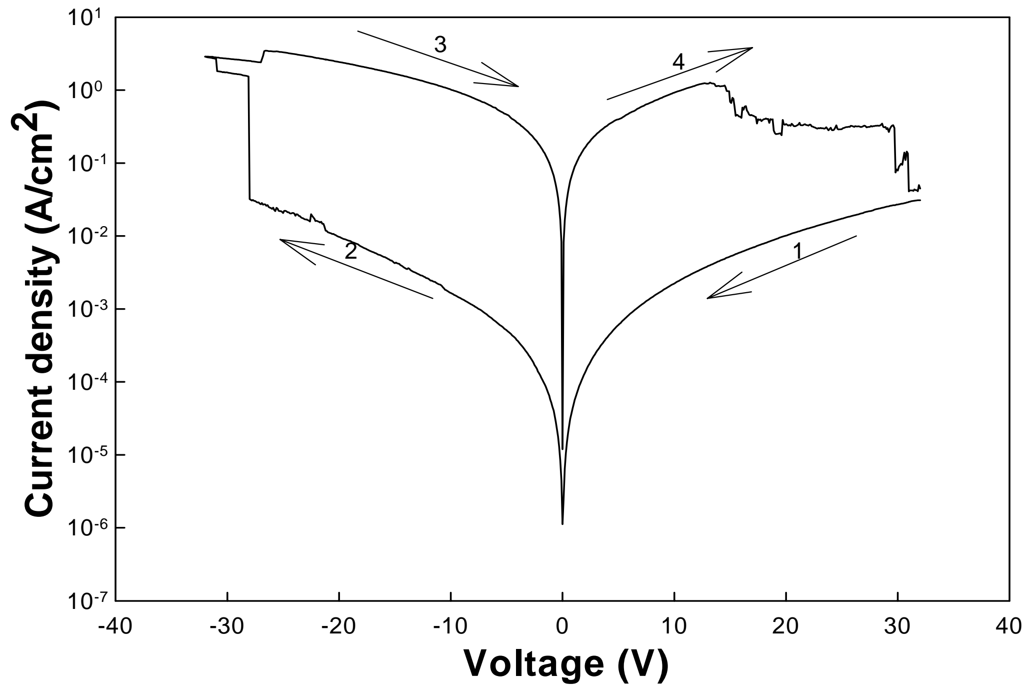

Fig. 3.3.4-4 I-V curve of the sample with thickness of 82 nm, sweeping of first time

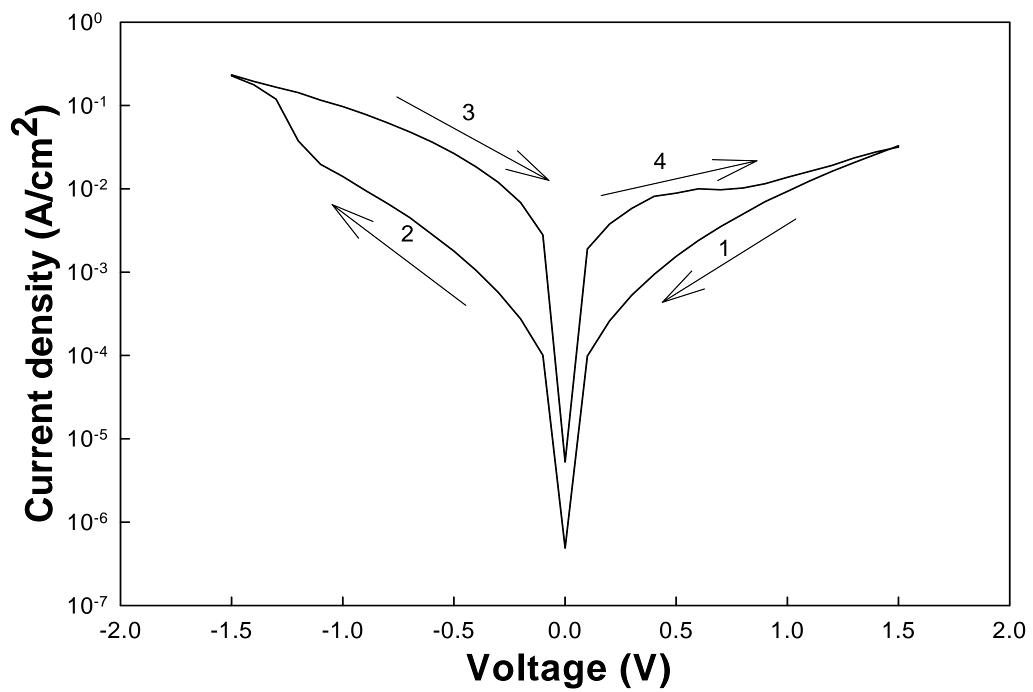

Fig. 3.3.4-5 I-V curve of the sample with thickness of 20 nm, sweeping of 5th time

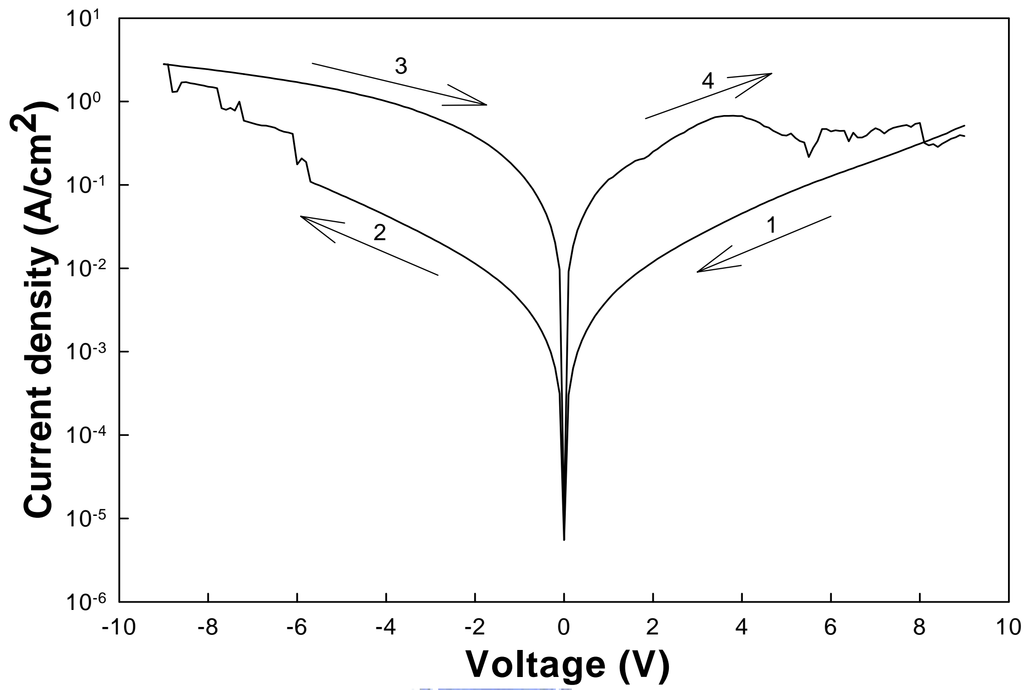

Fig. 3.3.4-6 I-V curve of the sample with thickness of 30 nm, sweeping of 5th time

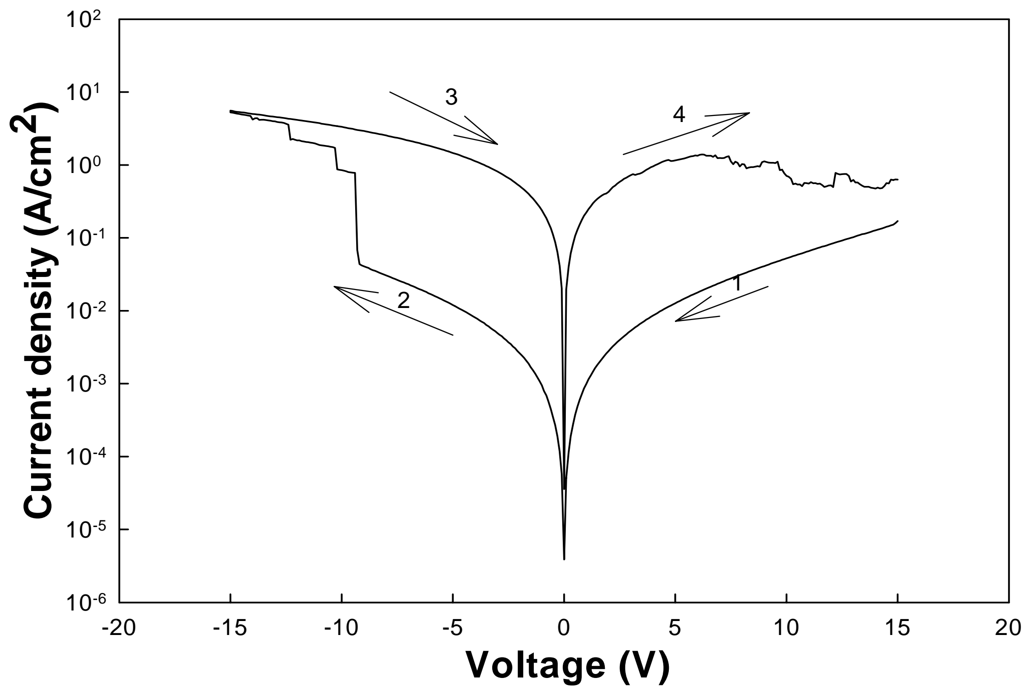

Fig. 3.3.4-7 I-V curve of the sample with thickness of 45 nm, sweeping of 5th time

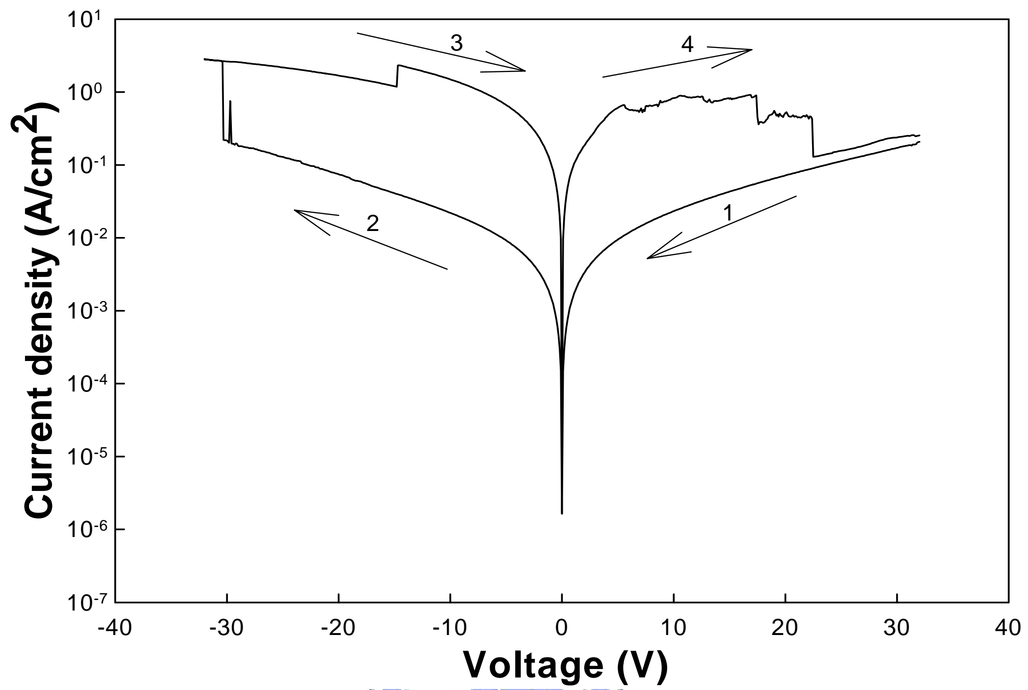

Fig. 3.3.4-8 I-V curve of the sample with thickness of 82 nm, sweeping of 5th time

[watermark]

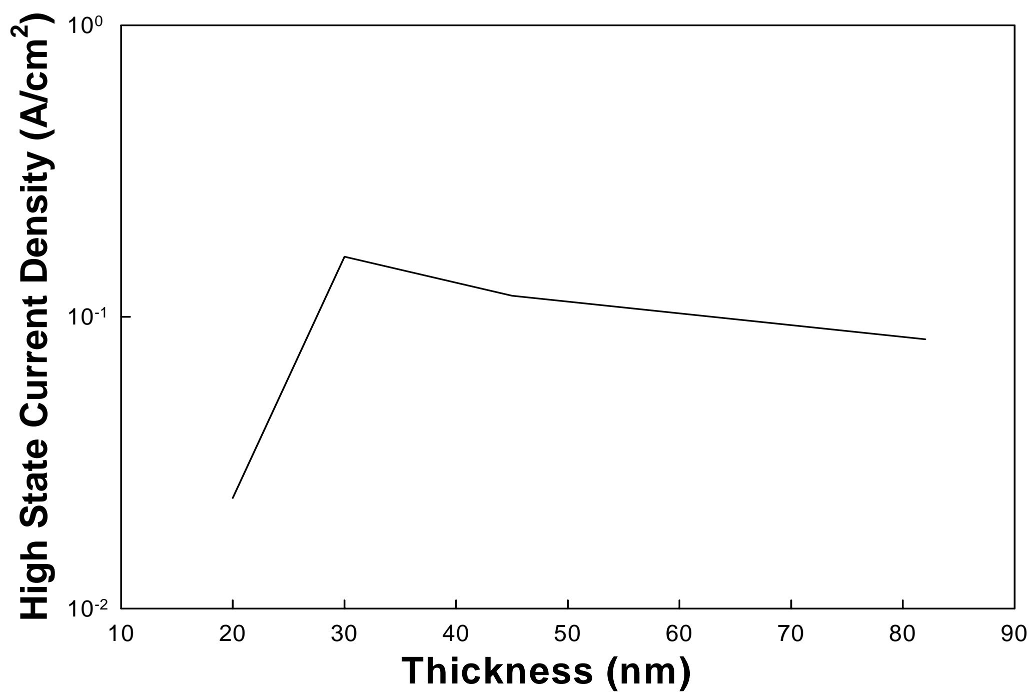

Fig. 3.3.4-9 the order of the current density versus thickness of the ZrO_2 film, sweeping of 1 time

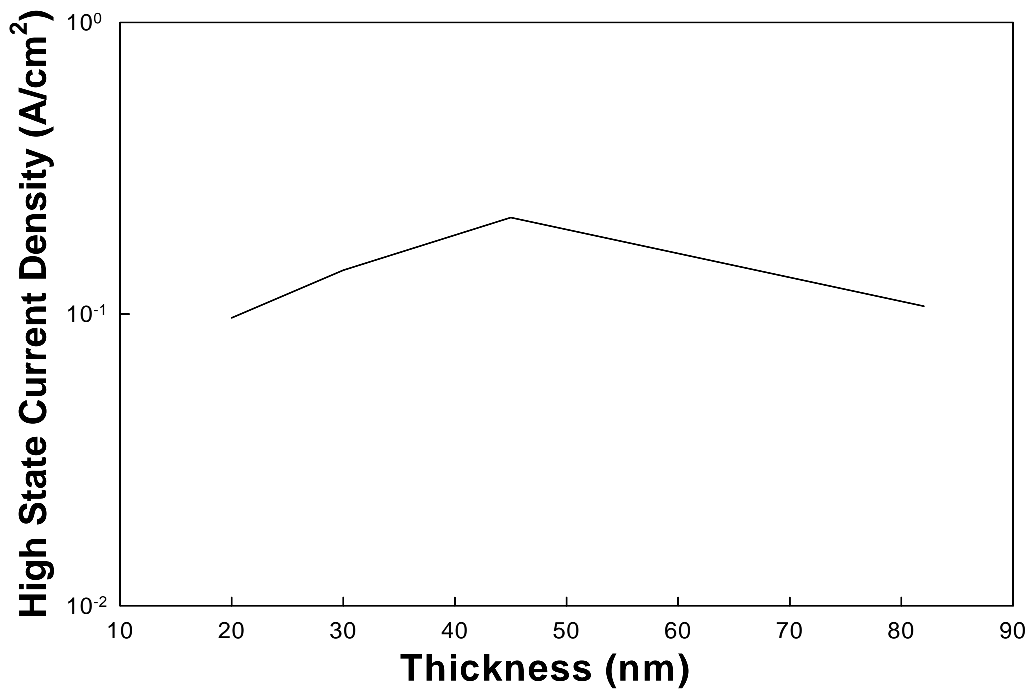

Fig. 3.3.4-10 the order of the current density versus thickness of the ZrO_2 film, sweeping of 5 times

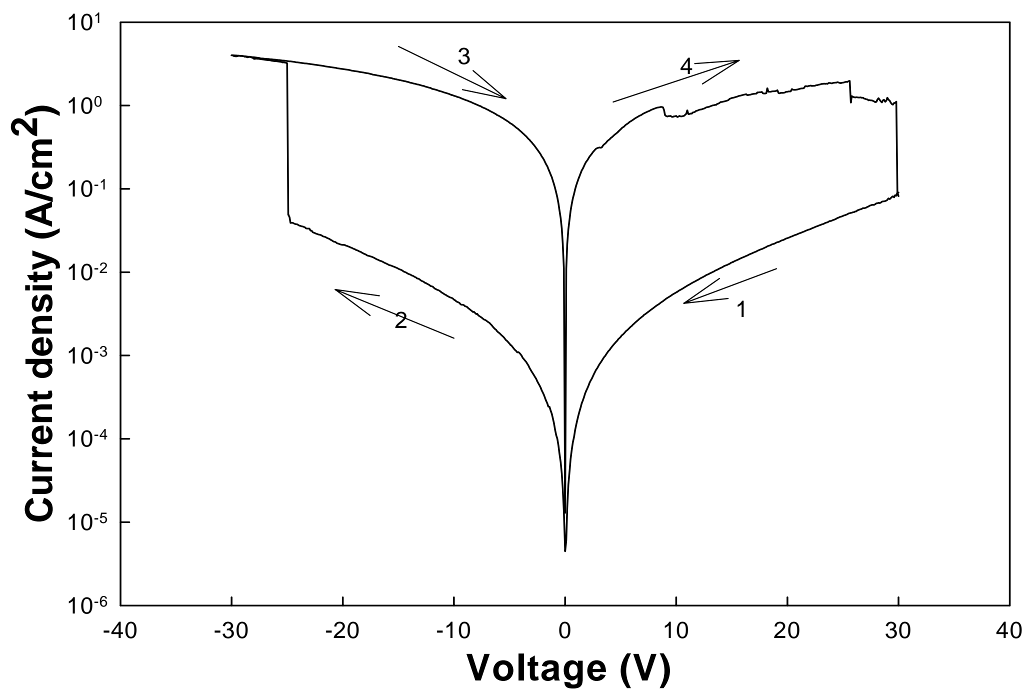

Fig. 3.3.5-1 I-V curve of ZrO_2 film deposited by solution of 0.5 mole concentration and thermal treatment in the furnace at temperature 600 ^oC for 30 min, 1st sweeping time

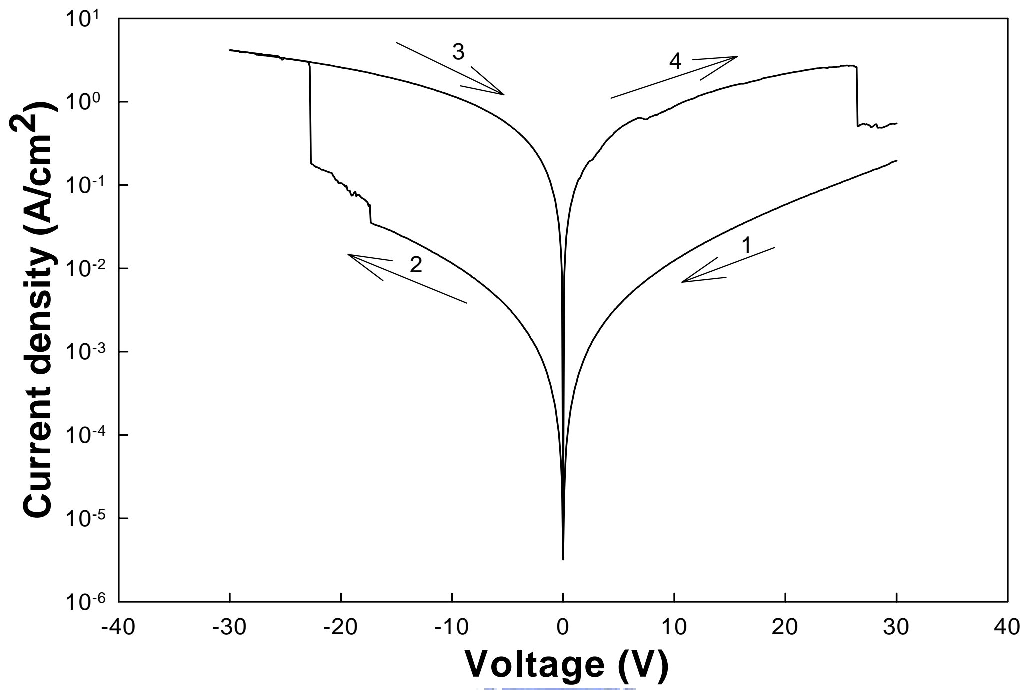

Fig. 3.3.5-2 I-V curve of ZrO_2 film deposited by solution of 0.5 mole concentration and thermal treatment in the furnace at temperature 600 ^oC for 30 min, 5th sweeping time

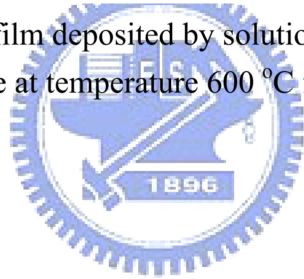

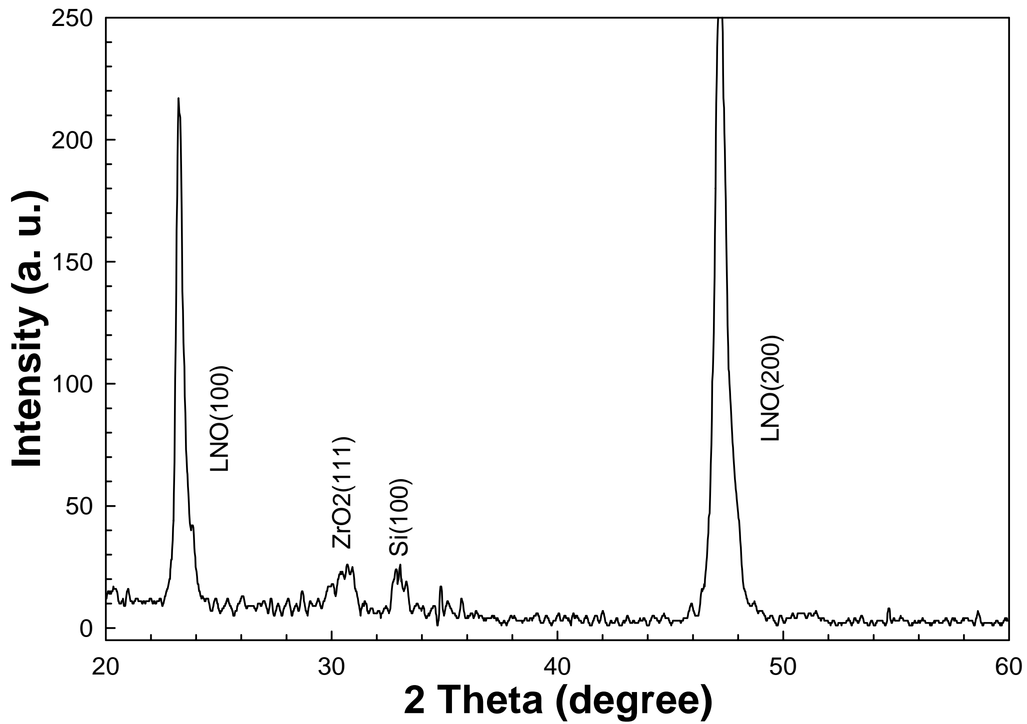

Fig. 3.3.5-3 X-Ray diffraction pattern of the ZrO_2 film deposited by solution of 0.5 mole concentration and thermal treatment in the furnace at temperature 600 ^{o}C for 30 min

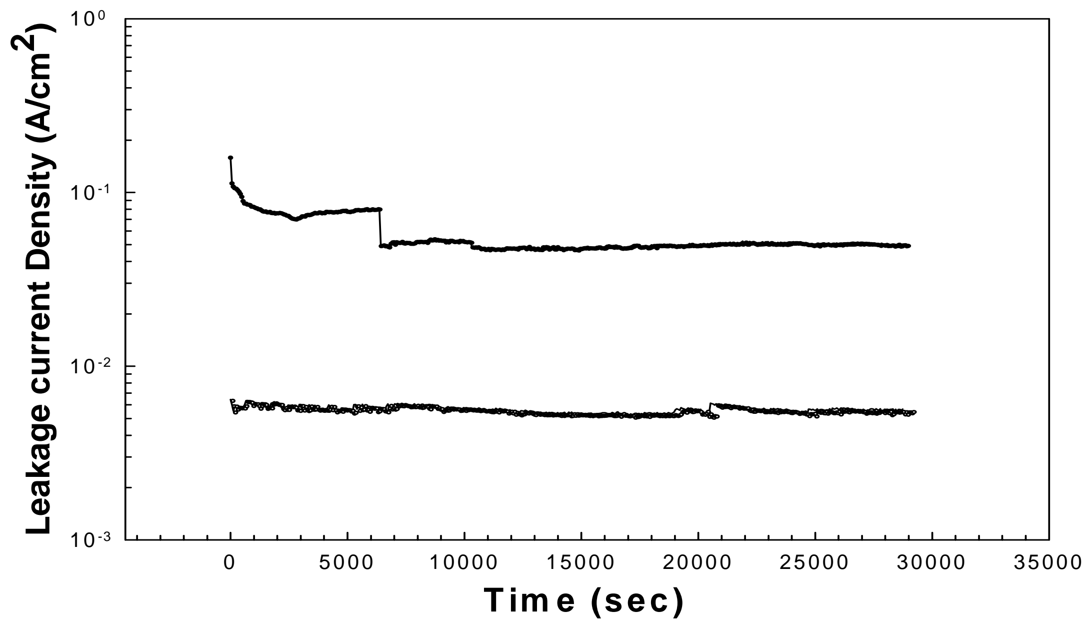

Fig. 3.3.6-1 Retention for this sample, the magnitude of the pulse voltage is 30 volts and the pulse width is 0.5 s

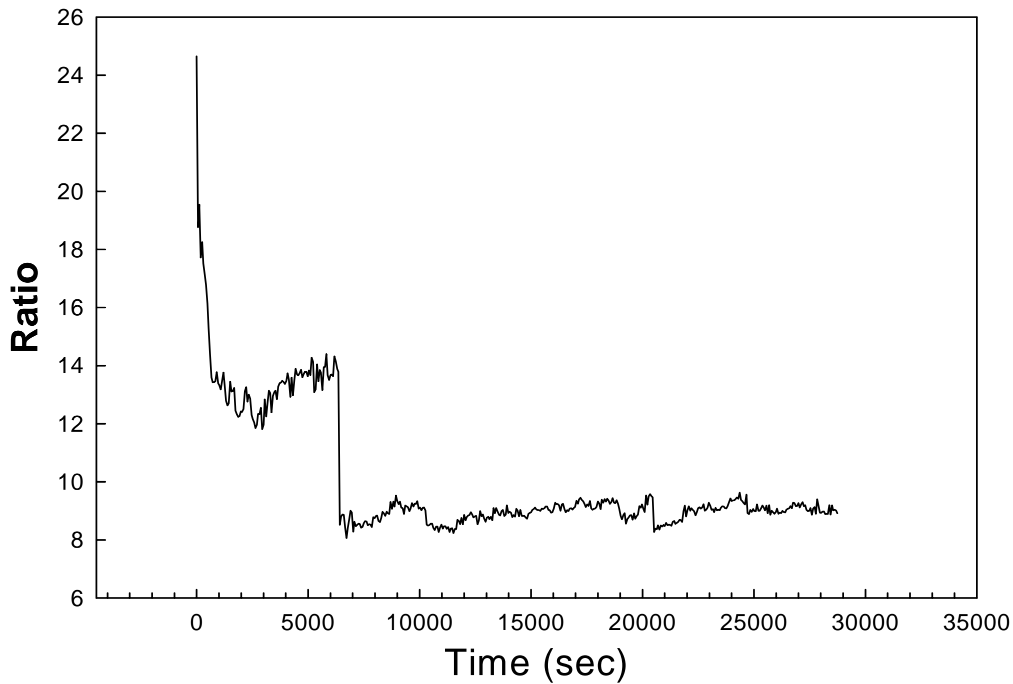

Fig. 3.3.6-2 High-low leakage ration variation during retention test for this sample, the magnitude of the pulse voltage is 30 volts and the pulse width is 0.5 s

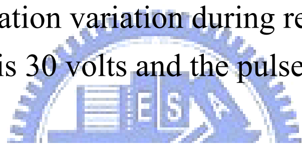

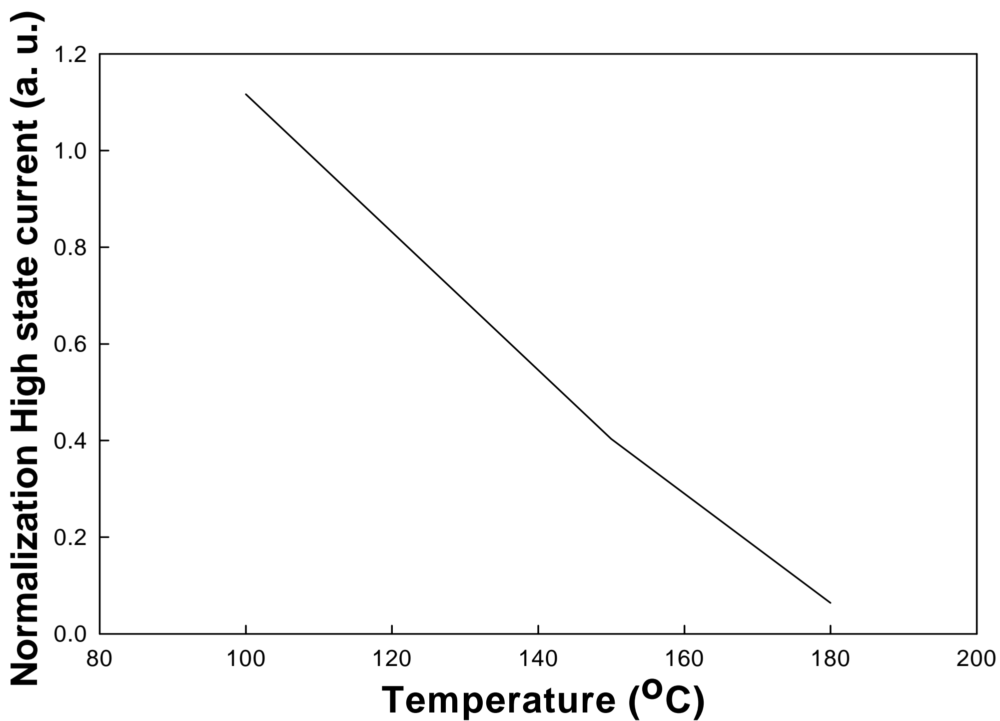

Fig. 3.3.7 High state current after thermal treatment divide by high state current before thermal treatment versus temperature

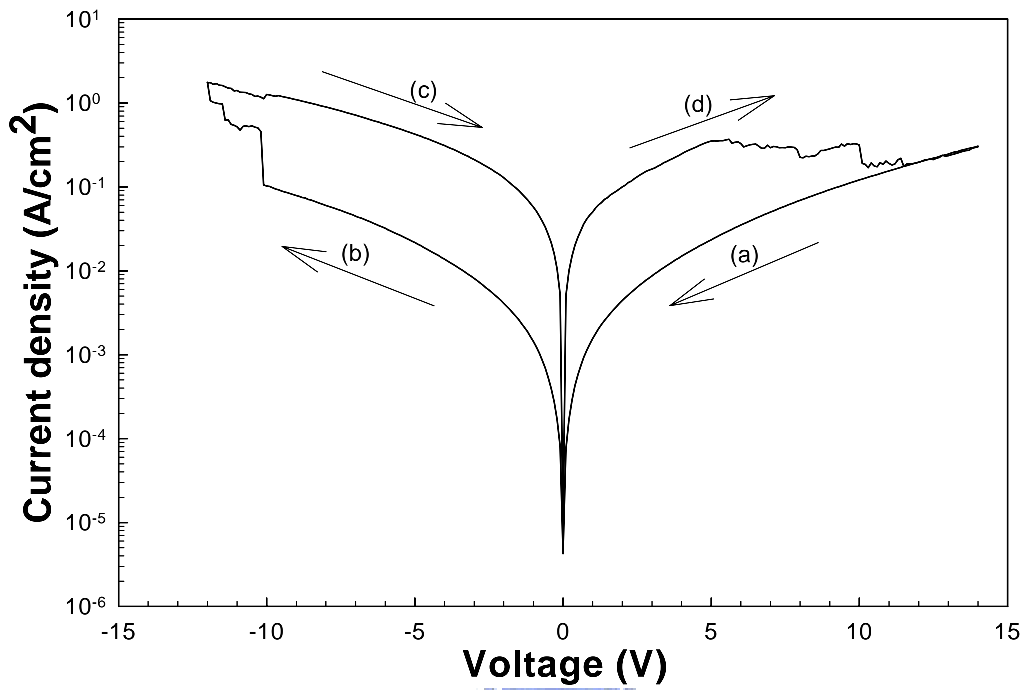

Fig. 3.3.8-1 Static I-V curve of 0.1 M two layers ZrO_2 film

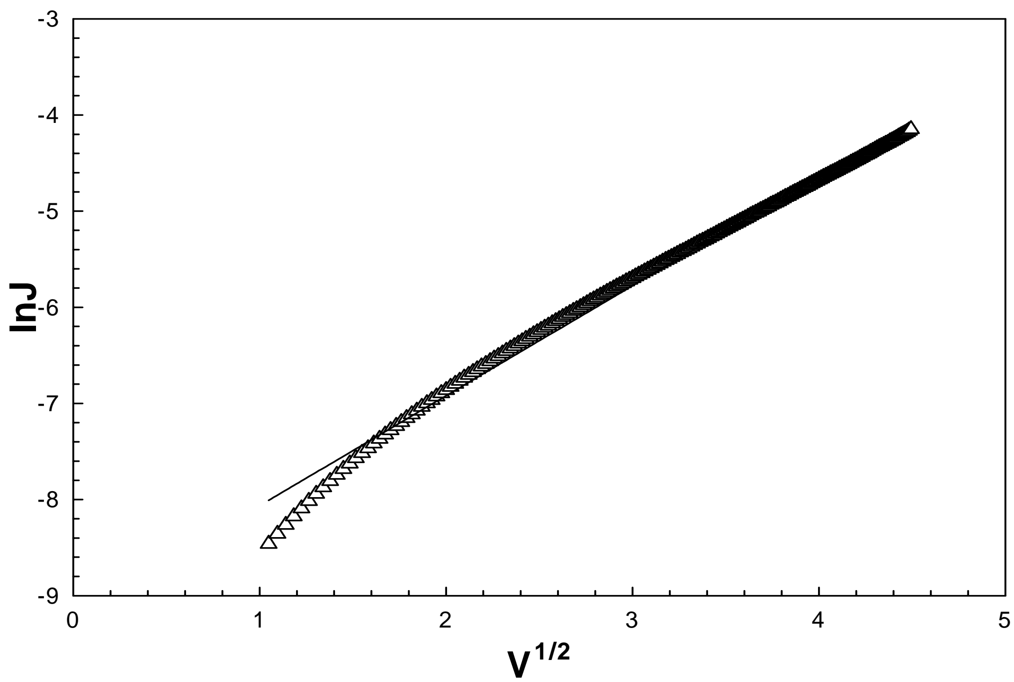

Fig. 3.3.8-2 Schottky emission process fitting of curve (a)

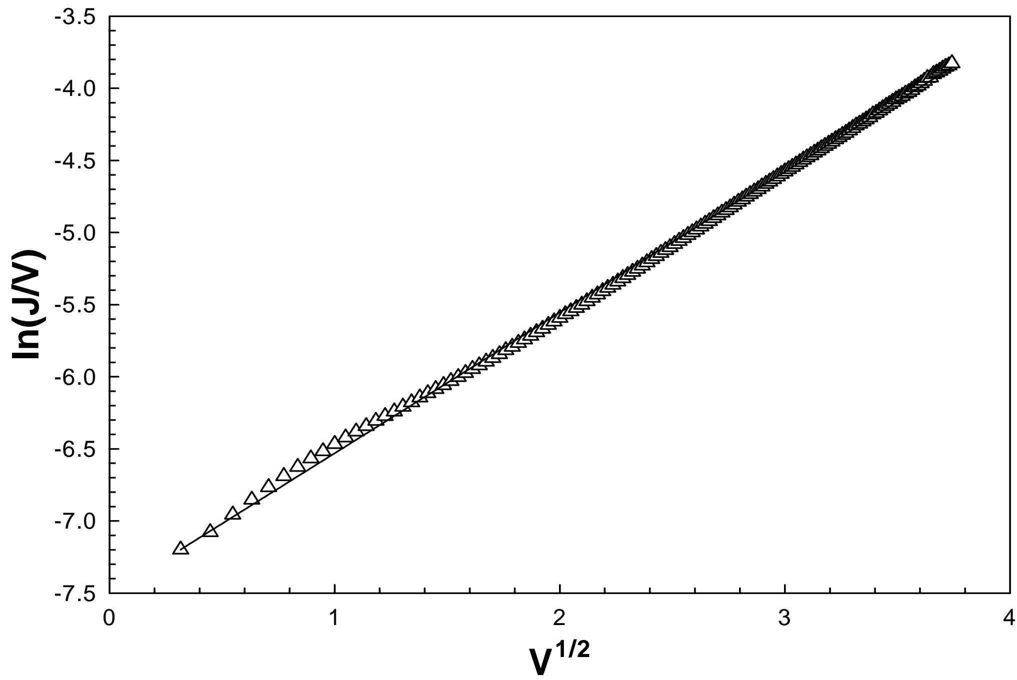

Fig. 3.3.8-3 Frenkel poole process current fitting of curve (a)

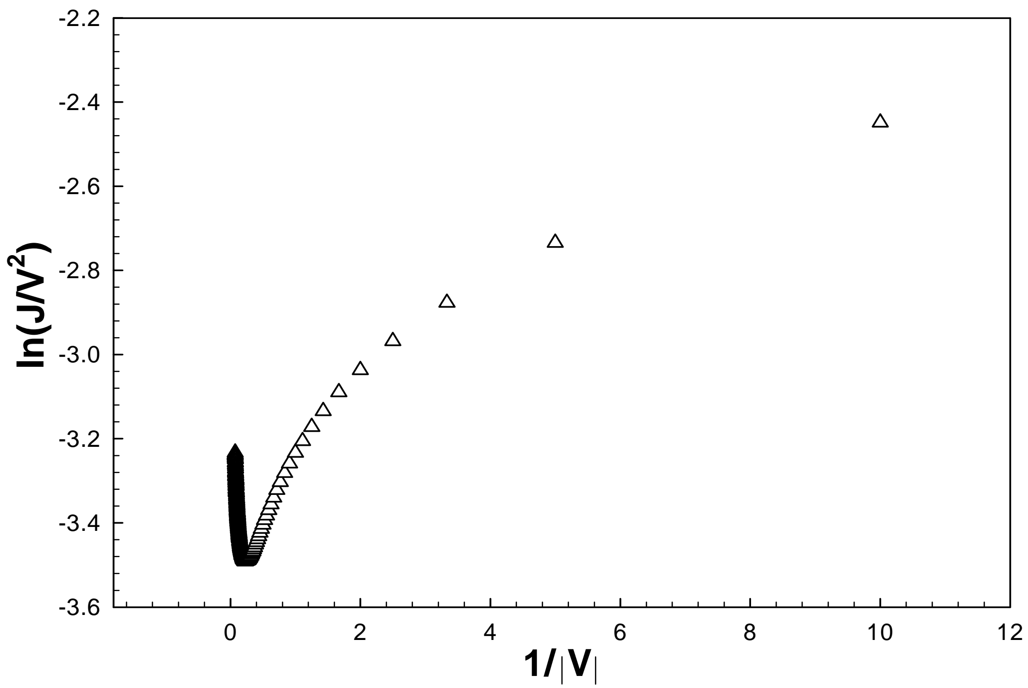

Fig. 3.3.8-4 Field emission process fitting of curve (a)

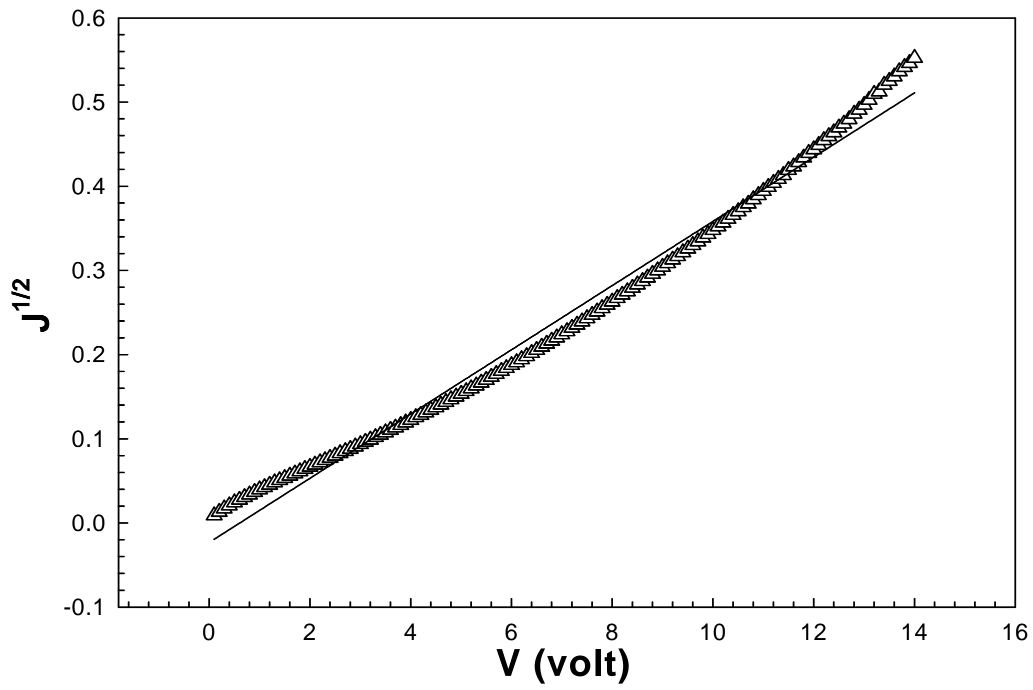

Fig. 3.3.8-5 Space-charge-limited process fitting of curve (a)

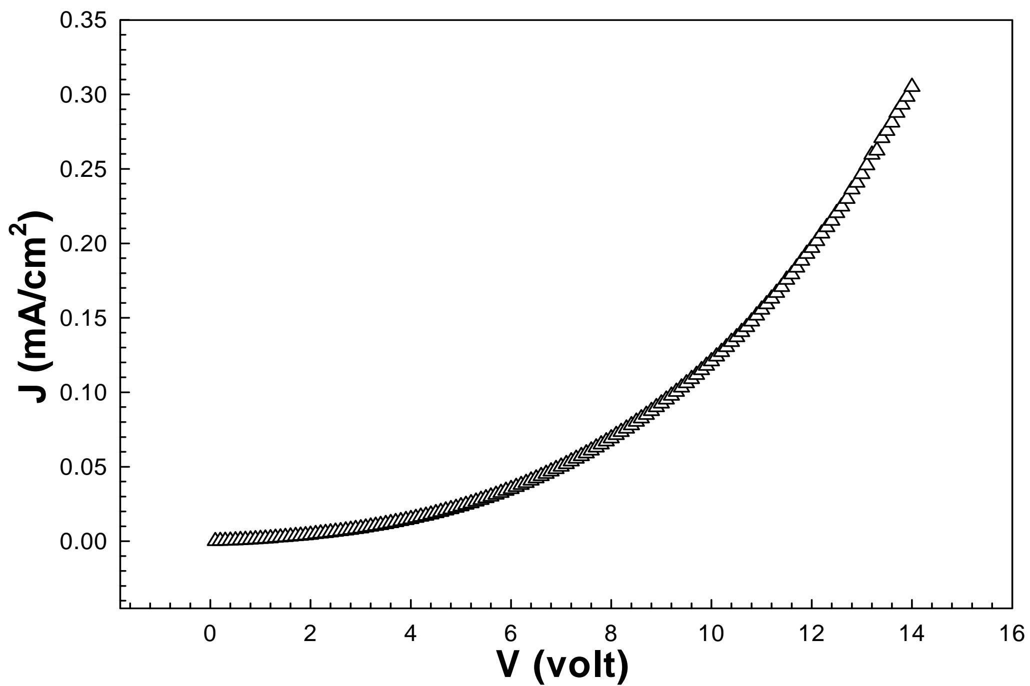

Fig. 3.3.8-6 Ohmic fitting of curve (a)

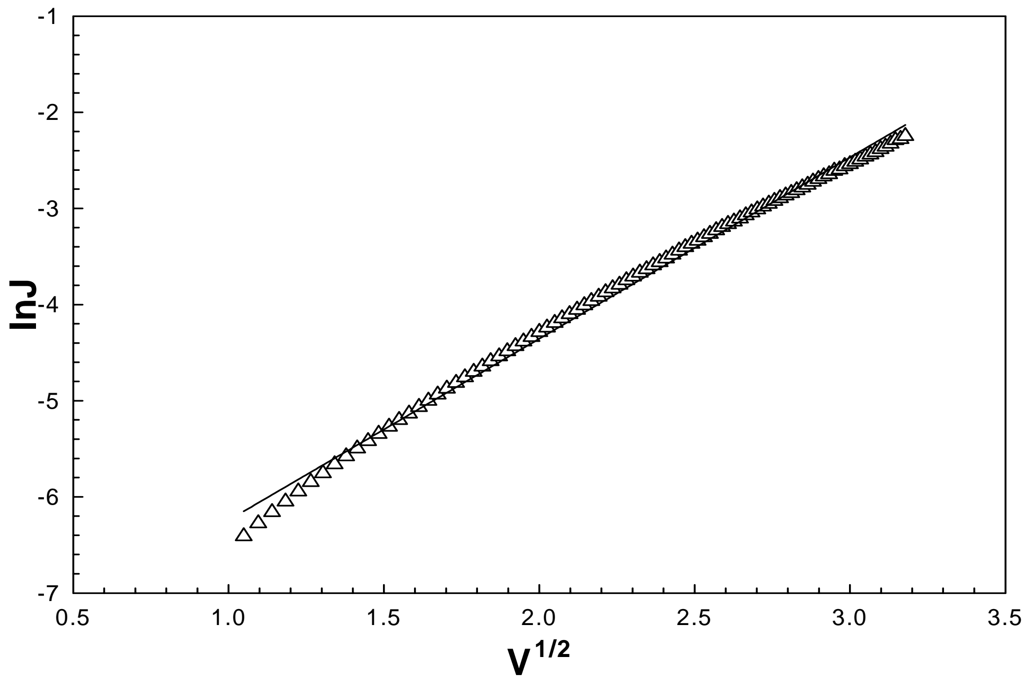

Fig. 3.3.8-7 Schottky emission process fitting of curve (b)

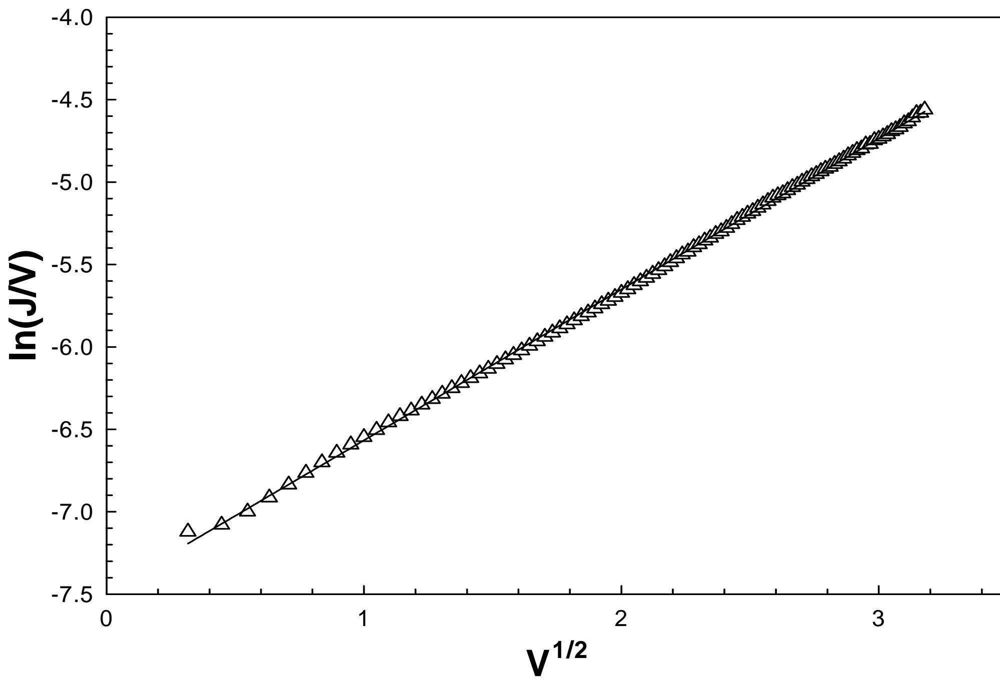

Fig. 3.3.8-8 Frenkel poole process current fitting of curve (b)

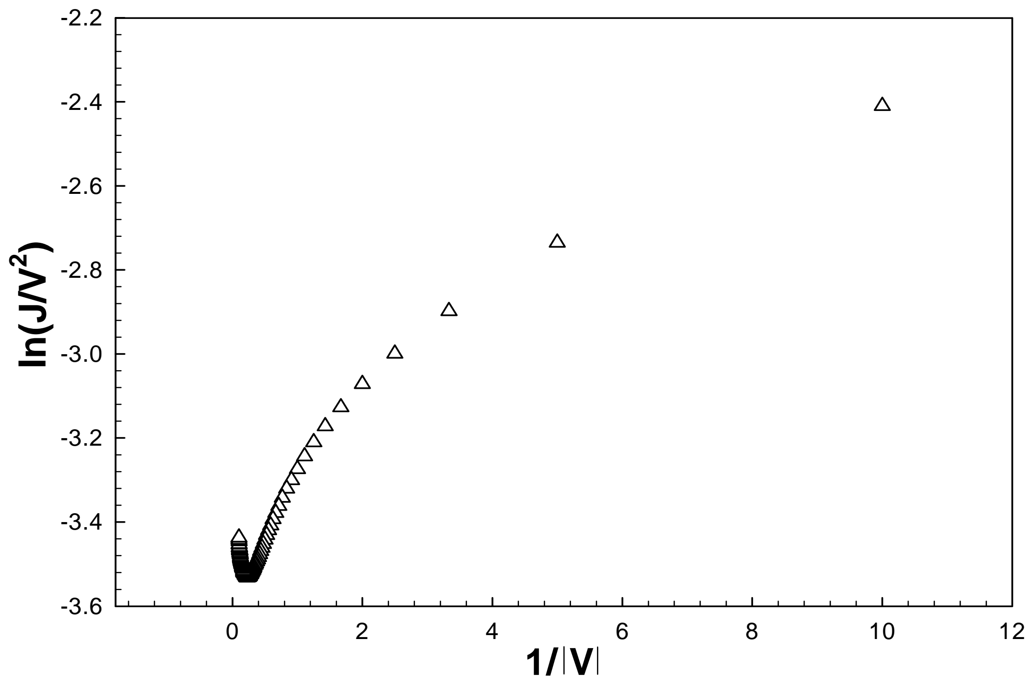

Fig. 3.3.8-9 Field emission process fitting of curve (b)

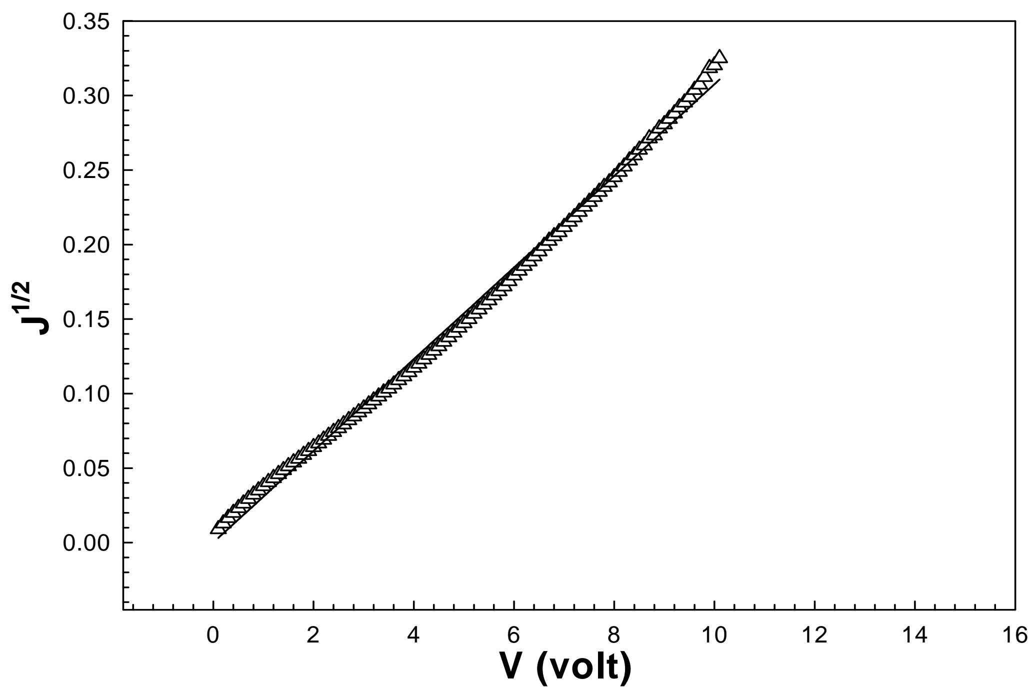

Fig. 3.3.8-10 Space-charge-limited process fitting of curve (b)

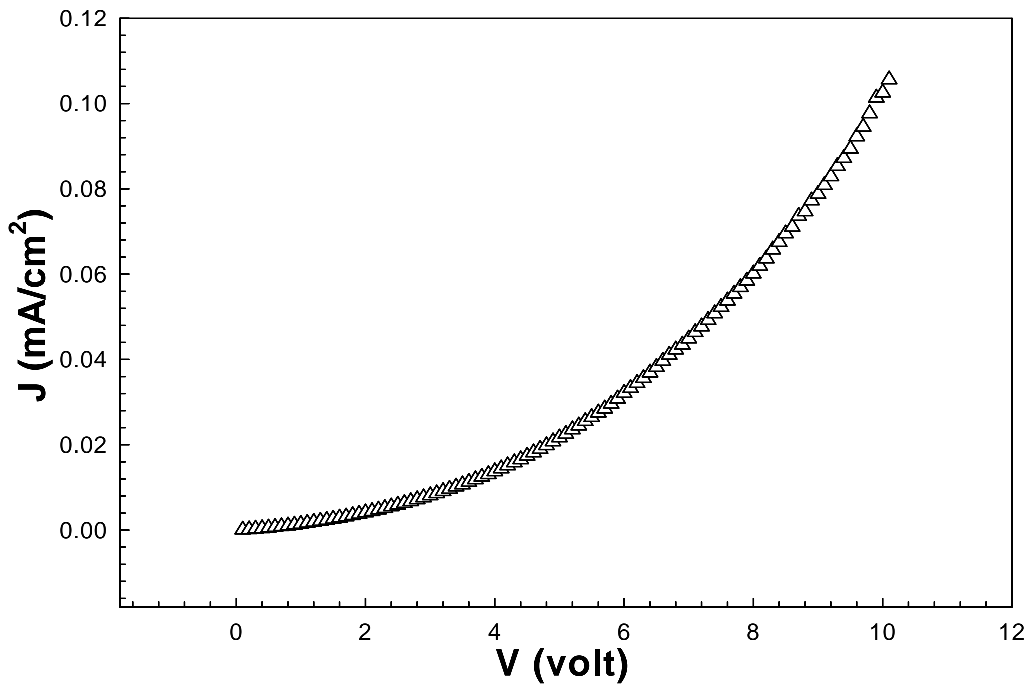

Fig. 3.3.8-11 Ohmic fitting of curve (b)

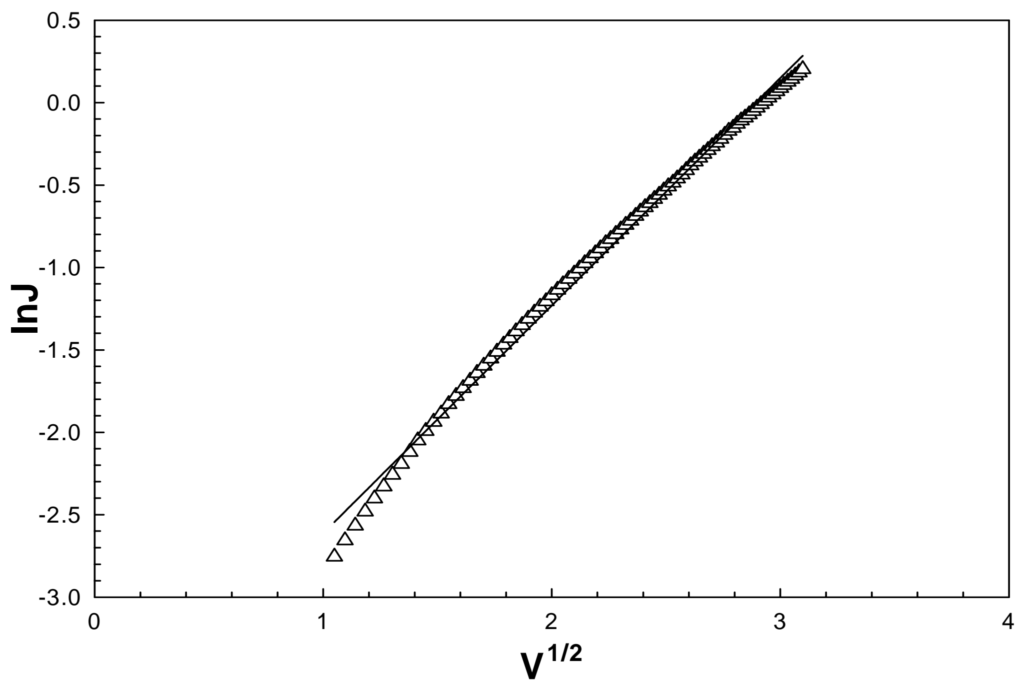

Fig. 3.3.8-12 Schottky emission process fitting of curve (c)

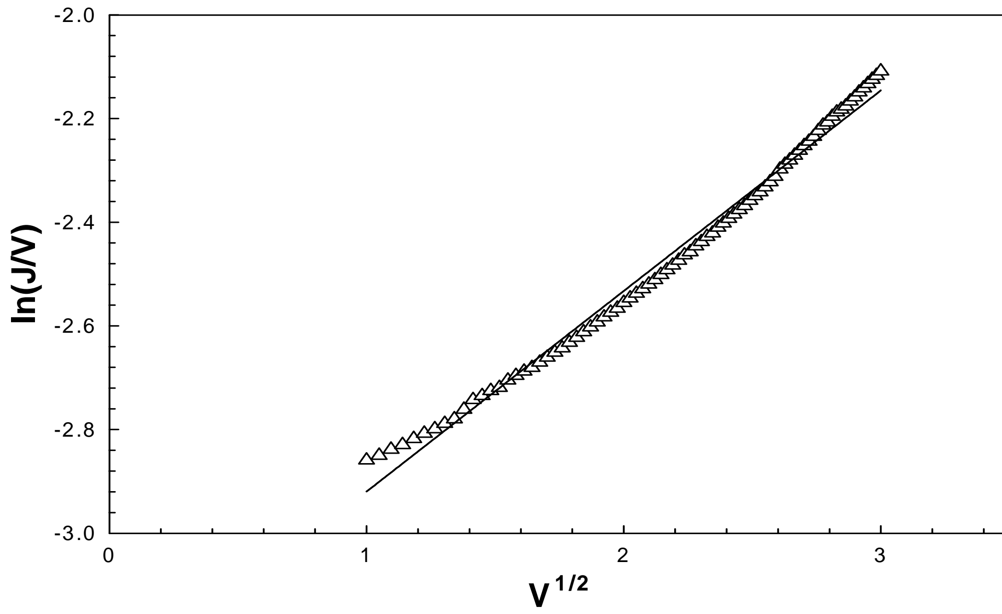

Fig. 3.3.8-13 Frenkel poole process current fitting of curve (c)

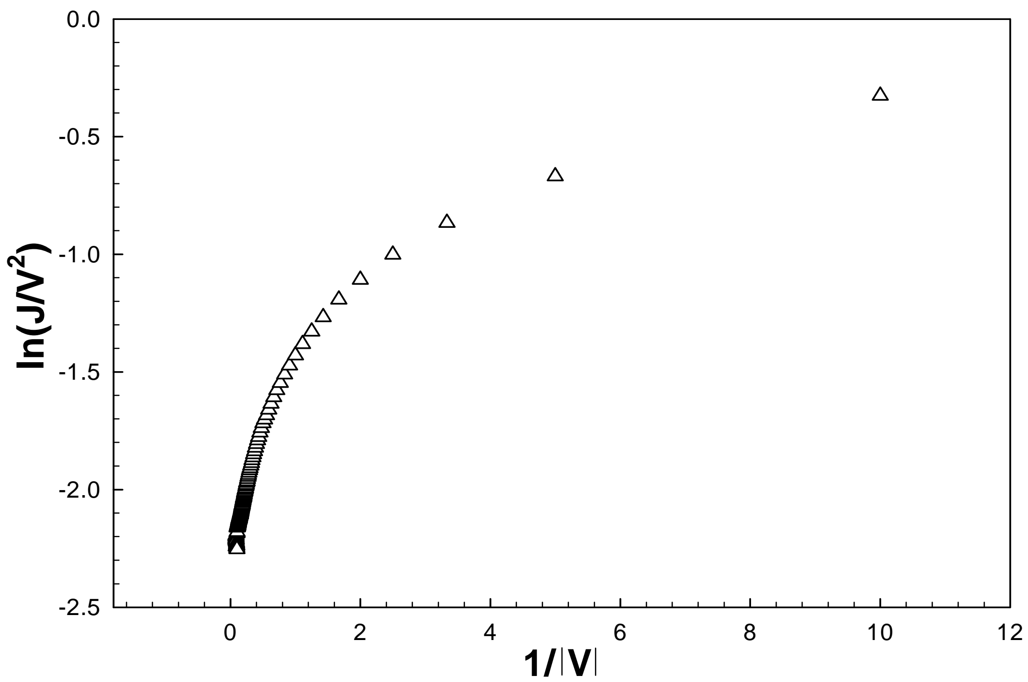

Fig. 3.3.8-14 Field emission process fitting of curve (c)

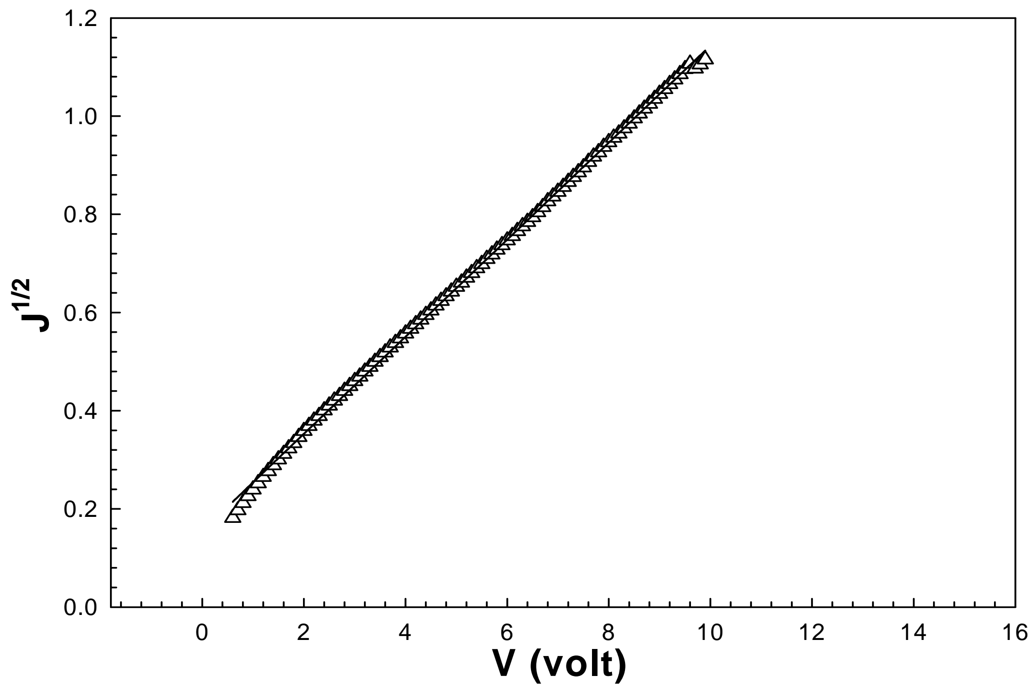

Fig. 3.3.8-15 Space-charge-limited process fitting of curve (c)

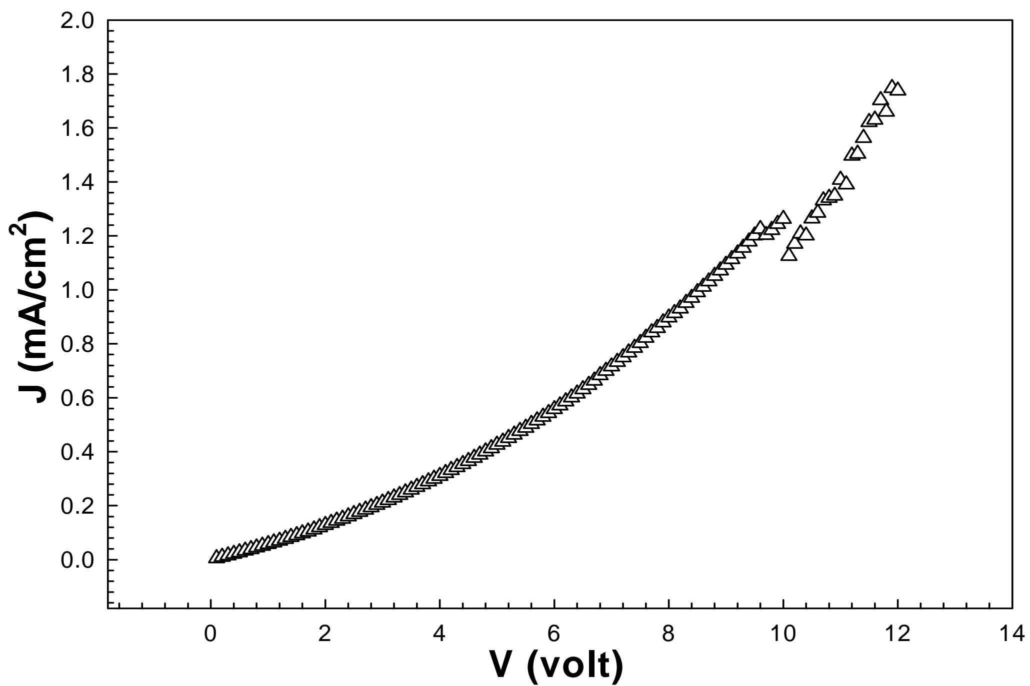

Fig. 3.3.8-16 Ohmic fitting of curve (c)

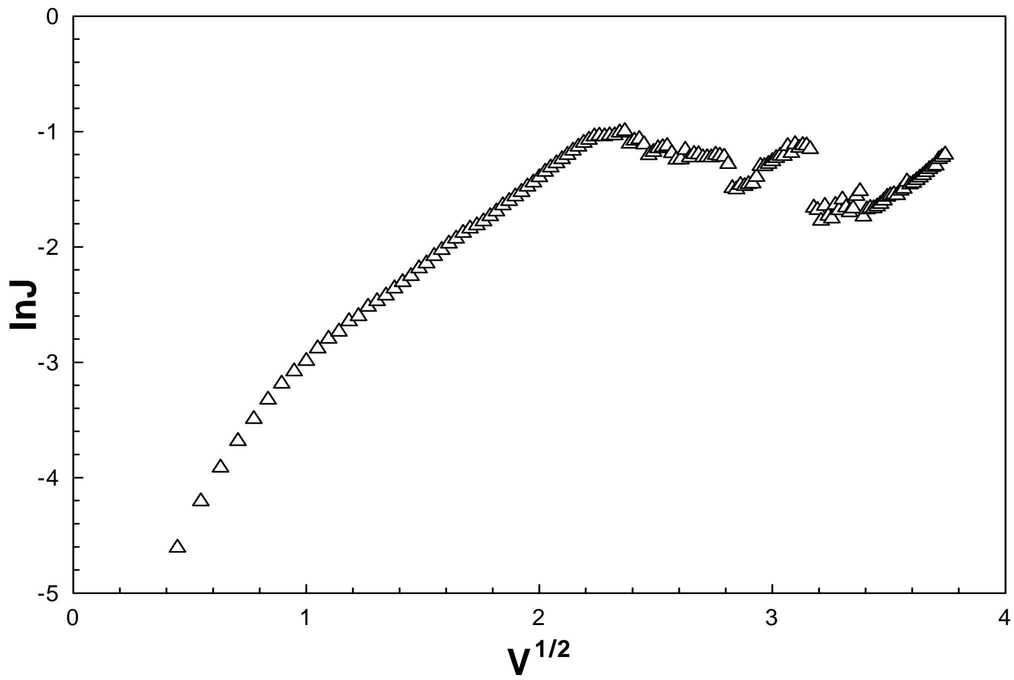

Fig. 3.3.8-17 Schottky emission process fitting of curve (d)

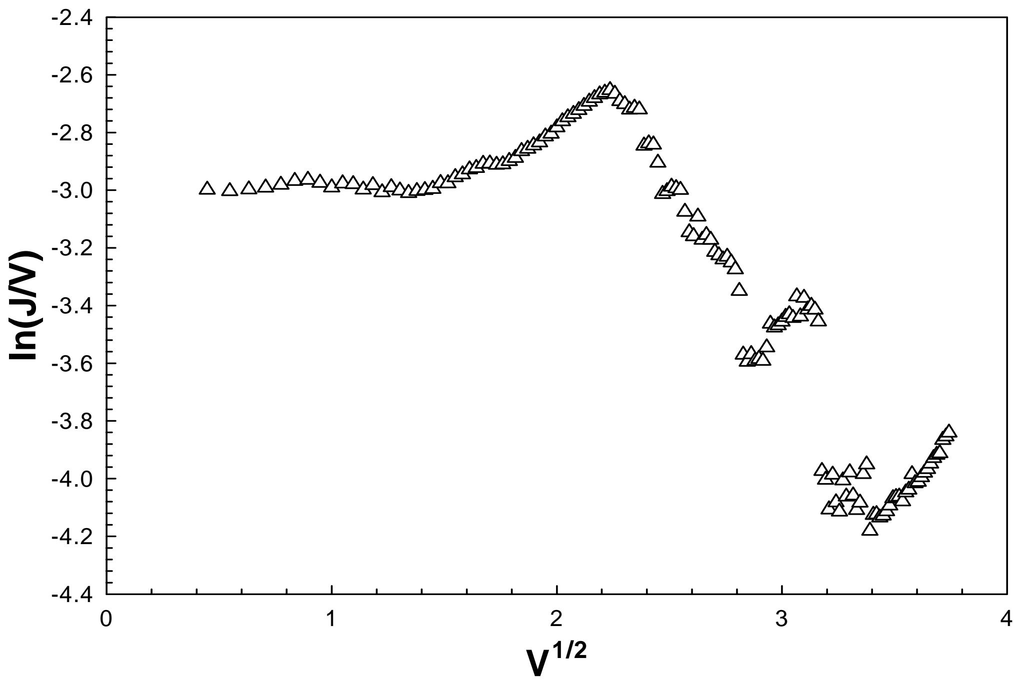

Fig. 3.3.8-18 Frenkel poole process current fitting of curve (d)

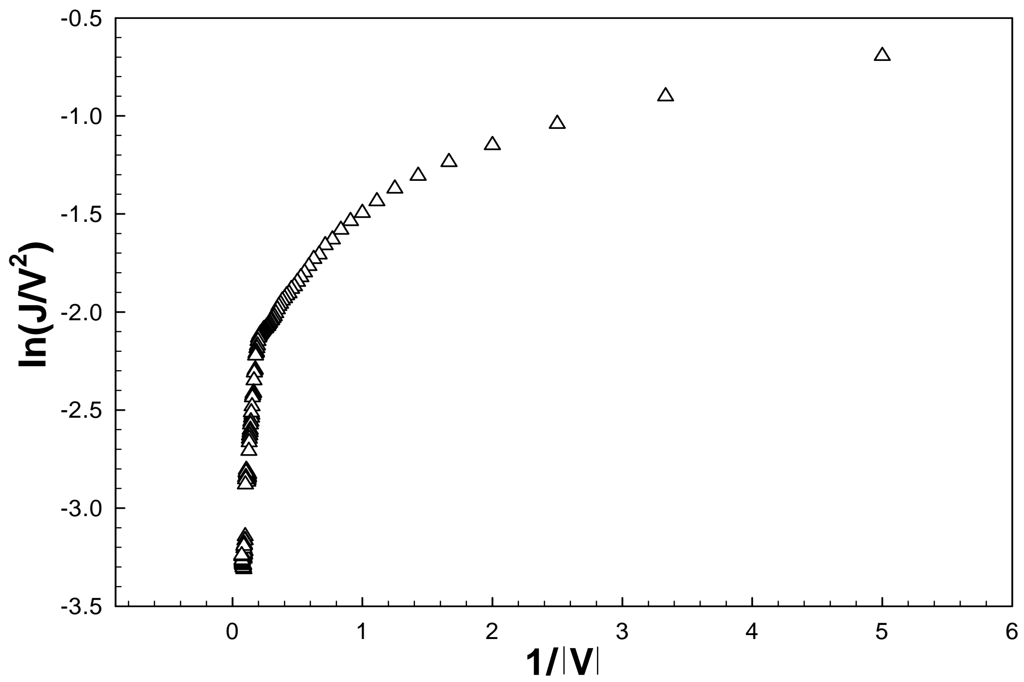

Fig. 3.3.8-19 Field emission process fitting of curve (d)

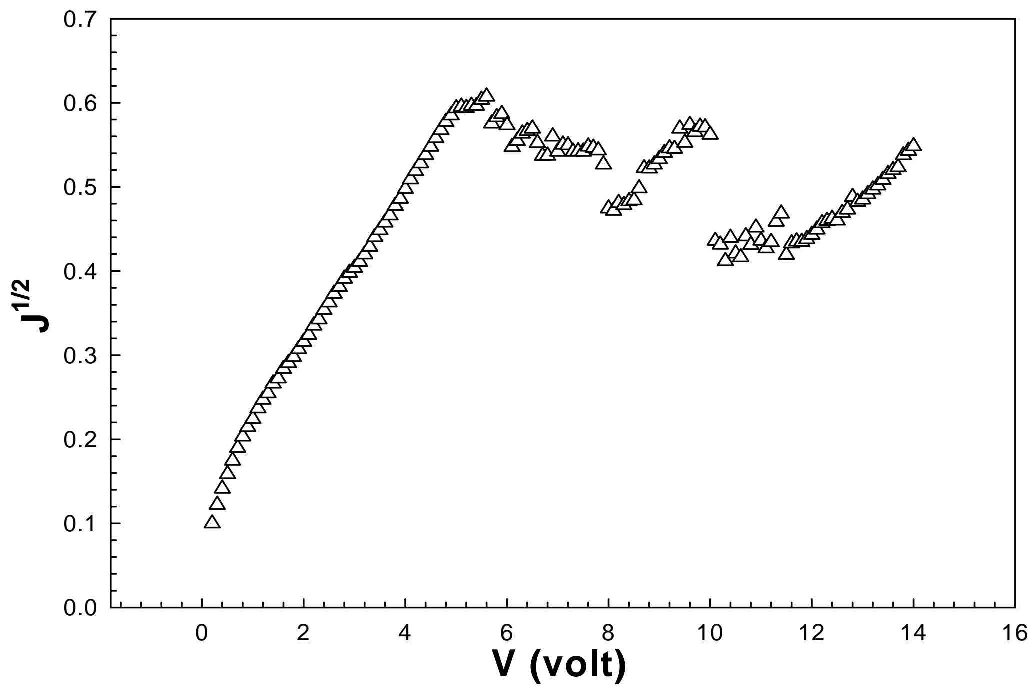

Fig. 3.3.8-20 Space-charge-limited process fitting of curve (d)

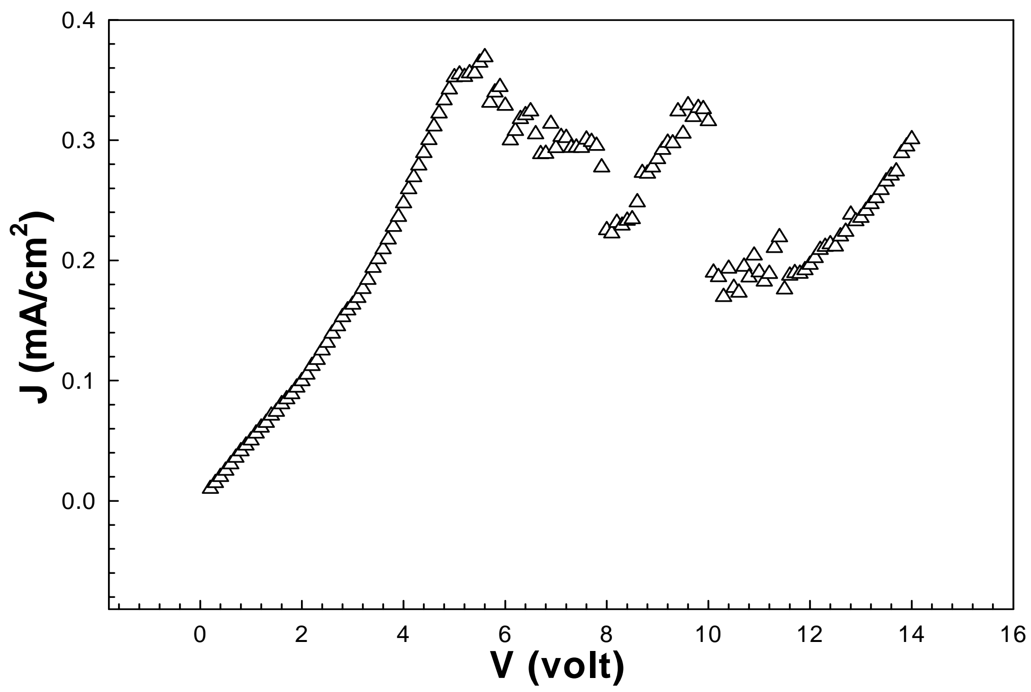

Fig. 3.3.8-21 Ohmic fitting of curve (d)

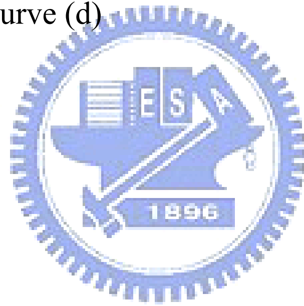

Chapter 1

[1] D. Kahng and S. M. Sze, “A Floating Gate and Its Application to Memory Devices“, Bell Syst. Tech. J., 46, pp. 1283, 1967.

[2] H. Ishiwara, "Recent Progress in FET-type Ferroelectric Memories", IEDM, Tech. Dig., ,2003.

[3] N. Takaura et al., "A GeSbTe Phase-Change Memory Cell Featuring a Tungesten Heater Electrode for Low-Power, Highly Stable, and Short-Read-Cycle Operations", IEDM, Tech. Dig., 2003.

[4] L. Ma, S. Pyo, J. Ouyang, Q. Xu, and Y. Yang, “Nonvolatile electrical bistability of organic/metal-nanocluster/organic system”, Appl. Phys. Lett., 82, pp. 1419-1421, March 2003.

[5] F. Argall, “Switching Phenomena in Titanium Oxide Thin Films”, Solid-State Electronics, 11, pp. 535-541, July 1968.

[6] S. Basavaiah, and K. O. park, “Bistable switching and conduction mechanisms in Nb-Nb_2O_5-Bi junctions, “ IEEE Trans. Electron Devices, ED-20, pp. 149-157, Feb. 1973.

[7] W. R. Hiatt, T. W. Hickmott, “Bistable Switching in Niobium Oxide Diodes”, Appl. Phys. Lett., 6, pp. 106-108, March 1965.

[8] J. C. Bruyere and B. K. Chakraverty, “Switching And Negative Resistance In Thin Films of Nickel Oxide”, Appl. Phys. Lett., 16, pp. 40-43, Jan. 1970.

[9] S. Seo et al., “Reproducible Resistance Switching in Polycrystalline NiO films”, Appl. Phys. Lett.,85, pp. 5655-5657, Dec. 2004.

[10] I. G. Baek et al., “ Highly Scalable Non-volatile Resistive Memory Using Simple Binary Oxide Driven by Asymmetric Unipolar Voltage Pulses”, IEDM 2004.

[11] S. Seo et al., “Conductivity Switching Characteristics And Reset Currents in NiO films”, Appl. Phys. Lett., 86, pp. 093509-1 – 093509-3, Mar 2005.

[12] K. C. Park and S. Basavaiah, “Bistable Switching in Zr-ZrO_2-Au Junctions”, Journal of

Non-Cryst. Solids, 2, pp. 284-291, 1970.

[13] J. F. Gibbons and W. E. Beadle, Solid-State Electronics, 7, p785, 1964

[14] A. Pirovano et. al, “Scaling Analysis of Phase-Change Memory Technology”, IEDM2003

[15] J. G. Simmons and R. R. Verderber, “New conduction and Reversible Memory Phenomena in Thin Insulating, Proc. R. Soc. London, Ser. A301, 77, 1967.

[16] Y. Watanabe, J. G. Bednorz, A. Bietsch, Ch. Gerber, D. Widmer, and A. Beck, “Current-Driven Insulator-conductor transition and nonvolatile memory in chromium-doped $SrTiO_3$ single crystals”, Applied Physics Letters,

[17] S. M. Sze, Physics of Semiconductor Devices, 林在高,2rd, Taiwan, 1981 July.

自　　　傳

學生：林昭正

性別：男

生日：民國 68 年 11 月 03 日

出生地：台灣省

學歷：

國立台北科技大學電機工程學系　　　　　（90 年 9 月~92 年 6 月）

國立交通大學電子研究所碩士班　　　　　（92 年 9 月~94 年 6 月）